TOTAL ATMOSPHERIC ATTENUATION

AT

MILLIMETER WAVELENGTHS

A THESIS

Presented to

The Faculty of the Graduate Division

by

Robert Deming Hayes

In Partial Fulfillment

of the Requirements for the Degree

Doctor of Philosophy in the

School of Electrical Engineering

Georgia Institute of Technology

June, 1964

"In presenting the dissertation as a partial fulfillment of the requirements for an advanced degree from the Georgia Institute of Technology, I agree that the Library of the Institution shall make it available for inspection and circulation in accordance with its regulations governing materials of this type. I agree that permission to copy from, or to publish from, this dissertation may be granted by the professor under whose direction it was written, or, in his absence, by the dean of the Graduate Division when such copying or publication is solely for scholarly purposes and does not involve potential financial gain. It is understood that any copying from, or publication of, this dissertation which involves potential financial gain will not be allowed without written permission.

TOTAL ATMOSPHERIC ATTENUATION

AT

MILLIMETER WAVELENGTHS

Approved:

Dr. F. K. Hurd, Chairman

Dr. M. W. Long

Dr. E. W. McDaniel

Date approved by Chairman May 27, 1964

ACKNOWLEDGMENTS

The author is grateful to Dr. F. K. Hurd for his patience, guidance, and advice during this investigation. The encouragement, guidance, and support of Dr. M. W. Long will always be remembered and appreciated; in addition, Dr. E. W. McDaniel's suggestions and interest in this investigation are appreciated.

I also express appreciation to my close associate, Mr. W. K. Rivers, Jr., for technical assistance and many long and interesting discussions, to Mr. Rezin Pidgeon, Jr. for assistance in constructing the radiometer, to Mrs. Elizabeth Bone for assistance in reducing the data, and to the many others who have worked to make the completion of my graduate studies possible.

My deepest appreciation goes to my wife and children for their patience, understanding, and encouragement.

TABLE OF CONTENTS

TABLE OF CONTENTS (Continued)

LIST OF ILLUSTRATIONS

LIST OF ILLUSTRATIONS (Continued)

LIST OF TABLES

SUMMARY

The effect of the atmosphere on the propagation of signals through it is generally described in terms of the attenuation and reflection characteristics of the atmosphere. Low frequency waves are reflected by the ionosphere, while medium frequency waves are essentially unaffected by the atmosphere and propagate without being reflected or absorbed. Very high frequency waves (for example radar and infrared waves) are attenuated by the uncondensed vapors which constitute the atmosphere.

This investigation was undertaken to determine experimentally the total vertical atmospheric attenuation at very high frequencies and thus provide additional basic information which theorists can use to make more realistic assumptions concerning the atmosphere. Measurements were made to help clarify existing conflicts between previously predicted values of the atmospheric attenuation as a function of frequency. In particular, the present investigation provides new experimental values of atmospheric attenuation throughout the frequency region from 40 to 140 gc/s for use in future calculations and theoretical studies.

The sun offers a good source of electromagnetic energy over the entire radio spectrum, and the techniques of radio astronomy have been employed to determine the vertical attenuation by measuring the energy from the sun as a function of the total atmospheric path length through which the energy passes.

Of the approximately 20 natural gases which occur in the atmosphere, only oxygen and water vapor exist in sufficient quantity and with

the proper molecular properties to cause appreciable absorption of electromagnetic energy in the frequency region from 40 to 140 gc/s. The Van Vleck-Weisskopf theory of gaseous absorption due to molecular resonances has been accepted by most investigators studying the earth's atmosphere. Using this theory, with laboratory measured molecular parameters and estimated dependencies of absorption linewidth on temperature and pressure, Schmelzer and Theissing and Caplan predicted the total vertical atmospheric attenuation resulting from oxygen and from uncondensed water vapor at frequencies above 40 gc/s. In order to anticipate the general type of relationship between detected power and atmospheric path length, the author used these predicted values of atmospheric attenuation to calculate the expected total vertical attenuation which should be obtained from using a wide band detecting system. In this approach, it has been assumed that the frequency response of the radiometer is altered only by the waveguide filters. Bandwidths of 5 to 15 gc/s were used; the atmospheric attenuation is thus not expected to be constant across each frequency band and average values of attenuation per air mass have thus been calculated.

A direct-detection radiometer constructed at Georgia Tech under National Science Foundation Grant G-15063 was used to collect the data. The radiometer consists of a 60 inch parabolic reflector antenna, a 30 cps chopper, a waveguide feed horn, ten high-pass waveguide filters, a bolometer square-law detector, a 30 cps amplifier, a phase-sensitive or synchronous detector, and recorders. Since the bolometer is a square-law detector and the synchronous detector is a linear second detector, the output voltage is linearly proportional to the power received at the antenna. The

large bandwidths provided by the waveguide systems result in large signal levels at the bolometer. The small bandwidth of the 30 cps amplifier and synchronous detector permit small changes in the input signal to be detected. The effective time constant of the system can be made either 1 second or 10 seconds by adjusting the integration time of the output medium.

High-pass waveguide filters employed between the antenna feedhorn and the microwave detector provided frequency selectivity. Frequency cut-off values were preselected for the filters to divide the electromagnetic spectrum into bands appropriate to reveal the predicted characteristics of the oxygen and the water vapor absorption lines. Five filters were constructed to mate with the RG-98 waveguide and have cut-off frequencies at 40.1, 49.6, 59.7, 69.4, and 74.6 gc/s. Also five filters were constructed in the RG-138 waveguide with cut-off frequencies at 72.7, 92.4, 107.7, 121.5, and 138.3 gc/s. Two double linear taper waveguide sections were constructed to transform the RG-98 waveguide of the feedhorn and detector holder to the filters constructed in RG-138 waveguide size. Attenuation characteristics as a function of frequency were calculated for these filters and tapers using equations presented by Kuhn and Ragan. The results are presented.

Signals from the sun and sky were recorded in half day intervals to obtain power level as a function of frequency and number of air masses. The sun was tracked through an optical telescope, attached to the radiometer, while the radiometer was manually positioned. System operation is restricted to one filter at a time. Data were taken sequentially for each of the five filters of a set. Since the sun is continuously changing position in the sky, each filter observation was at a different zenith

angle and the recorded signal levels could not be subtracted directly to obtain the effective received signal over the frequency band defined by two filters. Therefore, a set of curves was drawn which simultaneously best fit the collected data for five adjacent filters. The total vertical attenuation was calculated from these simultaneously best fit curves. It is estimated that the value of atmospheric attenuation (decibels per air mass) has an error of less than 0.6 db, which results primarily from curve fitting and daily fluctuations.

Water vapor content of the lower atmosphere (below 9.6 km) was determined from radiosonde data obtained from the U. S. Weather Bureau for the same days that the radiometer was operated.

Standard statistical tests were performed to establish the dependency of atmospheric attenuation (db/air mass) on water vapor content (gm/sq cm) in each of the frequency bands between 40 and 140 gc/s. These tests show straight lines to be best fits to the data in each frequency band except the region of 59 to 69 gc/s.

These measurements indicate the values calculated by Schmelzer are accurate in the frequency region from 40 to 80 gc/s, but are too high in the region from 80 to 140 gc/s, apparently because of an incorrectly large attenuation attributed to water vapor at frequencies removed from the resonant water lines. It appears to be appropriate for his calculations to be made again, using a smaller linewidth parameter for water vapor in the far-wing regions removed from the water lines.

Theissing and Caplan used a simple approximation of the attenuation function for oxygen, which was valid for their analysis in the frequency region near 300 gc/s, but which produces a large attenuation near

the oxygen resonant lines. To quote Theissing and Caplan, "The effective line width of the envelope of many individual components, greater than the theoretical value, compensates for the neglected oxygen continuum in this approximation." With a revised oxygen linewidth, their excellent work would be appropriate for frequencies down to 40 gc/s. In the frequency region between 125 and 138 gc/s, their calculated values of total atmospheric attenuation are smaller than the values obtained by this investigation. They reached two conclusions which agree with the data of this investigation except near 110 gc/s; that is, 1) the Van Vleck-Weisskopf equation properly describes the general shape of the relation of atmospheric attenuation as a function of frequency, but 2) fails to give the proper absolute magnitude of attenuation in frequency regions between resonant absorption lines.

In the frequency region from 107 to 121 gc/s, no measurable dependence of atmospheric attenuation on water vapor was obtained for water vapor content from 0.65 to 2.65 gm/sq cm. This is indicative of a broad resonant absorption line causing a large value of attenuation throughout the bandpass region and preventing an analysis of the separate influences from oxygen and water vapor. The oxygen line at 120 gc/s has a strong influence in this frequency band, but, with a predicted linewidth of 600 mc/s, it should not be so large as to predominate and completely mask the influence of water vapor. Measurements by Straiton et al., at the University of Texas also indicate anomalies in absorption at these frequencies. If true, as postulated by Straiton, that either additional water vapor lines of strong water vapor-oxygen interaction exists in this region, then the total attenuation would be large and a wide band system would not reveal separate influences by the two gases.

Meeks used an electronic digital computer at Georgia Tech to calculate the atmospheric attenuation resulting from dry air in the spectral region from 45 to 75 gc/s. He used previously reported laboratory and free space values of attenuation resulting from oxygen absorption to establish the oxygen linewidth parameter and integrated the Van Vleck-Weisskopf equation from sea level to 55 km altitude. The values of attenuation calculated by Meeks are only slightly larger than the values obtained from data measured during this investigation in the frequency regions from 40 to 50 and from 70 to 80 gc/s. The slight difference appears to be caused by the value of oxygen linewidth parameter which he calculated based on atmospheric measurements in air containing water vapor although he considered the air to be dry.

Using the sun as a source of electromagnetic energy, attenuation measurements have been made through the atmosphere by several investigators employing superheterodyne systems (5 to 10 mc/s bandwidth) at certain frequencies in the 40 to 140 gc/s region. University of Texas personnel have also made measurements in a chamber containing simulated atmospheres. Values of total vertical atmospheric attenuation reported by Nicoll, Royal Radar Establishment, by Coates, U. S. Naval Research Laboratory, by Whitehurst *et al.*, University of Alabama, and by Straiton *et al.*, University of Texas, are consistent with the values obtained during this investigation. The wide band technique reported here appears to be reliable, and measurements should be extended to higher frequencies.

CHAPTER I

INTRODUCTION

Transparency, absorption, and reradiation characteristics of the earth's atmosphere in relation to electromagnetic energy have interested many scientific groups. More knowledge of these characteristics would enhance physicists' understanding of the composition of the atmosphere, aid in developing the theory of gaseous absorption, and contribute to the understanding of interactions between various gases. Attenuation characteristics are important to the communication engineer interested in signal propagation at continually higher frequencies because of the prospects for more communication channels, smaller antennas for a given resolving power, and lighter weight equipment. Modern astronomers are using radio and radar techniques, in addition to visual observation, to study celestial objects. A knowledge of atmospheric characteristics will enable these scientists to perform their studies with greater accuracy and understanding.

The effect of the atmosphere on the propagation of signals through it is generally described in terms of the attenuation and reflection characteristics of the atmosphere. Low frequency waves are reflected by the ionosphere, while medium frequency waves are essentially unaffected by the atmosphere and propagate without being reflected or absorbed. At very high frequencies, for example radar and infrared, waves are attenuated by the many uncondensed vapors which constitute the atmosphere.

This investigation was undertaken to determine experimentally the total vertical atmospheric attenuation and provide additional basic information which theorists can use to make more realistic assumptions concerning the atmosphere. The sun offers a good source of electromagnetic energy over the radio spectrum. The techniques of radio astronomy have been employed to determine the vertical atmospheric attenuation by measuring the energy from the sun with a wide band direct detection radiometer as a function of the atmospheric path length through which the energy passes. Measurements were made to help clarify existing conflicts between previously predicted values of the atmospheric attenuation as a function of frequency.

Examination of the entire electromagnetic spectrum reveals the earth's atmosphere to be a complicated substance. This investigation was limited to the gigacycle frequency region of the spectrum where electromagnetic energy is attenuated by uncondensed vapors, by dust and smoke, and by meteorological phenomena such as rain, fog, snow, and turbulent air. So many problems are associated with establishing and maintaining homogeneous conditions that the component of total atmospheric attenuation due to each individual effect is very difficult to determine experimentally. On clear, sunny days, however, gaseous absorption produces most of the observed attenuation and the degree of the attenuation is, in theory, predictable from quantum-mechanical molecular models.

Atmospheric attenuation above 10 gc/s occurs as a series of spectral lines. The center line frequencies and intensities have been theoretically predicted and experimentally determined for pure oxygen. Less is known about uncondensed water vapor and about mixtures of water vapor

and oxygen as they normally occur in the atmosphere. The expected attenuation of the atmosphere due to oxygen and water vapor has been calculated by several investigators, but consistent results have not been obtained because of conflicting assumptions made for the parameter values required in the theoretically developed equations. Furthermore, some of the calculations conflict with measurements made by other investigators at isolated discrete frequencies.

A discussion of gaseous absorption and predicted atmospheric attenuation as calculated by other investigators is presented in Chapter II. The direct-detection radiometer used to collect the basic data for this investigation is described in Chapter III. Theory of the radiometer technique for measuring atmospheric attenuation, and the procedures used to obtain and analyze the recorded data are discussed in Chapters IV and V. Values of atmospheric attenuation obtained during this investigation are presented and compared with previously measured and predicted values in Chapter VI. Conclusions derived from this investigation and recommendations for future work are presented in Chapter VII. Appendices give more detailed information on model atmospheres and high-pass waveguide filters.

CHAPTER II

ATMOSPHERIC ATTENUATION

Early investigations (1,2,3,4) coupled with recent studies (13) have shown that certain uncondensed gases in the earth's atmosphere cause absorption of energy in the microwave region of the electromagnetic spectrum. There are approximately 20 natural gases occurring in the atmosphere; however, theory and experiment indicate that only oxygen and uncondensed water vapor exist in sufficient quantity and with the appropriate molecular structure to cause appreciable absorption at microwave frequencies. These vapors exist as molecules and possess dipole moments, oxygen has a magnetic dipole and water vapor has an electric dipole, which can couple with an electromagnetic field to produce molecular resonances.

Spectral Lines

For truly isolated, free, and undisturbed molecules, the absorption associated with molecular resonances can occur only at certain definite discrete frequencies, according to the quantum mechanical principle which holds that transitions between bound energy states can occur only in discrete steps. In reality, however, disturbances occur, and these discrete characteristic frequencies (called spectral lines by spectroscopists) are not monochromatic. Spectral lines are broadened by 1) collision between molecules, 2) Doppler shifts caused by molecular velocities, and 3) inherent uncertainty in the quantum energy levels in the molecular

system. Collision broadening is the predominant factor causing line broadening at pressures between 760 mm and 0.5 mm Hg. Doppler broadening becomes comparable in magnitude to collision broadening only at pressures below 0.5 mm Hg (about 55 km altitude). The "natural line broadening" caused by uncertainty phenomena is negligible in comparison with the molecular collision effect and the Doppler effect for temperatures, pressures, and excitation encountered in the atmosphere.

Broadening of an absorption line caused by the Doppler effect has been calculated by spectroscopists using the principles of kinetic theory. Rogers (1) has tabulated values of linewidth associated with the Doppler effect, in the absence of collision broadening, as a function of temperature for the characteristic water vapor lines at 22 gc/s 184 gc/s, and 327 gc/s, as well as the characteristic oxygen lines at 60 gc/s and 120 gc/s. These values are in the order of kilocycles per second and are thus very small compared to the values obtained for collision broadening. Hence, the Doppler effect is not considered important to this study.

The most generally accepted theory of collision broadening effects on the spectral linewidth has been developed by Van Vleck and Weisskopf (2,3,4). They extended the earlier theoretical work by Lorentz and Debye to the microwave region and developed a general equation for absorption due to vapors (see Appendix C). This equation is complicated by the quantum mechanical properties which must be considered when a molecule makes a transition from one energy state to another. In the case of oxygen and uncondensed water vapor, the Van Vleck-Weisskopf absorption coefficient, $\gamma(f)$, can be reduced with good approximation, in

the region $f_{ij} \pm 2\Delta f$, to

$$\gamma(f) = \frac{Kf^2p}{T^2} e^{-W/kT} \left[\frac{\Delta f}{(f_{ij}-f)^2 + (\Delta f)^2} + \frac{\Delta f}{(f_{ij}+f)^2 + (\Delta f)^2} \right] \text{ in db/km}$$

where:

K = molecular constant (see Appendix C)

p = partial gas pressure,

T = absolute temperature,

W = energy associated with changes from level i to level j,

k = Boltzmann's constant,

f = source frequency,

f_{ij} = characteristic frequency associated with the energy level change, and

Δf = linewidth; half-power half-width of the resonant spectral line.

Characteristic frequencies, f_{ij}, and molecular quantities required for determining K, have been calculated for oxygen and water vapor by several groups. Ghosh and Edwards (5) have tabulated frequencies, f_{ij}, and molecular quantities related to K for 12 of the oxygen lines and 658 of the water vapor lines between 22 gc/s and visual light; Meeks (6) has tabulated these parameters for 25 of the oxygen lines in the region of 60 gc/s; Schmelzer (7) has tabulated these parameters for 26 of the oxygen lines between 50 and 150 gc/s and 60 of the water vapor lines between 22 gc/s and 6,800 gc/s; and Theissing and Caplan (8) have tabulated these parameters for 11 of the water vapor lines between 22 gc/s and 1,500 gc/s. The absorption lines of most importance to this investigation

are a group of 25 lines caused by oxygen near 60 gc/s and one oxygen line near 120 gc/s, and those resulting from water vapor at 22, 184, 327, 380, and 750 gc/s. With these data and a knowledge of the atmosphere, all the quantities in the Van Vleck equation can be specified except the linewidth.

Experimental Measurements

The appropriate value of the linewidth parameter in the Van Vleck-Weisskopf equation has been a subject of investigation since the equation was introduced in 1945. Laboratory measurements have led spectroscopists generally to agree that the linewidth for gases consisting of a single type of molecule is linearly related to total pressure up to about one atmosphere of pressure (1). These measurements also show the linewidth to be inversely related to the absolute temperature. In the case of a mixture of gases, the linewidth is a linear function of the partial pressure of the absorbing gases in the mixture and is proportional to the total pressure. However, uncertainty in defining the time between collisions of various molecules in a mixture of gases prevents an explicit definition for the linewidth. Thus, the exact relationship must be determined experimentally. Researchers have attacked the problem experimentally by making laboratory measurements in waveguide structures, and by atmospheric measurements both horizontally and vertically to the earth's surface. Crawford and Hogg (9) and others have used laboratory measured values of parameters in the Van Vleck-Weisskopf equation to calculate the atmospheric absorption for paths parallel to the earth's surface. Figure 1 is taken from Crawford and

Hogg and shows the results of similar calculations for the absorption caused by oxygen in the 60 gc/s frequency region for the conditions of pressure and temperature which exist for several different altitudes.

The absorption due to uncondensed water vapor in the air was measured at Columbia University (4, 10) in the frequency region of the resonant line at 23.4 gc/s. The measurements show the half power linewidth to be 3 gc/s at typical ground level temperature and pressure (293° K, 760 mm Hg). Van Vleck (4) used this value of linewidth to calculate the expected atmospheric attenuation for a one percent partial pressure of uncondensed water vapor at ground level conditions. He used the same value of linewidth for all the water lines at higher frequencies and then calculated absorption values shown by the solid curve in Figure 2. Measurements made for ground level conditions at the Bell Telephone Laboratories and the University of Texas (11) in isolated portions of the spectral region between 60 and 150 gc/s have given larger values of attenuation than those predicted by Van Vleck, as shown in Figure 2. Most workers attribute these discrepancies to the linewidth value of 3 gc/s as being too small for the absorption lines in the submillimeter and near infrared regions.

Sinton (12), using infrared techniques at 750 gc/s, has made measurements of atmospheric attenuation over a path length of 9.3 meters. His interpretation of these measurements indicates a linewidth of 3 gc/s to be correct for the water vapor line at this frequency.

In addition to the work done over paths parallel to the earth's surface, there have been several investigations of the attenuation vertically through the atmosphere. Rosenblum (13) has presented a summary

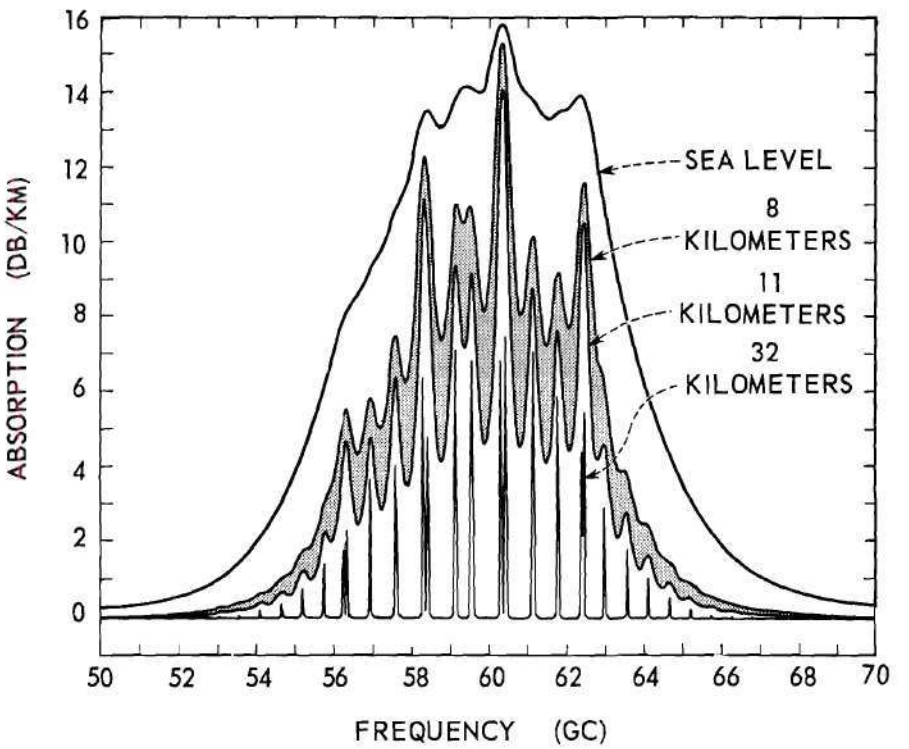

Figure 1. Spectrum of Oxygen Absorption Near 60 gc/s.

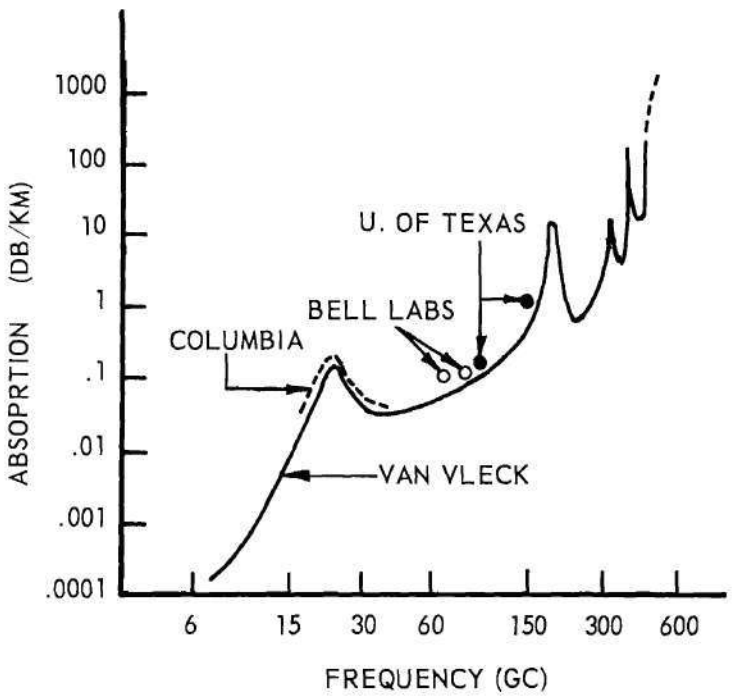

Figure 2. Atmospheric Absorption at Sea Level Due to Uncondensed Water Vapor. One Percent Partial Pressure of Water Vapor.

of the work completed through 1960. Figure 3 is a graphical presentation of his summary, with notations of the investigations included.

The solid curves showing total atmospheric attenuation due to oxygen and water vapor for frequencies less than 40 gc/s were calculated for various angles from the zenith by Hogg (14, 15, 16) using the Van Vleck-Weisskopf theory of attenuation. The relationships of temperature and pressure to altitude used by Hogg are essentially those of the International Standard Atmosphere from ground level to 20 km altitude (see Appendix A). Since this standard atmosphere does not contain water vapor, Hogg made the additional assumption that the water vapor density varies linearly from 10 gm/m^3 at ground level to zero gm/m^3 at 5 km. In addition, the attenuation due to the atmosphere above 20 km was assumed to be negligible.

Theissing and Caplan (8) also used the Van Vleck-Weisskopf theory of gaseous absorption to predict the total atmospheric attenuation due to oxygen and uncondensed water vapor. A summary of their calculations is shown by the dashed lines in Figure 3 in the 50 gc/s to 400 gc/s frequency interval. Since their investigation was primarily concerned with the influence of water vapor on atmospheric attenuation, a simplified equation was used for the portion of attenuation due to oxygen. In the 60 gc/s and 120 gc/s regions, they used the broadest oxygen linewidths of all the investigations encountered during this study, which will be discussed in more detail later. The three curves shown were computed for three typical conditions of water vapor content obtained from radiosonde observations made in the Fort Monmouth, New Jersey area.

Following the analysis by Rogers (1) of water resonant linewidth

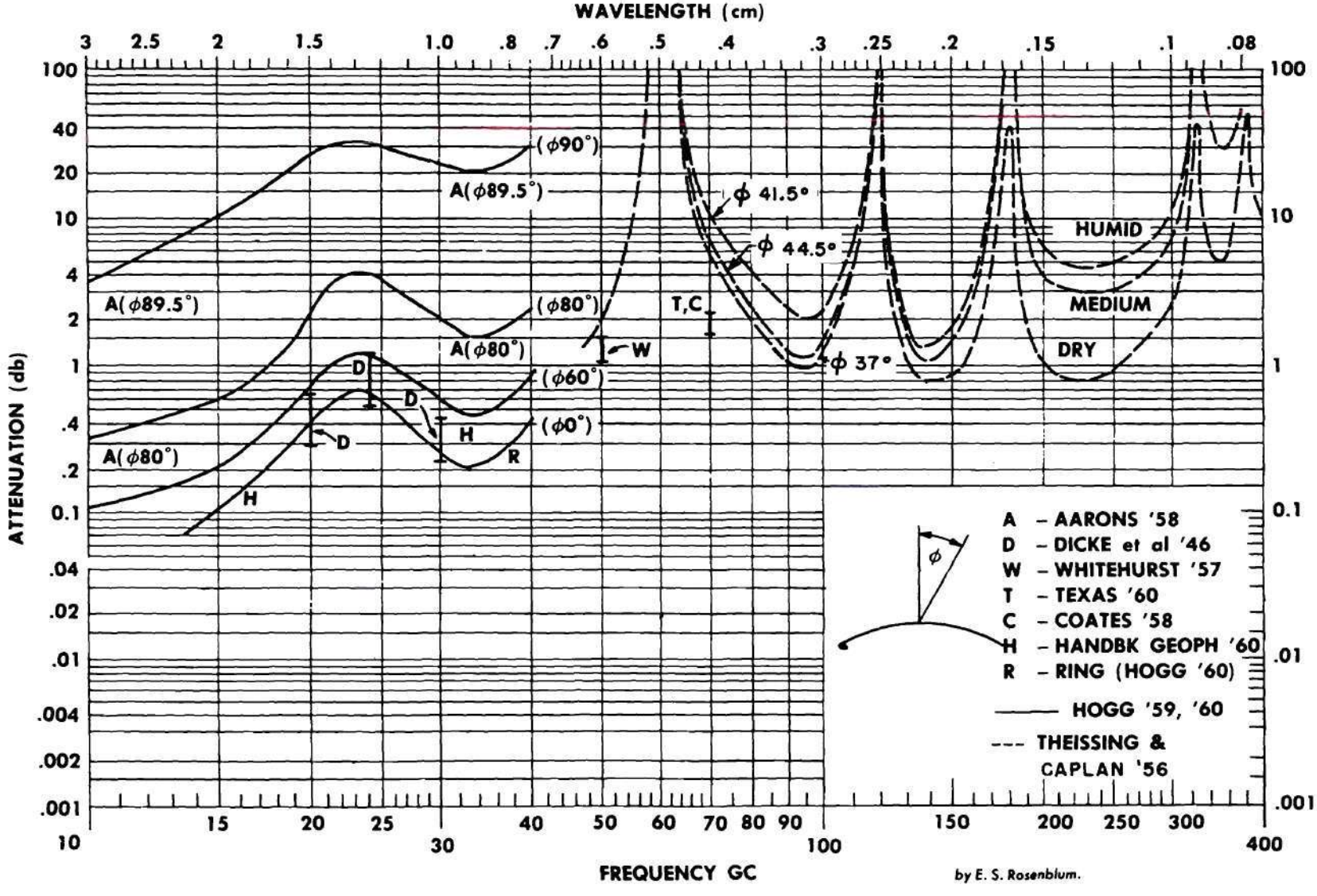

Figure 3. Total Attenuation for One-way Transmission Through the Atmosphere.

variation as a function of pressure, temperature, and water vapor Theissing and Caplan used the following equation to determine the linewidth as a function of the actual atmospheric conditions.

$$\Delta f = \Delta f_o \frac{(1 + 0.012\ \rho/\rho_o)}{1.012} \frac{P}{P_o} \sqrt{\frac{T_o}{T}}$$

The zero subscript denotes standard ground level conditions. They, like Van Vleck, assumed a value of $\Delta f_o = 3$ gc/s for all water vapor lines. Radiosonde data (see Appendix A) were used to define the pressure and temperature conditions with altitude. In calculating the atmospheric attenuation by the Van Vleck-Weisskopf equation, absorption resulting from water vapor was assumed negligible above 6100 meters altitude.

In order to obtain experimental data for comparison with the calculated attenuation, Theissing and Caplan (17) used a thermal detector to observe the power received from the sun on clear days. From these data, they concluded that the general shape of atmospheric attenuation as a function of frequency is correctly defined by the Van Vleck-Weisskopf equation, but that the absolute magnitude predicted by the equation is too small in the spectral region between resonant lines. They conjectured that the predicted values of attenuation are lower than the measured values because the linewidth parameter does not completely describe the absorption at frequencies away from a resonant line, and that all the various lines in the millimeter region may not have the assumed linewidth of 3 gc/s at sea level.

Calculated Attenuation

Since Rosenblum presented his original summary in 1960, publications

by Meeks (6) and Schmelzer (7) have appeared which are pertinent to this investigation. Meeks (6) used an electronic digital computer at Georgia Tech to investigate theoretically the absorption by dry air in the spectral region from 45 to 75 gc/s. He first considered the attenuation parallel to the earth's surface using ground level conditions and then the vertical attenuation through the earth's atmosphere. This attenuation by dry air is the result of 25 closely spaced oxygen absorption lines which overlap and blend together at ground level temperature and pressure conditions to produce high absorption over a wide range of frequencies. The measured values of attenuation by laboratory (18) and free-space experiments (9, 11) were used by Meeks to determine the pressure, temperature, and pure oxygen influence on the linewidth parameter in the Van Vleck-Weisskopf equation. Figure 4 shows the comparison of the experimental data with Meeks' calculation for ground level conditions.

The second phase of Meeks' work was to calculate the total vertical attenuation of the atmosphere from ground level to 55 km altitude by integrating the attenuation values obtained from the Van Vleck-Weisskopf equation. The narrow linewidth (1 mc/s) at low pressures, such as occur above 55 km altitude, results in negligible attenuation away from a resonant line and thus Meeks justified termination of the integration process at this height. The atmospheric temperature and pressure variation with altitude were assumed to be those of the 1960 ARDC Model Atmosphere (see Appendix A).

Investigations by Artman and Gordon (18) revealed that absorption near the oxygen lines is affected by the presence of nitrogen in

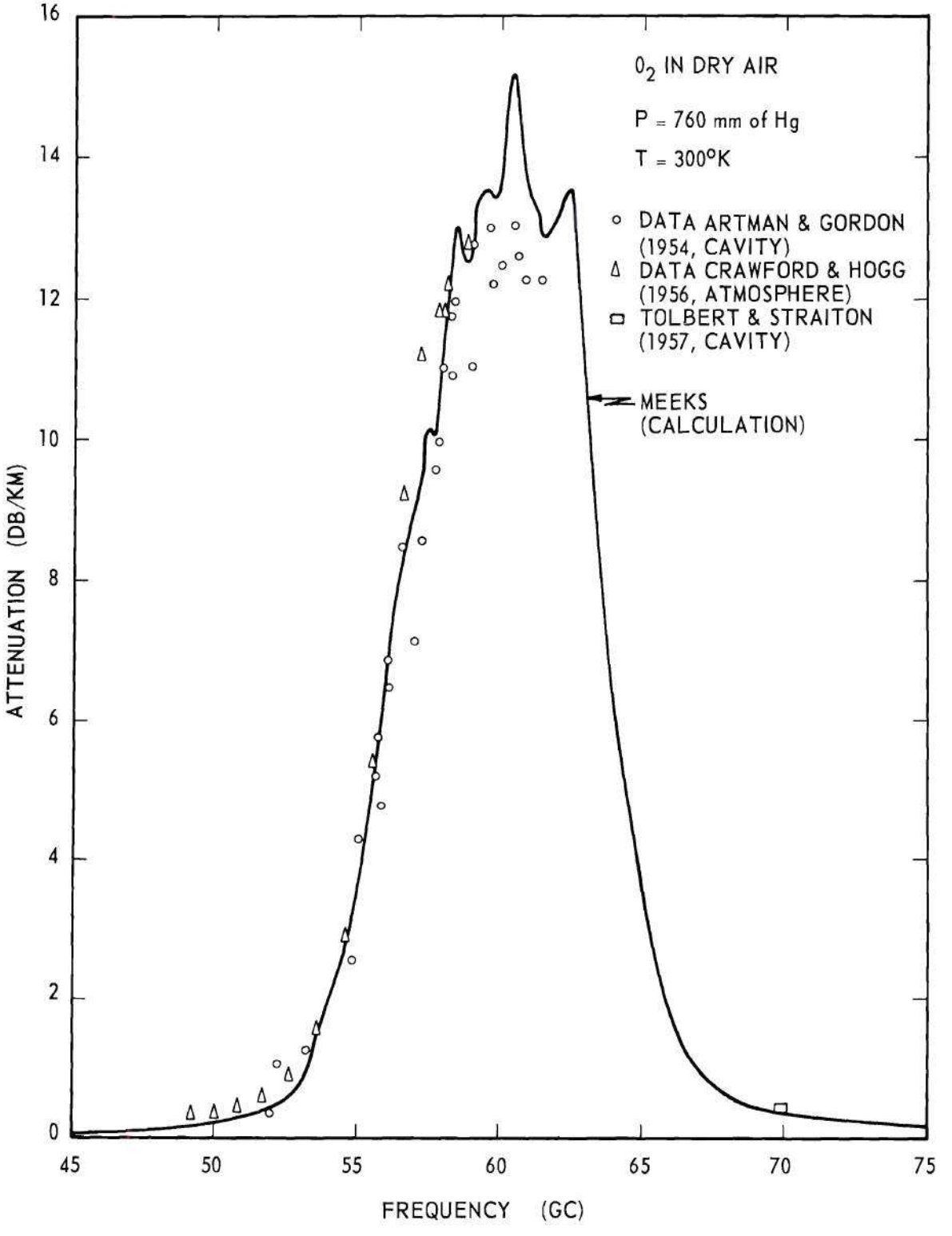

Figure 4. Attenuation of Dry Air at Sea Level.

dry air. Meeks used the mole fractions of oxygen and nitrogen in the air in assuming the following equation to hold for the oxygen linewidth parameter in the Van Vleck-Weisskopf equation

$$\Delta f = \alpha P(0.21 + 0.78\,\beta)\,(300/T)^{0.85} \text{ in mc/s}$$

where

α = 1.95 mc/s $(\text{mm Hg})^{-1}$, a value Meeks determined from ground level measurements by Crawford and Hogg (9),

β = 0.25, a measure of the effectiveness of N_2-O_2 collisions with that of O_2-O_2 collisions from data by Whitehurst (19) and Coates (20),

P = total pressure in mm Hg, and

T = temperature in °K.

By the process of repeated approximations, Meeks assumed values of Δf and β, and calculated the total atmospheric attenuation using the Van Vleck-Weisskopf equation until the experimentally measured values of total vertical attenuation by Whitehurst, et al. (19) at 50 gc/s and by Coates (20) at 70 gc/s were satisfied. It should be noted that the experimental measurements (19, 20) were made through the atmosphere, which contains water vapor, but Meeks considered the air to be dry. Also it is noted from measurements made by Schulze and Tolbert (21) on pure oxygen in a laboratory chamber, and at frequencies near the 120 gc/s absorption line, that α is not independent of pressure, but varies from 1.90 mc/s $(\text{mm Hg})^{-1}$ at 760 mm to 2.08 mc/s $(\text{mm Hg})^{-1}$ at 4 mm Hg.

Schmelzer (7) used the Van Vleck-Weisskopf equation to predict the total vertical atmospheric attenuation due to the combined effects

of oxygen and water vapor in the frequency region from 15 gc/s to 385 gc/s. Atmospheric temperature and pressure variation with altitude were taken from the 1957 ARDC Model Atmosphere (see Appendix A). In addition water vapor content was calculated from an assumed 50 percent relative humidity between ground level and 12 km. He obtained the attenuation due to oxygen by integrating the Van Vleck-Weisskopf absorption coefficient from ground level to 100 km, "since oxygen molecules are dissociated above this elevation and absorption per km is small--being less than one percent of the value computed in the lower range of altitude." The linewidth parameter for the 26 oxygen lines under consideration was selected as

$$\Delta f = 198\ P/T \text{ in mc/s.}$$

This gives a value of 502 mc/s at one atmosphere pressure and 300° K, which is smaller than the value of 600 mc/s used by Meeks. In addition, the different temperature influence on the linewidth parameter and the different atmosphere models result in the linewidth suggested by Meeks being larger than that used by Schmelzer for all altitudes considered.

To obtain the total atmospheric attenuation, Schmelzer added to the attenuation values obtained for oxygen, the attenuation values obtained for water vapor. The Van Vleck-Weisskopf equation was also used in calculating the water vapor absorption. Schmelzer used two linewidth parameters for water vapor: near a resonant line he used

$$\Delta f = 655\ P/(T)^{0.9} \text{ in mc/s}$$

and away from a resonant line he used

$$\Delta f = 2330\ P/(T)^{0.9} \quad \text{in mc/s}$$

At standard ground level conditions the value of the linewidth parameter near a resonant line is 3 gc/s, which is the same value used by all previous investigators.

Comparisons

The values of atmospheric attenuation in the spectral region between 40 and 250 gc/s presented by Theissing and Caplan, Meeks, and Schmelzer have been normalized to the total zenith attenuation and are presented in Figure 5 for comparison. Differences in these curves can be accounted for by considering the parameters used in the calculations. Meeks did not include the attenuation caused by water in his calculations; therefore, his values of attenuation are lower than those for other investigators in the frequency regions above and below the resonant oxygen lines at 60 gc/s. Theissing and Caplan used a simplified approximation, which results in a large linewidth for oxygen absorption, and thus gives higher attenuation values than would be expected in the region of oxygen absorption around the group of lines at 60 gc/s and the one line at 120 gc/s. Schmelzer used a large linewidth parameter for water vapor absorption in the regions removed from water vapor resonant lines resulting in large values of predicted attenuation between 90 and 180 gc. This more than outweighs the added 2 percent correction Theissing and Caplan used on the water vapor linewidth due to water vapor density.

The influence of temperature on the linewidth parameter is different for each investigator. In the case of oxygen, Meeks used a relation of $T^{-0.85}$, while Schmelzer used $T^{-1.0}$. In the case of water vapor,

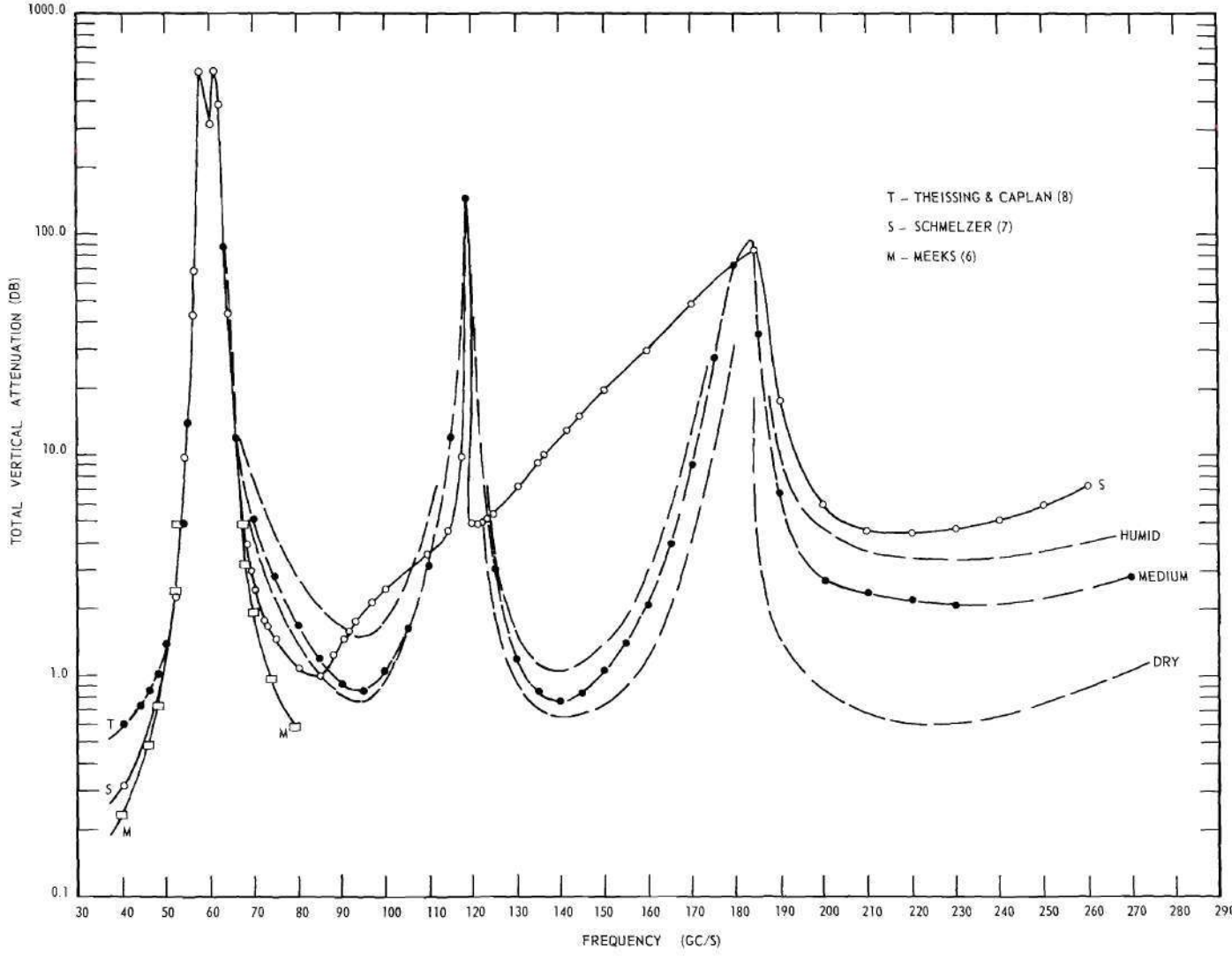

Figure 5. Calculated Vertical Atmospheric Attenuation in Frequency Region from 30 to 260 gc/s.

Theissing and Caplan used a relation of $T^{-0.5}$, while Schmelzer used $T^{-0.9}$; which causes linewidth parameters for water vapor to vary by a factor of ten for the temperature range normally encountered in the atmosphere.

In addition, different atmospheric models were used by each investigator to relate temperature, pressure, and water vapor content with altitude.

The present investigation provides new experimental values of atmospheric attenuation in the frequency region from 40 to 140 gc/s for use in future calculations and theoretical studies.

CHAPTER III

INSTRUMENTATION

A direct-detection radiometer was constructed at Georgia Tech under National Science Foundation Grant G-15063 and has been used to record signal strength of the sun as a function of zenith angle in the frequency region from 40 to 140 gc/s. The radiometer consists of a 60 inch parabolic reflector antenna, a 30 cps chopper, a waveguide feed horn, ten high-pass waveguide filters, a bolometer square-law detector, a 30 cps amplifier, a phase-sensitive or synchronous detector, and recorders. Figure 6 is a simplified diagram of the radiometer. When the antenna is directed at the sun, then the radiation from the sun is alternately passed and then blocked by the chopper wheel from the parabolic reflector to the bolometer detector. This produces a square wave signal which has an amplitude proportional to the received radiation. This signal is amplified, detected, and filtered as shown in Figure 6. The output voltage is recorded for each waveguide filter used as a function of the zenith angle and processed to obtain the atmospheric attenuation.

Since the bolometer is a square-law detector and the synchronous detector is a linear second detector, the output voltage is linearly related to the power received at the antenna. The large bandwidths provided by the waveguide systems result in large signal levels at the bolometer. Yet, the small bandwidth of the 30 cps amplifier permits

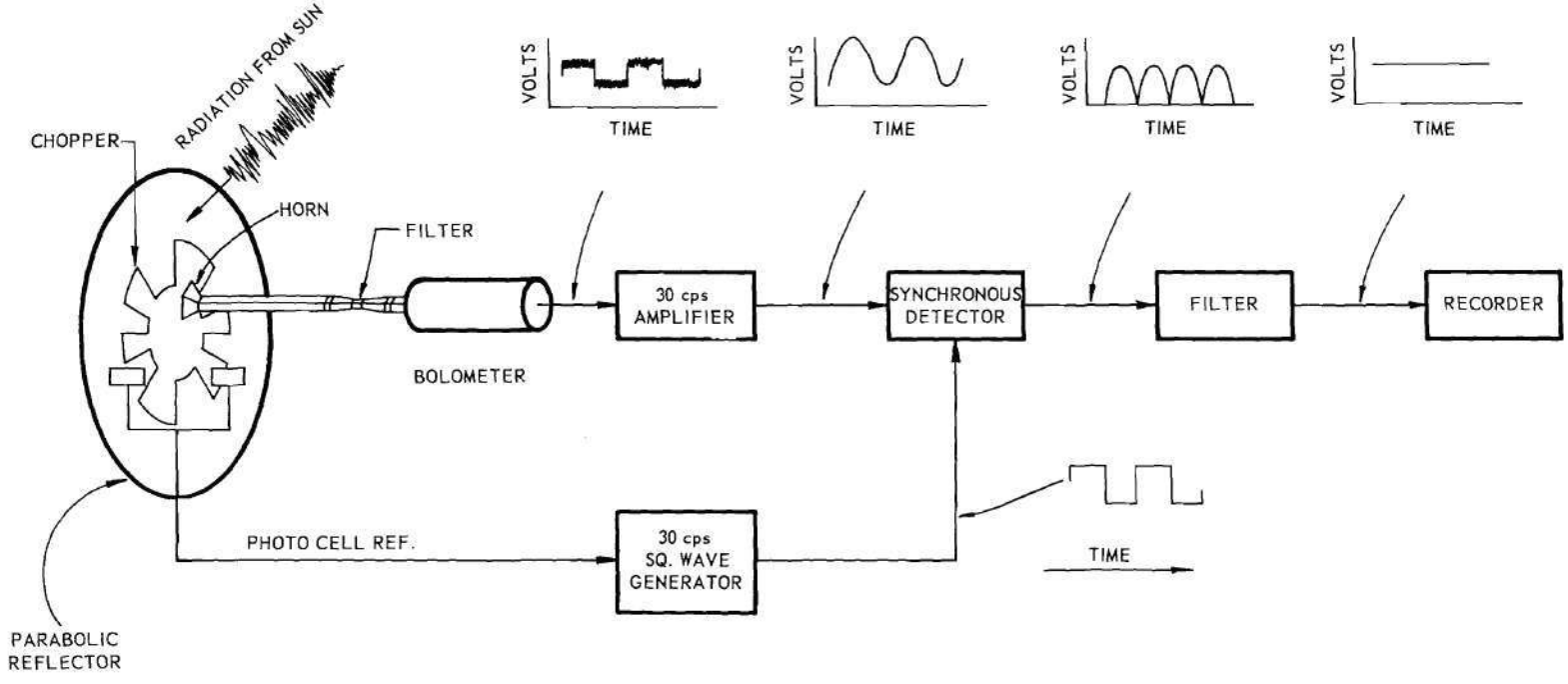

Figure 6. A Simplified Diagram of the Radiometer.

small changes in the input signal to be detected (28). The effective time constant of the system can be made either 1 second or 10 seconds by adjusting the integration time of the output medium. A photograph of the antenna and associated microwave equipment is presented in Figure 7. Figure 8 is a photograph of the amplifiers, recorders, and associated equipment.

Microwave System

A war surplus 60 inch searchlight was obtained for the antenna reflector and mount assembly. This unit contains a silver-surfaced, copper-based parabolic reflector which has a focal length of 25.45 inches and an F/D ratio of 0.427. The parabola can be seen in Figure 7 inside the support frame of the antenna. The carbon arc, front glass cover, and arc feed assembly were removed and a mount for the chopper, microwave feed horn, waveguide filters, and bolometer detector was installed. Servo-dc motor drive controls, originally used to position the searchlight, were disabled, and manually operated cranks were used to position the antenna in azimuth and elevation. An eight-power optical elbow telescope, with optical filters to protect the eye and cross-hair sights for ease in tracking, has been installed on the assembly. This telescope was boresighted with the antenna and is used by the operator to track the sun as a function of position in the sky. A scale, calibrated in degrees from the zenith, is located near the telescope and can be conveniently read by the operator. This arrangement permits one operator to specify the elevation angle of the antenna while tracking the sun.

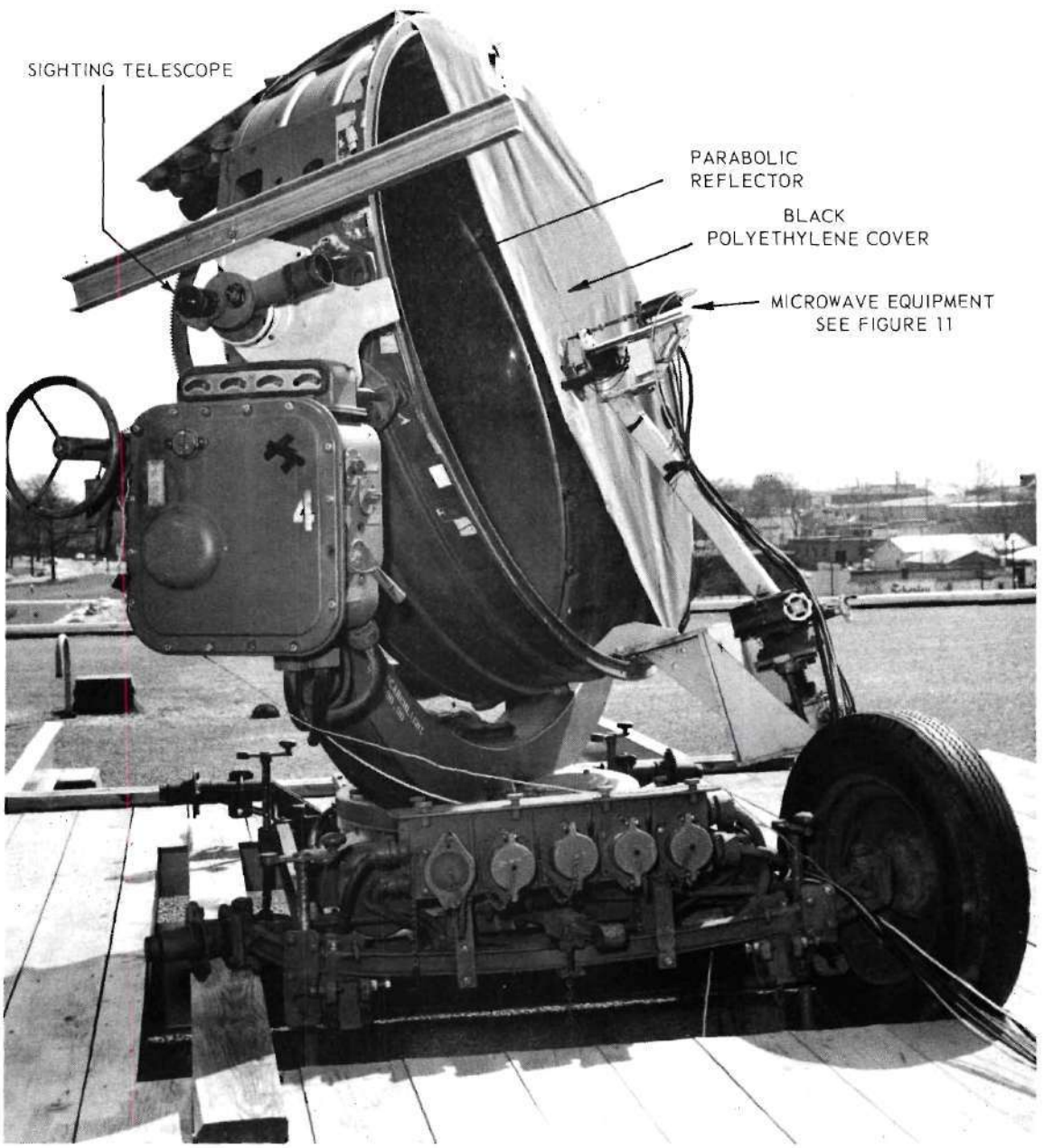

Figure 7. A View of the Antenna and Microwave Components.

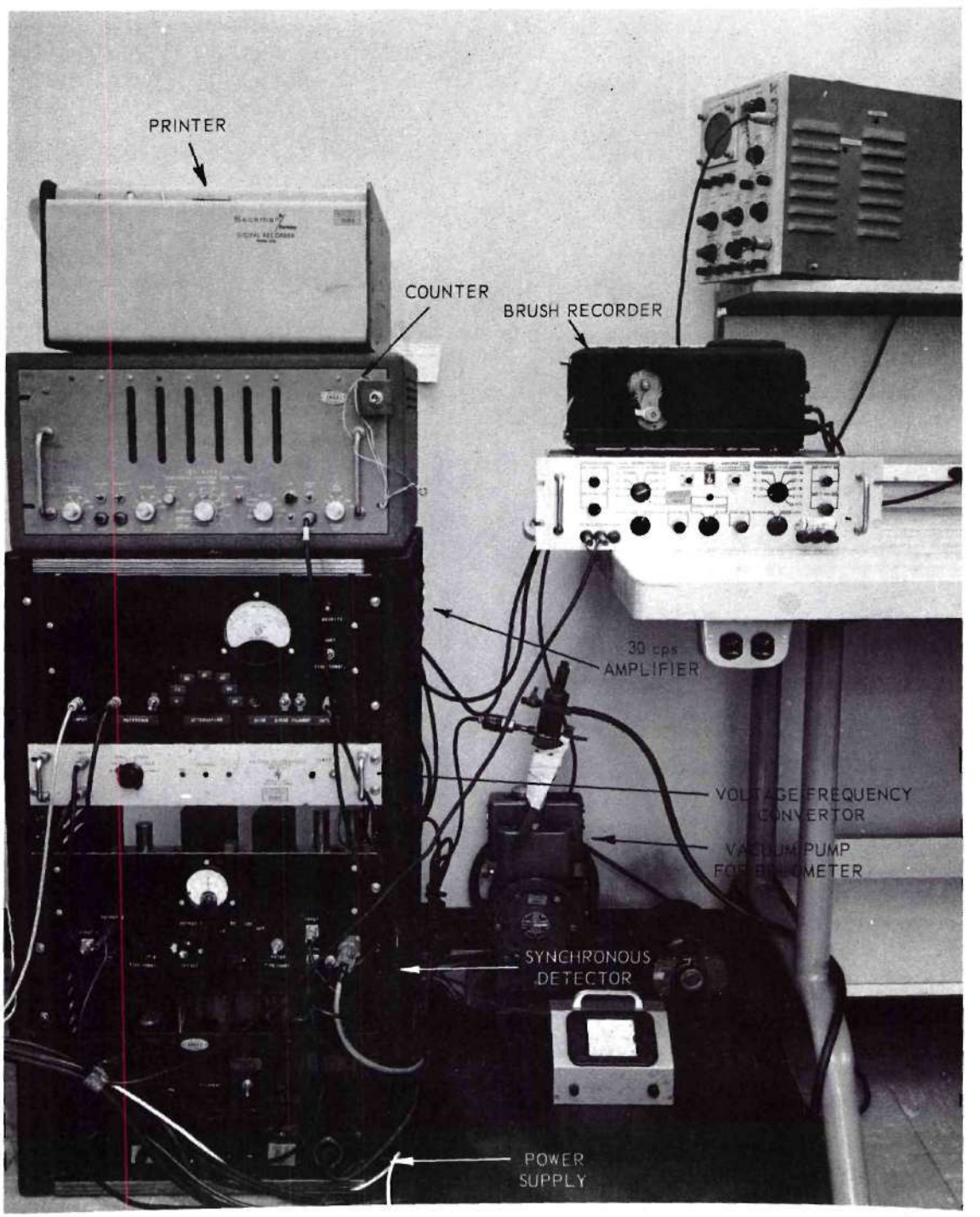

Figure 8. A View of the Amplifiers, Recorders, and Other Equipment.

Standard microwave techniques were used in constructing the waveguide feedhorn used with the radiometer. The horn is linearly flared in both the E and H planes to inside dimensions of 3.43 by 4.72 mm from standard RG-98 waveguide (1.88 by 3.76 mm inside dimensions). Low reflections in the flared horn over the frequency band of interest are insured by a taper length of 3.51 mm. Calculations using standard equations for sectorial horns (22) show the variation in horn path length to be less than 10 per cent at the highest frequency used, thus establishing the focal center of the horn to be very near the open aperture. The calculated half-power beamwidth of the far field pattern for the horn is less than 100 degrees for frequencies greater than 40 gc/s, and the 1/10 power beam width is less than 120 degrees for frequencies above 70 gc/s. Since the angle subtented by the edge of the parabolic reflector is 120 degrees at the focal point, the antenna-feed combination has been assumed to be reasonably efficient, and the energy arriving at the feedhorn is primarily from the parabola, with a negligible amount from other sources.

Alignment of the waveguide feedhorn and collimation of the optical telescope with the antenna have been determined by drift-scan measurements of the sun. The procedure was to orient the antenna a few degrees west of the sun and lock it in position. As the earth revolves, the antenna beam would pass across the center of the sun and the sun's radiation was recorded by the radiometer. Then the antenna was changed slightly in elevation, again advanced to the west of the sun, but in a position such that the center of the antenna beam just passed the edge of the optical circumference of the sun. The results of such drift scans are shown in Figure 9, where the lowest frequency passed by the radiometer was 40 gc/s.

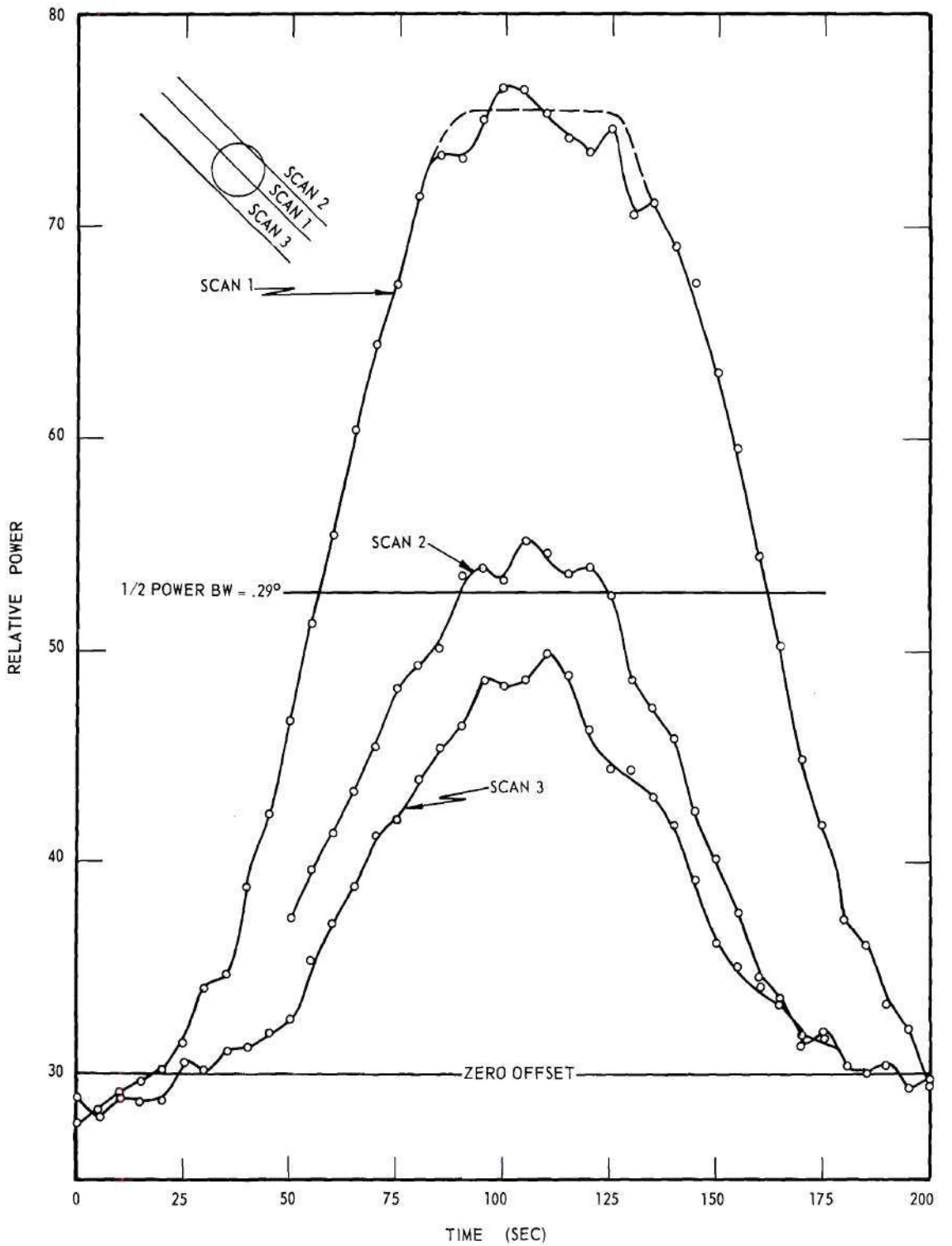

Figure 9. Drift Scans of the Sun with Filter No. 1.

Using these data, the calculated half-power beam width of the antenna is 0.29 degree, which agrees reasonably well with a calculated value of 0.297 degree obtained from standard antenna equations (22). Since the antenna beamwidth is smaller than the subtented angle of the sun (approximately 0.56 degree), a drift scan through the center of the sun (such as Scan 1) has a flat portion at the center of the scan period.

High-pass waveguide filters are employed between the antenna feedhorn and the microwave detector. Frequency cut-off values were preselected for the filters to divide the electromagnetic spectrum into appropriate bands which reveal the characteristics of oxygen and water vapor absorption lines, as discussed in Chapter II. Five filters (Nos. 1 - 5) were constructed to mate with the RG-98 waveguide and have cut-off frequencies respectively at 40.1, 49.6, 59.7, 69.4, and 74.6 gc/s. And five filters, (Nos. 6 - 10) were constructed in the RG-138 waveguide with cut-off frequencies at 72.7, 92.4, 107.7, 121.5, and 138.3 gc/s. Two double linear taper waveguide sections were constructed to transform the RG-98 waveguide of the feedhorn and detector holder to RG-138 for use with Filters No. 6 through 10. Attenuation characteristics as a function of frequency have been calculated for these filters and tapers using equations presented by Kuhn (23) and Ragan (24). The results are presented in Figure 10. The values presented for Filters No. 6 through 10 include the attenuations of the linear transitions, while the values for Filters No. 1 through 5 are for the filters only. The cut-off frequencies listed above were defined as the 10-db attenuation value for each filter curve present in Figure 10. More details relative to the construction and electrical properties of these filters are presented in Appendix B.

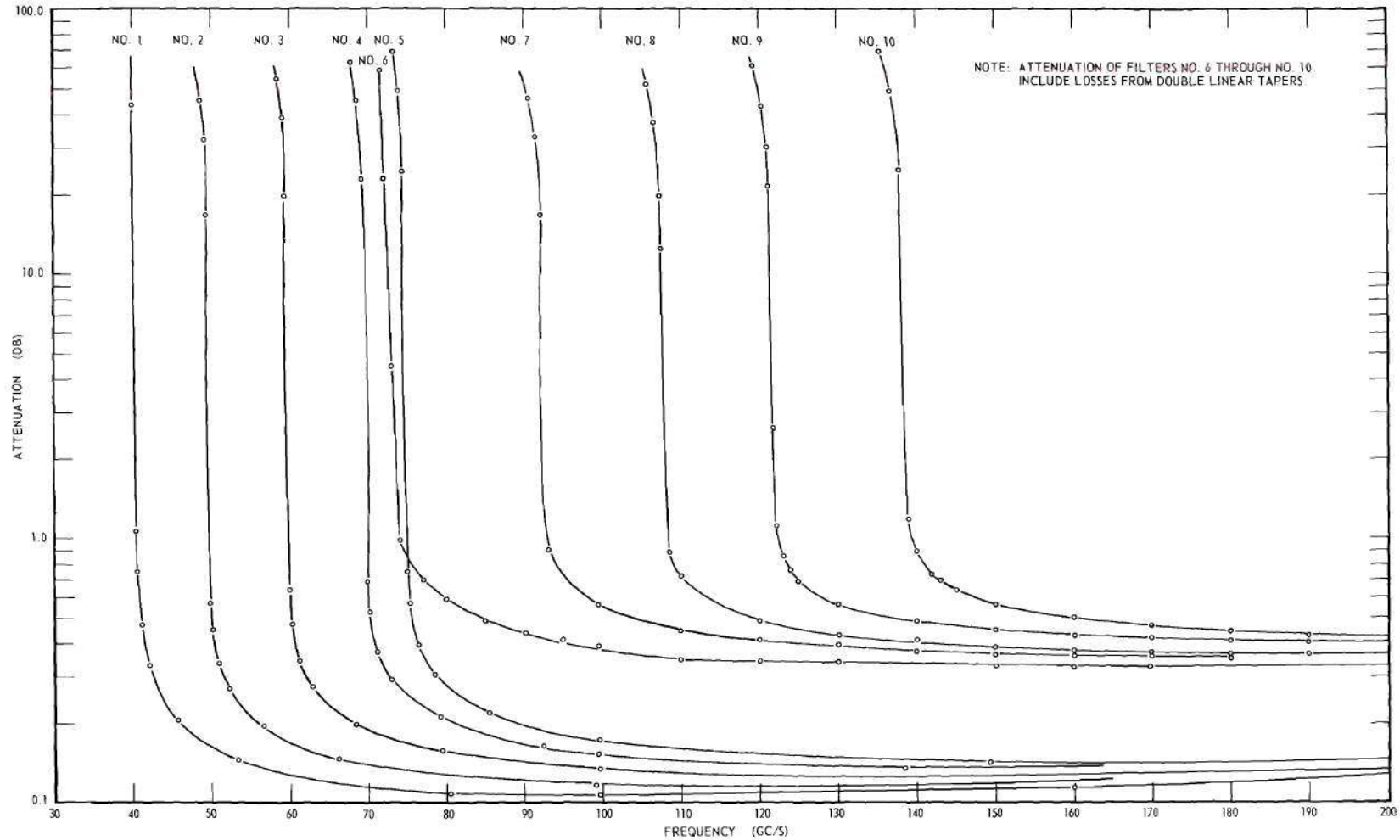

Figure 10. Attenuation Characteristics of the Waveguide Filters.

Black polyethylene sheet film[1] approximately 8 mils thick is placed over the antenna between the parabola and the feedhorn to eliminate energy in the visible and infrared region of the spectrum (25, 26) from reaching the parabolic reflector. In addition, the feedhorn is also covered to prevent any extraneous high frequency energy from entering the feedhorn directly. No appreciable change was observed in signal strength received from the sun when the thickness of the polyethylene sheet was doubled, thus verifying that the film is transparent to energy in the millimeter wavelength region of the spectrum. In Figure 7, the polyethylene sheet has been folded back so that the parabolic reflection can be seen.

The microwave square-law detector used in this system is a PRD-634 bolometer mounted in a PRD-632 waveguide holder.[2] An evacuated chamber was constructed to house the detector and a continuously operating vacuum pump maintains a pressure below 50 microns on the unit. As reported by Long and Butterworth (27), the minimum detectable signal from typical waveguide barreters is reduced by a factor of 10 under evacuated conditions as compared to standard ground level pressures. A window of clear mylar, 5 mils thick, is used between the bolometer and the waveguide filters to form a vacuum seal at the waveguide junction. A BNC lead-through-connector was constructed by modifying standard UG-260A and UG-1094 connectors, installing in the endplate of the vacuum chamber, and applying glyptol to insure a proper vacuum seal. This special connector minimized lead-through

---

[1]The black material in the polyethylene film is carbon black powder which permits less than 1 percent transmission through a 3 mil thickness and effectively zero transmission through an 8 mil thickness in the visual region of the spectrum. (Private communication with Visking Co., Chicago, Illinois.)

[2]Polytechnic Research and Development Co., Inc., Brooklyn, New York.

lengths from the bolometer holder to an external coaxial line and essentially eliminated stray noise pickup in the connector to an input transformer located in the 30 cps amplifier. A 1.5 volt battery and resistive divider circuit provide an appropriate bias level for operating the bolometer at the manufacturer's recommended resistance of 200 ohms.

The minimum signal which can be detected by a wideband system is limited by spurious gain fluctuations in the amplifier and statistical noise variations occurring in a noise-like waveform. One common method for reducing gain fluctuations and incoherent noise variations is to modulate the incoming signal at a low audio rate and then synchronously detect the signal at the modulation frequency. Dicke (28) described such a system for a superheterodyne radiometer in which absorbing material was alternately inserted and removed at a 30 cycle rate from the waveguide between the antenna and the receiver. Comparison was thus obtained between thermal noise generated by the resistive material and the radiation signal received at the antenna. Each cycle of the square wave produced by this comparison technique contains one-half period of signal from the reference source and one-half period of signal from the antenna. For illustration, if the antenna is pointed at a black body of the same temperature as the absorbing material then the same thermal noise will be produced during each half cycle and the synchronous detector will have zero signal output.

At millimeter wavelengths, waveguides are very small and waveguide insertion techniques do not appear as a practical method for obtaining a switch reference. However, the radiation from the parabolic reflector can be blocked and prevented from reaching the feedhorn by placing a piece

of reflecting material in front of the feedhorn. A six-blade flat propeller, driven by a small synchronous motor through a gear reducer, was located between the feedhorn and the parabolic reflector on the antenna. This mechanical configuration offers a balanced load to the motor and permitted a small Borg fractional horsepower unit to be used.

A 30 cps phase reference signal is also produced at the chopper by placing a small light bulb on one side of the propeller opposite a photocell detector. The rotating propeller alternately passes and breaks the light beam from the bulb to the photocell, resulting in a 30 cps signal from the photocell which is phase coherent with the chopped bolometer signal. This bulb-photocell unit can be rotated through a 270 degree sector which facilitates adjusting the phase between the two detectors. Figure 11 is a photograph of the microwave horn, waveguide filter, bolometer detector mount, chopper, photocell 30 cps reference, and synchronous drive motor.

Amplifiers and Recorders

Signals from the bolometer detector are amplified by a high-gain, low-noise 30 cps amplifier, shown in block diagram form in the upper portion of Figure 12. The amplifier consists of a wideband 62 db gain preamplifier, high- and low-pass RC-active filters, notch filters at 60 and 15 cps, and two 30 db gain amplifiers each followed by 30 db resistive pad variable attenuators. Practical designs of RC filters for low frequency (less than 100 cps) applications have been discussed and formalized by Sallen and Key (29). The filters were constructed following these outlined methods and have symmetrical attenuation response for logarithmic

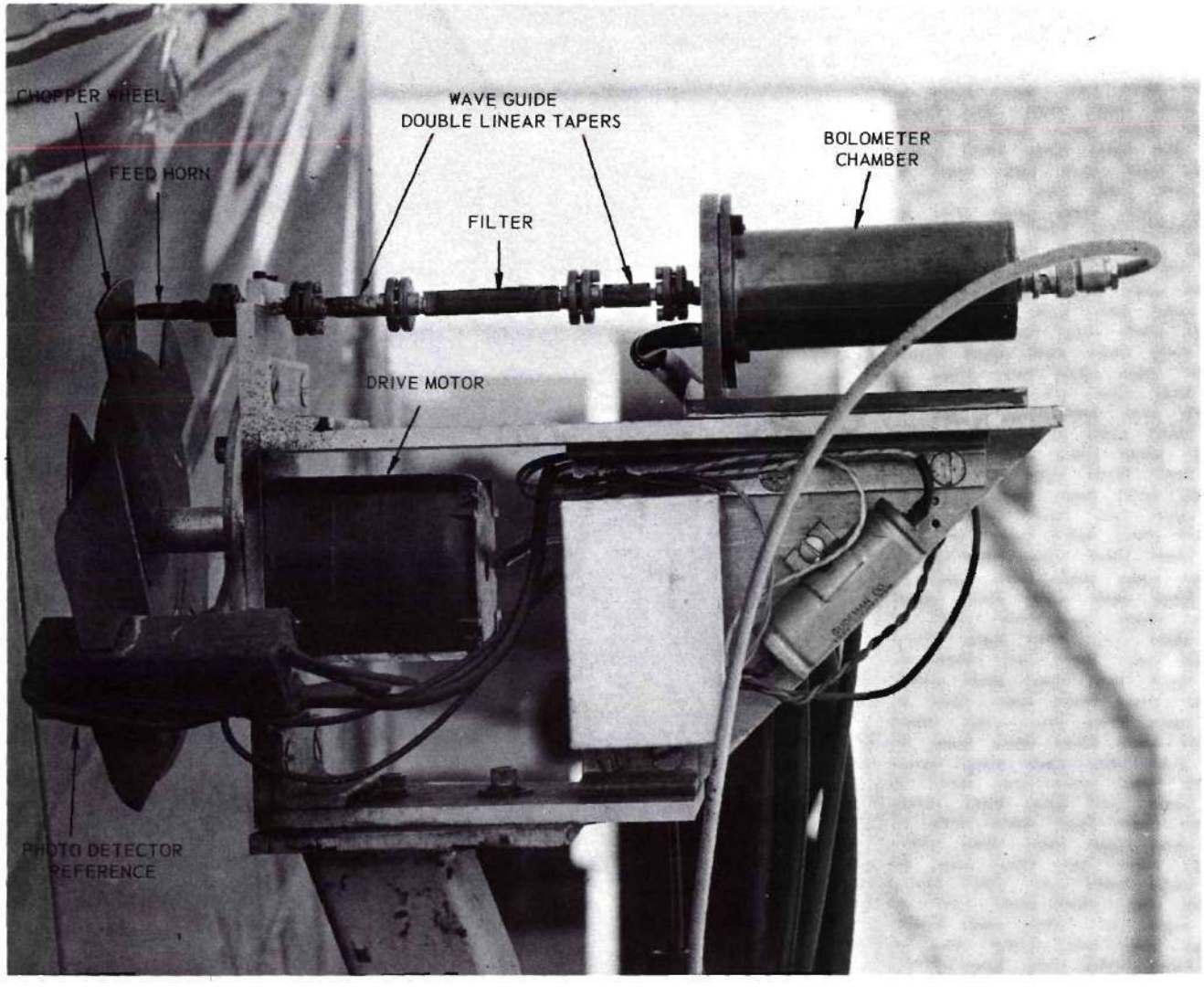

Figure 11. A Close-Up View of the Microwave Equipment.

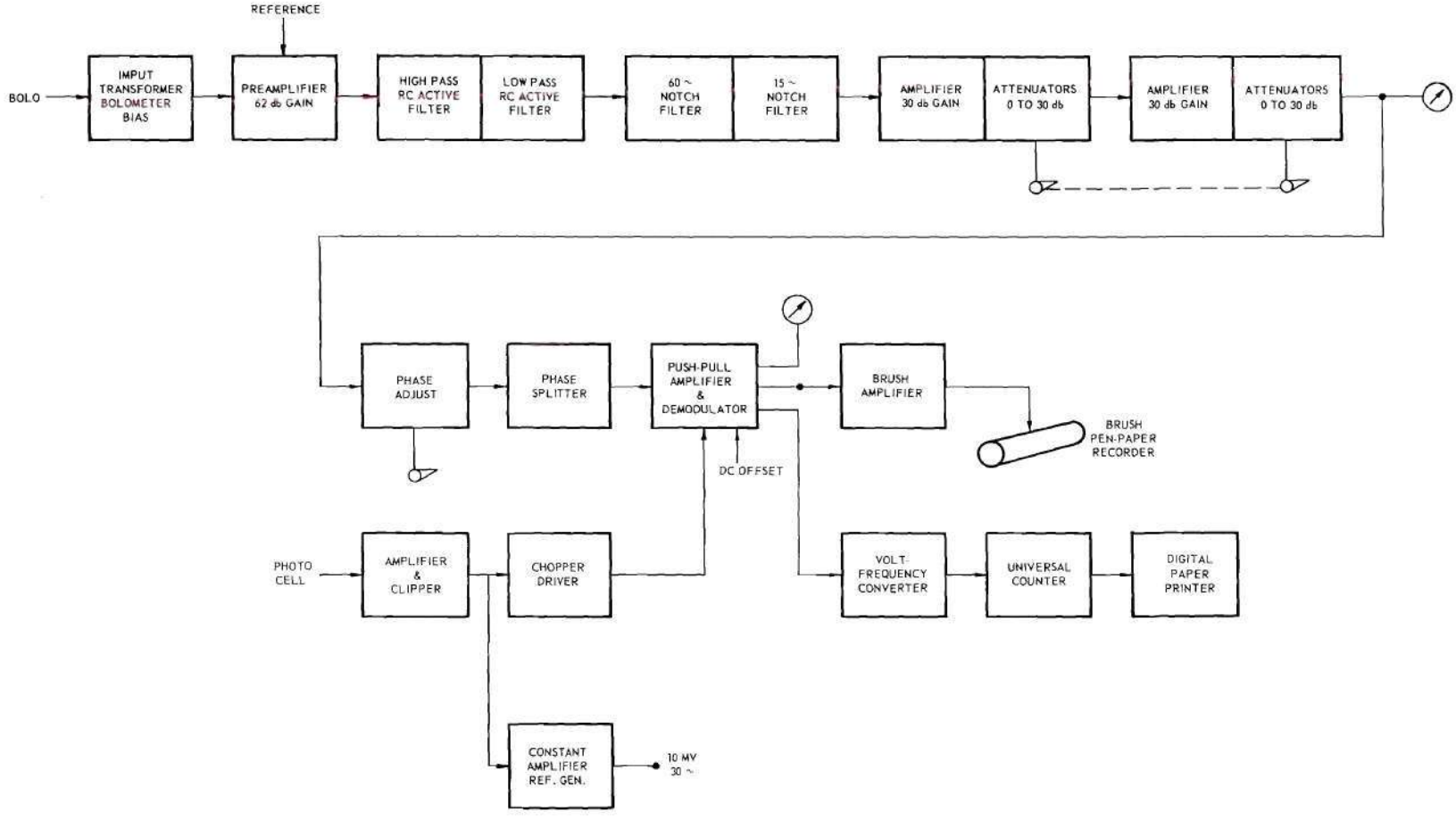

Figure 12. System Block Diagram.

changes in frequency about the bandpass region. Total gain of the amplifier is 132 db at 30 cps, and a 15.5 cps half-power bandwidth (23.5 to 39 cps) has been obtained. The attenuator pads are connected together for ease of operation, which provides 60 db of attenuation in 10 db ± 0.05 db steps. Special precautions were taken to reduce noise in the amplifier; for example, 1) the preamplifier has separate shock mounts, and 2) the separate ground circuits for each amplifier section are all connected at one common location.

An input transformer is used to match the ac impedance of the bolometer to the first stage of the 30 cps preamplifier. This transformer is enclosed in Mu-metal to reduce stray magnetic pickup at the critical input amplifier stage in the system. With the addition of the transformer, an overall amplifier gain of 170 db and a noise figure of 2.5 db have been obtained at 30 cps when a 200 ohm wirewound resistor is attached to the input terminals. This noise figure was measured by comparing the amplifier output power level when the 200 ohm resistor was at room temperature (295° K) and then at liquid nitrogen temperature (77° K).

Conventional techniques have been used in the design and construction of the phase-sensitive detector, which in principle of operation is similar to the unit described by Larsen (30). A block diagram of this unit is shown in Figure 12. Output voltage signals from the high gain 30 cycle amplifier have been time delayed by the amplifier and thus contain some phase shift relative to the original signal from the bolometer. An adjustable phase shifter is provided to compensate for this time delay. The corrected signal is then split into two parts of opposite phase to

drive a push-pull amplifier which is transformer coupled to the contacts of an electro-mechanical chopper relay. Since the coil of this relay is energized by a 30 cps signal from the photocell detector, the information bearing signal from the bolometer is demodulated and appears at the RC filtered output of the synchronous detector as a dc voltage which is proportional to the power received by the antenna. An offset bias is applied to the coupling transformer in the push-pull amplifier, thus preserving the sign of the phase between the bolometer detected signal and the photocell detected signal.

In radiometer detection, it is important to know if the energy received by the antenna and detected by the bolometer when the propeller chopper is in a space between two blades is smaller, equal to, or larger than the energy detected by the bolometer when a propeller blade is directly in front of the feedhorn. Preserving the phase sign in the synchronous detector is the technique which permits this to be accomplished. Thus if the synchronous detector voltage is less than the offset bias, the antenna is directed at an energy source which produces less signal than that from the chopper blade. An example of this is the zenith sky on a clear day.

Three output terminals are provided from the phase sensitive or synchronous detector, as shown in Figure 12. A zero centered direct reading meter is provided for quick reference during operational data collection. One output is provided for a Brush amplifier and pen-paper recorder which provides a graphical time presentation of the radiometer observations. The other output, which was used almost exclusively for data collection and analysis, is connected to a voltage-to-frequency

converter which is connected to a Universal frequency counter. Output from the Universal counter is recorded on paper tape by a digital printer. Minimum observation time with the radiometer is limited to one second by the RC filter on the output of the phase-sensitive detector. System integration time can be made either 1 second or 10 seconds by setting the counting scale on the Universal counter.

Gain stability of the 30 cps amplifier and synchronous detector is checked by an internally generated reference voltage, as shown in Figure 12. A portion of the phase reference signal generated by the photocell is amplified and hard clipped to produce a square wave which has the same frequency as the chopper wheel at the antenna. A calibrated 10 mv constant amplitude of the square wave is produced by applying this signal as a back biasing voltage on a Zener diode and using the voltage across the diode as the amplitude reference signal.

CHAPTER IV

THEORY OF MEASUREMENTS TECHNIQUE

Measuring the vertical atmospheric attenuation by placing a man-made transmitter outside of the earth's atmosphere and detecting the signal strength with a receiver on the earth's surface is not practical because of the high cost of locating such a transmitter in orbit and the large number of narrowband coherent sources required to cover wide regions of frequency. However, the sun offers a good source of electromagnetic energy over the entire radio spectrum, and the techniques of radio astronomy (31, 32, 33, 34, 35, 36) have been employed to determine the vertical atmospheric attenuation by measuring the energy from the sun as a function of the total path length through which the energy passes.

Power from Thermal Source

About 1900, Planck presented a radiation law relating the brightness, β, of a black body at a temperature, T, to frequency. The brightness is the amount of power arriving on a unit area, over a unit solid angle and in a given frequency interval; this can be stated as

$$\beta = \frac{2hf^3}{c^2} \frac{1}{e^{hf/kT} - 1}, \quad \text{in watts } m^{-2} \text{ rad}^{-2} \text{ cps}^{-1} \qquad (4.1)$$

where

h = Planck's constant (= 6.55×10^{-34} joule sec)

f = source frequency, cps

c = velocity of light

k = Boltzmann's constant (= 1.38 x 10^{-23} joules/deg K)

T = source temperature (deg K)

Assuming that the sun radiates as a thermal source (black body) at thousands of degrees Kelvin and that the observed frequency is in the region of a few hundred gigacycles or less, then $hf << kT$. The brightness, with this approximation, reduces to the Rayleigh-Jeans law of the form

$$\beta = \frac{2f^2 kT}{c^2} \tag{4.2}$$

For a source of random polarization, such as a thermal source, the power received by a radio telescope antenna is given by (36)

$$P = \frac{1}{2} \int \int A \cdot \beta \cdot d\Omega \cdot df \ , \quad \text{in watts} \tag{4.3}$$

where

A = effective antenna area in specified direction (m^2),

$d\Omega$ = element of solid angle from the antenna, and

df = frequency interval.

The effective antenna area, A, is related to the antenna gain, G, specified with respect to an isotropic antenna (36) by

$$A = \frac{c^2 G}{4\pi f^2}$$

Now by substitution

$$P = \frac{1}{2} \int \int \frac{c^2 G}{4\pi f^2} \cdot \frac{2f^2}{c^2} \cdot kT \cdot d\Omega \cdot df$$

$$= \frac{1}{4\pi} \int \int GkT \cdot d\Omega \cdot df \qquad (4.4)$$

It was shown that the angle subtended by the sun (0.56 degree) is approximately twice as large as the beamwidth of the antenna (0.29 degree) and that the brightness of the sun is independent of the beam position (see Figure 9). This is the case of an extended source where the temperature is constant in the region of solid angle, $d\Omega$, subtended by the antenna. If the antenna has a beamwidth less than the subtended angle of the sun and has low side lobes, so that radiation received from the earth is negligible and the integrated gain function, G, over the solid angle is 4π, then the received power becomes

$$P = k \int T df \qquad (4.5)$$

This equation is usually presented in the form

$$P = kT_a \int df \qquad (4.6)$$

where T_a is the effective black-body temperature of the extended source as seen by the antenna over the frequency region $\int df$. Since both the sun and the sky are extended sources for a narrow beam antenna, this equation applies when observing either one. The power received by a radiometer then is linearly related to the temperature of the source at which the antenna is pointed.

Atmospheric Attenuation Using Radiometer

Superheterodyne System

Coates (20) has presented a method for determining the atmospheric attenuation from measurements of effective sun and sky temperatures as a function of the zenith angle (air mass). He has shown that when the antenna is pointed at the sun, the effective temperature is given by

$$T_{sun} = t_{sun} \cdot \alpha \cdot \alpha_g + (1-\alpha) t_{sky} \cdot \alpha_g + (1-\alpha_g) t_g \tag{4.7}$$

and when the antenna is pointed at the sky, the effective temperature is given by

$$T_{sky} = (1-\alpha) t_{sky} \cdot \alpha_g + (1-\alpha_g) t_g \tag{4.8}$$

where

α_g = waveguide transmission,

α = atmospheric transmission,

t_{sun} = temperature of the sun,

t_{sky} = temperature of the sky, and

t_g = temperature of the waveguide.

If one assumes that the atmosphere is horizontally stratified in a homogeneous manner and that the zenith angle is less than 80 degrees, α can be expressed in terms of the zenith transmission, α_o, and the zenith angle, φ, by

$$\alpha = (\alpha_o)^{\sec \varphi} \tag{4.9}$$

Substituting this for α and taking the logarithm of the difference between T_{sun} and T_{sky}, one obtains

$$\log (T_{sun} - T_{sky}) = \sec \phi \log \alpha_o + \log \alpha_g t_{sun} \qquad (4.10)$$

The atmospheric attenuation at the zenith $(-10 \log \alpha_o)$ is obtained from the slope of a graph of $[\log(T_{sun} - T_{sky})]$ versus $[\sec \phi]$. This development assumes that the transmission coefficients are constant over the frequency interval of interest which is reasonable for the superheterodyne radiometer used by Coates. In the present wide band system the transmission coefficients are not constant over wide frequency intervals.

Wideband System

A direct-detection radiometer is a wide band system and thus the power detected is the integrated result of the received power over a wide range of frequencies. The bandpass of the radiometer used in this investigation is limited at its lower frequency boundary by the cut-off frequency characteristics of the waveguide filters and limited at the upper frequency boundary only by the bolometer detector. The frequency dependence of the waveguide filter transmission, α_g, has been discussed in Chapter III and the frequency dependence of the atmospheric transmission, α_o, has been discussed in Chapter II.

Following the approach used by Coates, but considering the dependence of the transmission coefficients on frequency, Equation (4.5) is written

$$P_{sun} = k \int T_{sun} \, df \qquad (4.11a)$$

and

$$P_{sky} = k \int T_{sky} \, df \qquad (4.11b)$$

Substituting Equations (4.7), (4.8), and (4.9) and taking the difference between (4.11a) and (4.11b) results in

$$P_{sun} - P_{sky} = kt_{sun} \int \alpha_g \alpha_o^{\sec \Phi} \, df \, . \tag{4.12}$$

In considering transmission of energy through a homogeneous lossy medium, where the transmission coefficient per unit length α_o is constant with frequency, the effective total transmission coefficient, α, is $(\alpha_o)^L$, for a path length L through the medium. When α_o is not constant, but varies with frequency, then a weighted or average value, $\overline{\alpha_o}$, of α_o may be obtained over a given bandwidth for a unit path length. However, $\overline{\alpha_o}$ is no longer constant per unit length as the path length, L, is varied, but decreases as the value of L increases.

Consider then, how to obtain the atmospheric attenuation by knowing the output voltage from a wide band direct-detection radiometer which employs high-pass waveguide filters when alternately observing the sun and the sky. Power received at the radiometer antenna is linearly converted to voltage by the square-law bolometer detector. This voltage is amplified and then detected by the synchronous detector. Thus, the voltage recorded on the digital printer is linearly related to the radiation power received by the antenna. For simplification, the relation between detected voltage and atmospheric attenuation will be considered for two filters that have cut-off frequencies f_{c_1} and f_{c_2} where

$$f_{c_1} < f_{c_2} < f_n \, ,$$

and the upper frequency limit of the detector response is f_n. Then for

filters No. 1 and No. 2, respectively, Equation (4.12) becomes

$$(V_{sun} - V_{sky})_1 = \frac{1}{K} \int_{f_{c_1}}^{f_n} \alpha_{g_1} \alpha_o^{\sec \Phi} \, df \tag{4.13a}$$

and

$$(V_{sun} - V_{sky})_2 = \frac{1}{K} \int_{f_{c_2}}^{f_n} \alpha_{g_2} \alpha_o^{\sec \Phi} \, df \tag{4.13b}$$

in which V_{sun} and V_{sky} are the measured detector output voltages and K is a constant. Now divide the bandwidths, $(f_n - f_{c_1})$ and $(f_n - f_{c_2})$, into small subintervals so that α_{g_1}, α_{g_2}, and α_o can be considered constant over the particular subinterval of interest; then

$$K(V_{sun} - V_{sky})_1 = \alpha_{g_{1a}} \alpha_{o_a}^{\sec \Phi} (f_a - f_{c_1}) + \alpha_{g_{1b}} \alpha_{o_b}^{\sec \Phi} (f_b - f_a) + \ldots + \alpha_{g_{1n}} \alpha_{o_n}^{\sec \Phi} (f_n - f_{n-1}) , \tag{4.14a}$$

and

$$K(V_{sun} - V_{sky})_2 = \alpha_{g_{2a}} \alpha_{o_a}^{\sec \Phi} (f_a - f_{c_1}) + \alpha_{g_{2b}} \alpha_{o_b}^{\sec \Phi} (f_b - f_a) + \ldots + \alpha_{g_{2n}} \alpha_{o_n}^{\sec \Phi} (f_n - f_{n-1}) \tag{4.14b}$$

Subtracting Equation (4.14b) from Equation (4.14a) and collecting terms in the same frequency range gives

$$K(V_{sun} - V_{sky})_1 - K(V_{sun} - V_{sky})_2 = \sum_{f_{c_1}}^{f_{c_2}} (f_x - f_{x-1})\, \alpha_{o_x}^{\sec \Phi} (\alpha_{g_1} - \alpha_{g_2})$$

$$+ \sum_{f_{c_2}}^{f_n} (f_y - f_{y-1})\, \alpha_o^{\sec \Phi}\, (\alpha_{g_1} - \alpha_{g_2}) \qquad (4.15)$$

In the frequency region between f_{c_1} and f_{c_2}, $\alpha_{g_2} << \alpha_{g_1}$, thus we may write $K(V_{sun} - V_{sky})_1 - K(V_{sun} - V_{sky})_2$

$$= \sum_{f_{c_1}}^{f_{c_2}} (f_x - f_{x-1}) \alpha_{o_x}^{\sec \Phi}\, \alpha_{g_{1x}} + \sum_{f_{c_2}}^{f_n} (f_y - f_{y-1}) \alpha_{o_y}^{\sec \Phi} (\alpha_{g_1} - \alpha_{g_2}) \qquad (4.16)$$

In the frequency region above f_{c_2}, the difference in waveguide transmission $(\alpha_{g_1} - \alpha_{g_2})$ is small enough that the term $\sum_{f_{c_2}}^{f_n}$ can be neglected and the equation can be further reduced. To a first order approximation, the difference in voltage can be represented by the equation

$$(V_{sun} - V_{sky})_1 - (V_{sun} - V_{sky})_2 = \frac{1}{K} (f_{c_2} - f_{c_1})\, \bar{\alpha}_o^{\sec \Phi}\, \bar{\alpha}_{g_1} \qquad (4.17)$$

where $\bar{\alpha}_o$ and $\bar{\alpha}_{g_1}$ are the weighted average values of atmospheric transmission and waveguide transmission, respectively, in the frequency pass band between cut-off filters No. 1 and No. 2. It is to be noted here

that the frequency dependence of the radiometer, excluding the waveguide filters, needs to be constant only over the frequency region f_{c_1} to f_{c_2}. Over the rest of the frequency range, any nonlinearity occurring in the system for filter No. 1 also occurs for filter No. 2 and the contribution to the difference in the response is negligible.

Taking logarithms of both sides of Equation (4.17) gives

$$\log \left[(V_{sun} - V_{sky})_1 - (V_{sun} - V_{sky})_2 \right] = \sec \varphi \log \bar{\alpha}_o + \log \frac{\bar{\alpha}_{g_1}}{K} (f_{c_2} - f_{c_1}) \qquad (4.18)$$

Thus weighted atmospheric attenuation at the zenith ($-10 \log \bar{\alpha}_o$) is obtained from the slope of a graph of the logarithm of the voltage difference versus sec φ.

Average Attenuation Over Wide Bands

In order to anticipate the general type of relationship between detected power and secant zenith angle which would result from using a wide band radiometer, the integral in Equation (4.12) has been numerically evaluated with the use of a Burroughs 220 digital computer. As was discussed in Chapter II, atmospheric transmission is a function of the assumed linewidth parameters for oxygen and for water vapor as well as the temperature, pressure, and humidity of the atmosphere. Values of α_o were calculated from Figure 5 of Chapter II for the attenuation values presented by Schmelzer and by Theissing and Caplan (medium humidity). The values of α_g were obtained from Figure 10 in Chapter III for each of the ten filters. For ease of calculation, the maximum value of attenuation

was limited to 50 db for each filter and atmosphere, and the frequency band was limited to the region between 40 and 200 gc/s. Intervals of 0.5 air mass were used in each case for (sec ϕ) values from 1.0 to 6.0. The results of these calculations are shown in Table 1. A maximum value of 160 would be obtained for lossless atmospheric and waveguide transmission. The fractional power passed by each filter between 40 and 200 gc/s can be obtained by dividing each table entry by 160.

In this approach, it has been assumed that the radiometer, except for the waveguide filters, has a constant frequency response from 40 to 200 gc/s. This is not strictly true, for it is known that the power response of a bolometer in its holder is frequency dependent. However, as discussed previously, this is not a serious limitation when reasonably small frequency intervals are considered.

The Burroughs 220 computer was also used to obtain the weighted or average atmospheric attenuation per air mass, $\bar{\alpha}_o$, as a function of air mass in 0.5 air mass intervals from 1.0 to 6.0, from the values presented in Table 1. Results of these computations are shown in Table 2. Several conclusions can be drawn from these calculations for a wide band detector. The atmospheric attenuation per air mass remains reasonably constant when the change of atmospheric attenuation over the bandwidth considered is reasonably constant, as expected. Also the attenuation per air mass has the largest change, as a function of air mass, over those frequency bands where the atmospheric attenuation itself has the greatest variation, as expected. Another conclusion to be drawn from these calculations is that the attenuation per air mass always decreases as the number of air masses increases. This can be understood when one considers

TABLE 1. VALUES OF $\int_{40}^{200} \alpha_g \alpha_o^{L} \, df$, IN GC/S, FOR EACH FILTER

FILTER		AIR MASS (L)										
		1.0	1.5	2.0	2.5	3.0	3.5	4.0	4.5	5.0	5.5	6.0
1	SCHMELZER	44.7003	34.2312	27.4614	22.6587	19.0592	16.2618	14.0309	12.2168	10.7189	9.4667	8.4088
2		36.8321	26.9179	20.6506	16.3062	13.1269	10.7158	8.8409	7.3555	6.1615	5.1908	4.3940
3		34.7153	25.5062	19.6480	15.5673	12.5698	10.2895	8.5113	7.0986	5.9601	5.0319	4.2681
4		33.2853	24.5147	18.9473	15.0661	12.2070	10.0235	8.3136	6.9495	5.8460	4.9433	4.1984
5		29.8737	21.7638	16.7226	13.2624	10.7416	8.8307	7.3409	6.1550	5.1961	4.4109	3.7615
6		29.2299	21.3535	16.4342	13.0449	10.5681	8.6865	7.2172	6.0465	5.0993	4.3238	3.6826
7		15.9534	9.9327	6.5836	4.5329	3.2024	2.3049	1.6825	1.2418	.9247	.6936	.5235
8		8.0841	4.0583	2.1808	1.2217	.7042	.4146	.2481	.1504	.0922	.0570	.0356
9		4.2694	1.7915	.8115	.3847	.1880	.0939	.0477	.0245	.0127	.0066	.0035
10		1.5269	.5363	.2163	.0944	.0433	.0205	.0099	.0049	.0024	.0012	.0006
1	THEISSING & CAPLAN (MEDIUM HUMIDITY)	74.7998	61.2472	51.2210	43.4653	37.2782	32.2298	28.0397	24.5161	21.5221	18.9573	16.7453
2		67.3273	54.4993	45.1180	37.9390	32.2692	27.6856	23.9142	20.7680	18.1149	15.8581	13.9247
3		64.2330	52.3109	43.5330	36.7665	31.3857	27.0097	23.3903	20.3576	17.7905	15.5997	13.7176
4		63.2303	51.6985	43.1355	36.4919	31.1847	26.8550	23.2666	20.2559	17.7051	15.5270	13.6552
5		60.9123	50.1361	42.0665	35.7488	30.6595	26.4774	22.9902	20.0499	17.5487	15.4061	13.5600
6		58.6917	48.2196	40.3909	34.2750	29.3594	25.3287	21.9743	19.1508	16.7526	14.7008	12.9347
7		45.8054	37.3188	31.1212	26.3568	22.5688	19.4844	16.9284	14.7817	12.9598	11.4005	10.0569
8		35.2242	28.1726	23.1885	19.4575	16.5535	14.2285	12.3271	10.7463	9.4147	8.2815	7.3089
9		32.6649	26.4957	22.0224	18.6130	15.9223	13.7442	11.9469	10.4418	9.1666	8.0763	7.1369
10		22.3074	17.6894	14.4391	12.0259	10.1646	8.6874	7.4891	6.5002	5.6728	4.9728	4.3753

NOTE: FRACTIONAL TRANSMISSION IS OBTAINED BY DIVIDING TABULATED VALUE BY 160 GC/S

TABLE 2. ATTENUATION FOR BAND BETWEEN FILTERS IN DB/AIR MASS

FILTER		AIR MASS (L)									
		1.0	1.5	2.0	2.5	3.0	3.5	4.0	4.5	5.0	5.5	6.0
1–2	SCHMELZER	.635	.618	.605	.594	.584	.576	.568	.560	.553	.547	
2–3		3.518	2.973	2.649	2.453	2.325	2.234	2.165	2.108	2.060	2.018	
3–4		3.180	3.015	2.911	2.806	2.695	2.575	2.452	2.326	2.201	2.079	
3–5		2.236	2.139	2.071	2.012	1.960	1.913	1.871	1.833	1.800	1.769	
4–5		1.869	1.843	1.822	1.804	1.787	1.772	1.757	1.744	1.731	1.719	
6–7		1.307	1.284	1.268	1.256	1.245	1.236	1.228	1.220	1.213	1.207	
7–8		2.539	2.504	2.474	2.447	2.421	2.397	2.374	2.351	2.330	2.309	
7–9		3.138	2.987	2.869	2.773	2.692	2.622	2.561	2.508	2.460	2.418	
8–9		4.520	4.378	4.276	4.197	4.134	4.081	4.036	3.996	3.960	3.928	
9–10		6.788	6.479	6.236	6.045	5.896	5.778	5.686	5.612	5.552	5.503	
1–2	THEISSING & CAPLAN (MEDIUM HUMIDITY)	.885	.872	.862	.853	.846	.839	.833	.828	.822	.818	
2–3		3.008	2.801	2.618	2.459	2.324	2.212	2.119	2.042	1.977	1.921	
3–4		4.283	3.754	3.212	2.706	2.277	1.943	1.697	1.523	1.402	1.317	
3–5		3.676	3.422	3.173	2.931	2.698	2.480	2.278	2.095	1.932	1.788	
4–5		3.426	3.295	3.158	3.015	2.865	2.710	2.551	2.392	2.235	2.083	
6–7		1.453	1.407	1.368	1.334	1.303	1.275	1.251	1.228	1.208	1.189	
7–8		1.265	1.236	1.212	1.191	1.172	1.155	1.139	1.125	1.112	1.099	
7–9		1.685	1.507	1.400	1.327	1.273	1.231	1.197	1.169	1.146	1.126	
8–9		3.672	3.155	2.803	2.528	2.299	2.102	1.930	1.779	1.647	1.534	
9–10		1.409	1.298	1.223	1.168	1.127	1.095	1.068	1.047	1.029	1.013	

a wide frequency region which has two subregions of equal width, but different values of attenuation per air mass--for example, 10 db and 1 db. At one air mass, the higher attenuation region passes about 11 percent of the total power received over the two regions together; at two air masses, 1.6 percent; at three air masses, 0.2 percent; and at four air masses, 0.03 percent. Thus it is that as the number of air masses increases, the high attenuation region becomes less and less transparent, passing a smaller percentage of the total power with the result that the effective attenuation per air mass decreases. For the example considered, the limiting value which the effective attenuation per air mass will approach is twice the value of the lower loss region measured at unity air mass.

CHAPTER V

EXPERIMENTAL PROCEDURE

General

The radiometer described in Chapter III was installed on the roof of the Hinman Research Building at Georgia Tech during the month of August, 1961 and data were collected from this location for several months thereafter. With the arrival of cold weather in December, 1961, it became apparent that this location was not adequate for several reasons. The surrounding buildings are higher than the antenna and with the sun at a lower angle in the sky, observations of the sun were restricted to morning and early afternoon periods. The temporary structure housing the amplifier, recorders, and vacuum pump was unheated, creating operational instability in these units. Finally, the primary electrical distribution sub-station for the campus was located about 100 feet from the antenna and high voltage transmission lines were only 30 feet away. With cooler weather, an increase in electrical power resulted and a higher noise level from the sub-station and transmission lines was observed.

After the Van Leer Electrical Engineering building was completed on the Georgia Tech campus, a more suitable location was available. The radiometer was moved to this building in 1962. As can be seen in Figure 7, the antenna is located on a platform approximately 3 feet above the roof level, which provides a sturdy mount that is dry and above the surrounding buildings. From this location it is possible to observe the

sun from near the horizon to the zenith for any day of the year, morning or afternoon. The amplifier, recorders, vacuum pump, and auxiliary equipment, shown in Figure 8, are located inside the building, in an air conditioned laboratory having ample work space. Data were collected from this location during the fall, winter, and spring months of 1962-63.

Weather conditions were a prevailing factor during this investigation, and limited the available days for observing the sun. As discussed in the preceding chapters, this investigation's objective was to determine the total atmospheric attenuation for clear days. It soon became obvious that if this condition was to be rigorously adhered to, then a daily surveillance of the local weather forecasts was required. Cloudy and rainy days were relatively consistent with forecasting and these days could be avoided, but ground fog is more of a local condition and personal observation had to be made at the time. Many cloudless days were not suitable because of the local ground fog conditions. Moderate winds offered another local weather condition which limited data collection. When the wind speed exceeded about 15 mph, excessive noise was observed in the recorded output of the radiometer, primarily because mechanical vibration of the bolometer detector created excessive noise, and secondarily, because movement of the antenna and waveguide feed horn reduced tracking accuracy of the antenna.

On clear days suitable for operating the radiometer, a frequency region either from 40 to 74 gc/s or from 72 to 138 gc/s was used. This corresponded to using Filters No. 1 through 5, which are in RG-98 waveguide or using the double linear tapers and Filters No. 6 through 10 in RG-138 waveguide. The system was turned on approximately 1 hour prior to

collecting data, which allowed adequate time for the amplifiers and recorders to become electrically stable and for a low pressure to be obtained in the evacuated bolometer chamber. Before recording data, the radiometer was checked for gain stability of the amplifiers, synchronous detector, and recorders by applying the 10 mv reference signal to the 30 cps amplifier and recording the output voltage for 10 minutes. Operation was considered normal when this portion of the system had a gain deviation of less than 0.5 percent. If the gain of the system was stable, then the synchronous detector was adjusted for proper phase alignment between the photo cell and the bolometer detector output. A lighted cigarette was placed in front of the antenna feed horn and the photo cell was phase positioned until the output voltage from the synchronous detector was a series of half-sine waves having deep nulls, as shown in Figure 6. The voltage-to-frequency convertor was adjusted for zero voltage balance and proper level conversion as specified by the manufacturer. The dc offset bias in the output of the synchronous detector was recorded and considered stable when deviations were less than 0.1 percent.

Operating experience with the system has shown that signals from the sun will cause voltage saturation in the 30 cps amplifier and synchronous detector unless attenuation is used in the 30 cps amplifier. When operation in the frequency range of 40 to 74 gc/s (Filters No. 1 through 5), an attenuator value of 20 db is satisfactory and was used for all data collected in this frequency region. In the higher frequency region of 72 to 138 gc/s (Filters No. 6 through 10), an attenuator value of 10 db was used. More gain is required at the higher frequencies because less power is available at the bolometer as a result of the smaller bandwidth

in the microwave section of the system. A value of 50 db attenuation is required when the 10 mv reference signal is used for checking gain stability of the system.

Radiometer Operation

Signal strength levels from the sun and sky were recorded in half day intervals to obtain data as a function of frequency and number of air masses. The sun was tracked through the optical telescope, which is attached to the radiometer, while manually positioning the radiometer. Assuming that Filters No. 1 through 5 are used, then data recorded on 24 March 1963 can be used as an example of the procedure. Filter No. 5 is installed in the waveguide section, and the sun is tracked for five 10 second periods and the average signal level recorded for each 10 second period. The zenith angle is also recorded. Then the radiometer is moved off the sun in azimuth and the sky level recorded for each of five 10 second periods at the same zenith angle. Filter No. 5 is removed and replaced by Filter No. 4 and the tracking and recording procedures repeated. This procedure is repeated with Filters Nos. 3, 2, and 1, and again for No. 5, etc. The process is continued, changing filters, recording sun and sky signal levels at continuingly increasing zenith angles until the trees obstruct the viewing angle at approximately 75 degrees from the vertical. Several times during the afternoon, the gain of the amplifier is checked by applying the 10 mv reference signal, and the dc offset is recorded to reference the "no input" signal level.

The voltage outputs as recorded on the digital printer are transferred to IBM cards along with the appropriate zenith angle for data

processing by a Burroughs 220 Computer. Figure 13 is a photograph of the first input card for the afternoon of 24 March 1963. A zenith angle is used to indicate where the sun is located while the 10 mv reference signal and the dc bias offset signal are recorded. Figure 14 is a photograph of the IBM card containing the signal strength of the sun and the sky as recorded for Filter No. 5 at a zenith angle of 33.5 degrees. Since the zenith angle is different for each filter and thus each card, it can also be used as a reference for proper sequential order of all cards for this set of data. Figure 15 is a photograph of the IBM card containing values of sun and sky signals for Filter No. 1 at a zenith angle of 74.9 degrees. Figure 16 is a photograph of the IBM card containing signal level for the 10 mv reference input and the dc bias offset at the completion of operation on 24 March 1963. Instead of the day of the month, a 99 is listed on this card to signify it is the last card for this set of data.

For each set of five numbers, representing either sun, sky, reference level, or dc bias, the mean value and standard deviation are computed. Also the secant of the zenith angle is computed for the angle value listed on each card. These computed values are fed into an X-Y plotter and a graph is made of the recorded signal strength of the sun and the sky for each filter, the 10 mv reference, and dc bias as a function of secant zenith angle. The resulting graph for data recorded on 24 March 1963 is shown in Figure 17. Each dot represents the average of a 50 second observation and each bar represents twice the standard deviation for this same observation period.

In addition to the digital output, the signal levels were recorded

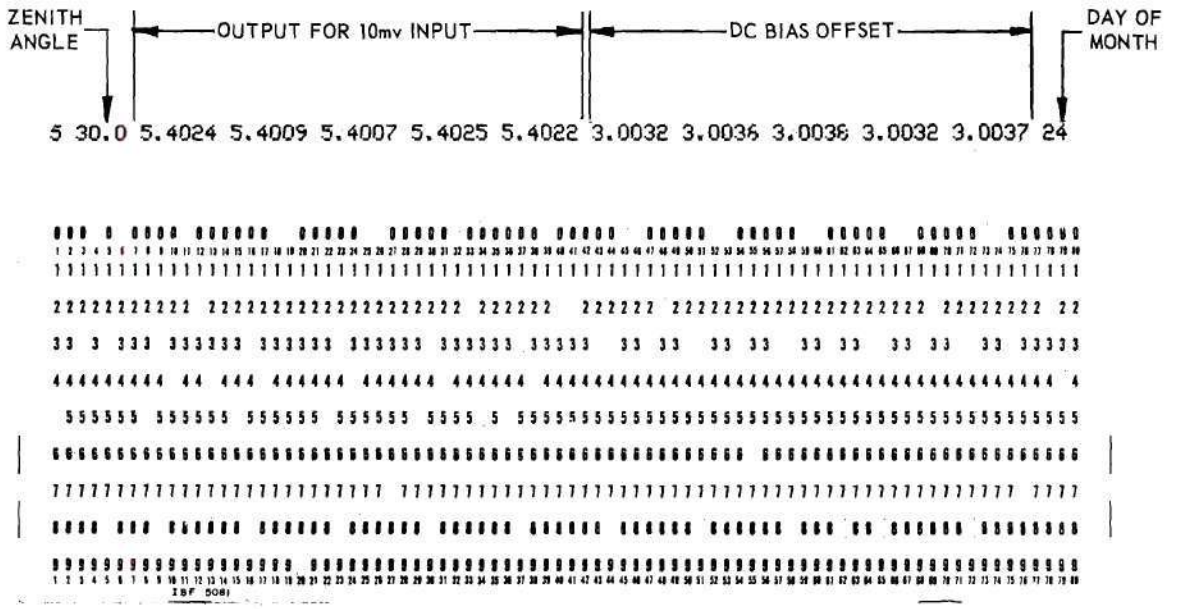

Figure 13. IBM Card Containing Reference and Offset Values.

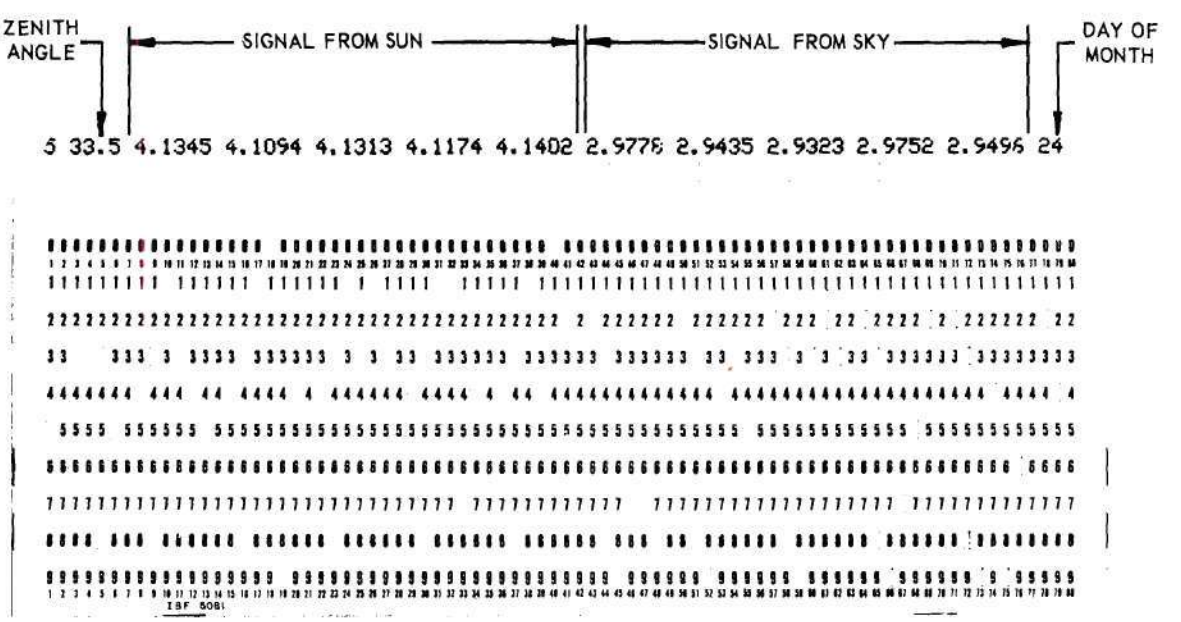

Figure 14. IBM Card Showing Filter No. 5 Data.

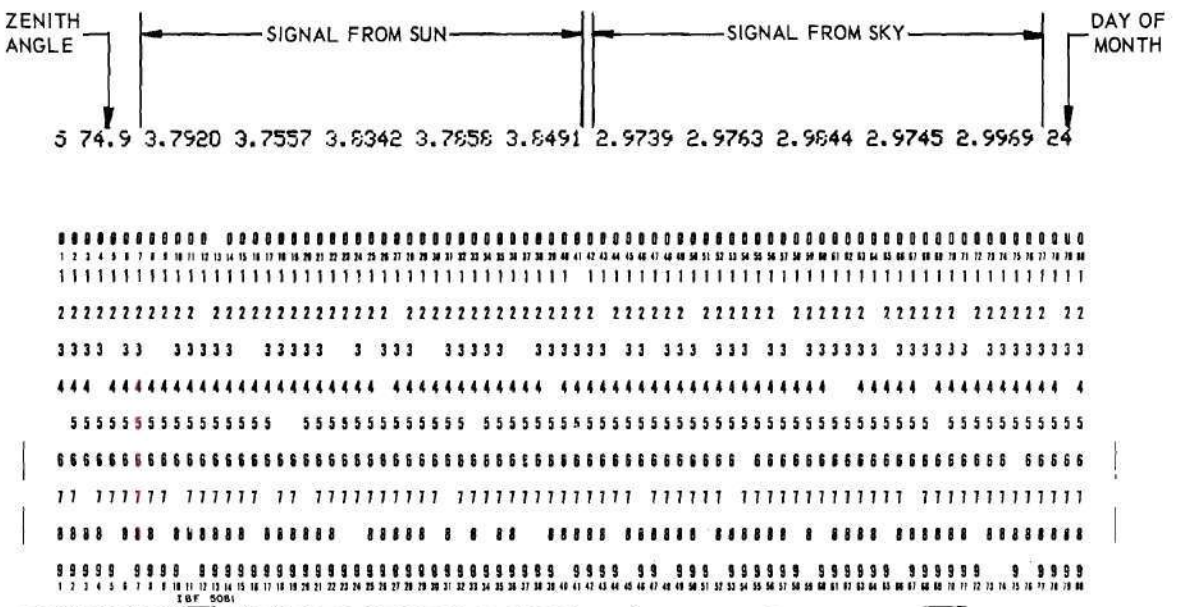

Figure 15. IBM Card Showing Filter No. 1 Data.

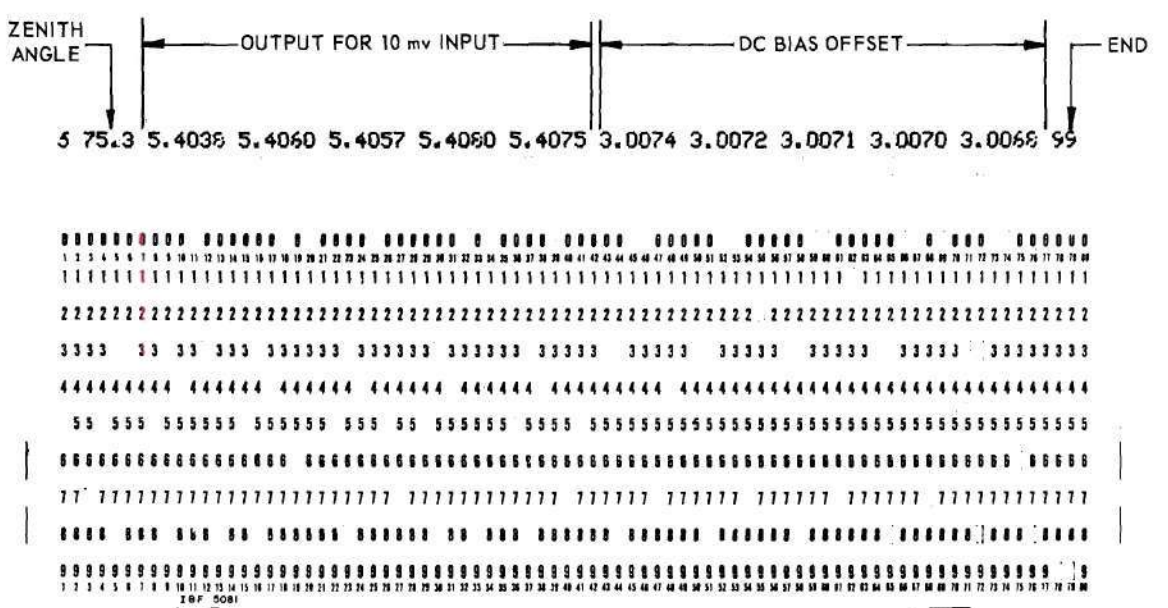

Figure 16. IBM Card Containing Final Data for March 24, 1963.

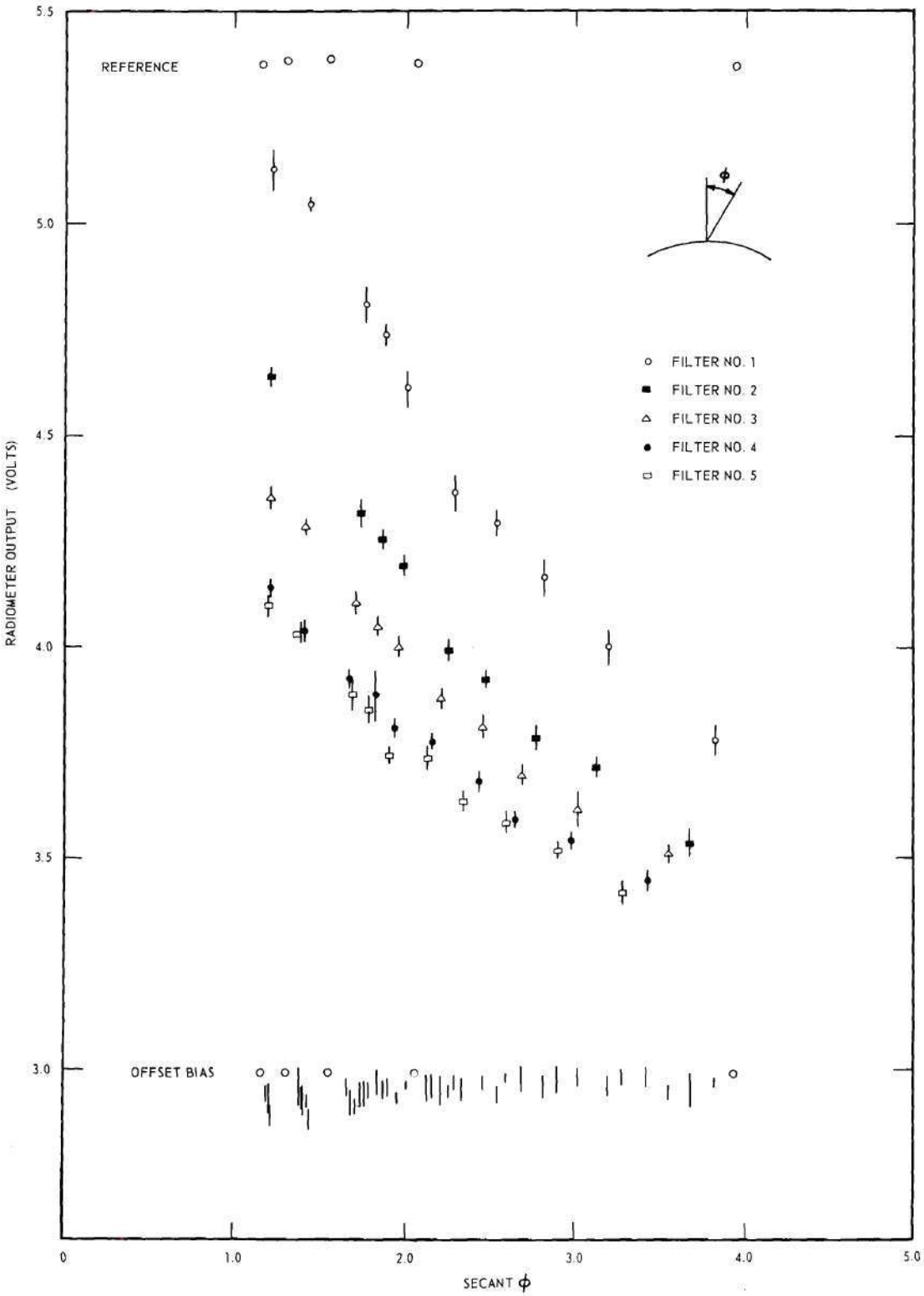

Figure 17. Sun and Sky Recordings for March 24, 1963.

on a Brush pen-paper recorder. This graphical output permitted a quick visual check to insure that no large extraneous signals occurred during any 10 second recording period with the digital printer. The integration time for the system using the Brush is approximately one second. Figure 18 shows the signal levels for Filters No. 1 through 5 at the beginning of data collection (zenith angles 33 to 35 degrees) and at the end (zenith angles 72 to 75 degrees) of the afternoon of 24 March 1963. These were recorded at the same time as the digital data presented on IBM cards in Figure 14 and 15.

These data obtained with the radiometer are processed to determine the total vertical atmospheric attenuation for the frequency regions specified by the cut-off frequencies of the waveguide filters. Again it is appropriate to discuss the procedure employed in this operation by using an actual set of recorded data as an example. The data presented in Figure 17 for 24 March 1963 are used for the following discussion.

System operation is restricted to one filter at a time. Since the sun is continuously changing position in the sky, each filter observation is at a different zenith angle and the recorded signal levels can not be subtracted directly to obtain the effective received signal over the frequency band defined by the two filters employed. Thus, a set of curves is drawn which best fit the collected data and from which the total vertical attenuation is calculated. First consider the dc bias offset and the 10 mv reference signals. They appear to be reasonably straight lines and show that the system was stable during the period of data collection. The sky data are considered next. The average value of the sky signal for any filter is sufficiently close to the average value for any

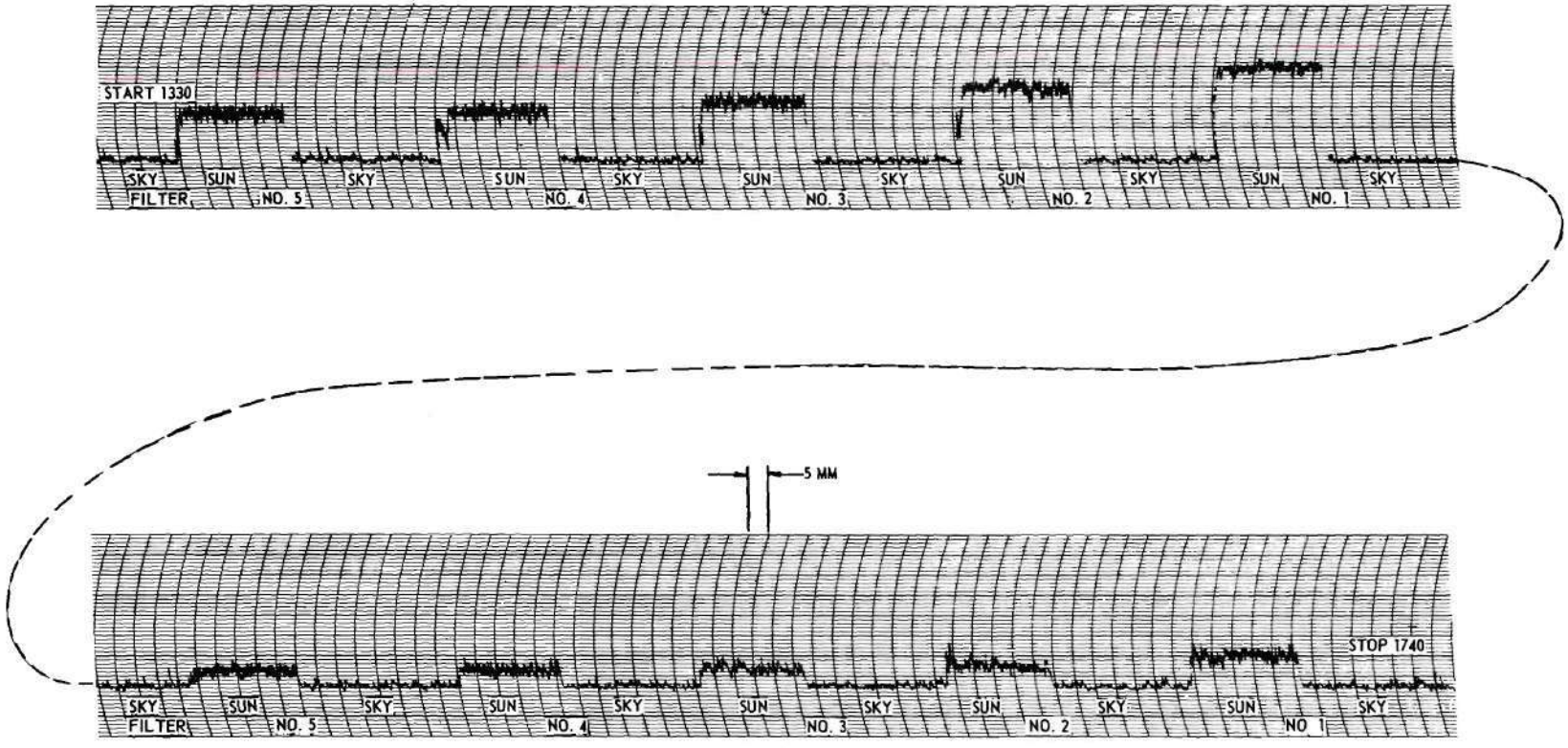

Figure 18. Photograph of Sample Brush Recording.

other filter and the standard deviations are sufficiently large that it is not possible to distinguish between filters over values of secant φ between 1 and 4. Although the sky signals are further below the dc bias near vertical zenith (secant φ = 1.0) than near horizontal (secant φ = 4), the sky signals from all the filters are essentially the same at any zenith angle. Thus there is no measurable difference in signal level when the antenna is pointed at the sky for Filters No. 1 through 5. The general shape of the average curve drawn from the sky signals is reasonable and expected. When the antenna is directed toward the zenith, most of the signal received comes from the atmosphere, which is at a lower average temperature than the chopper wheel and thus a signal appreciably below that of the dc offset is recorded. As the antenna is directed more toward the horizontal, it receives signals from more of the atmosphere which is closer to the earth and at a higher temperature which is closer to that of the chopper wheel. Thus a smaller signal difference is recorded between the dc offset and the sky.

Determining Atmospheric Attenuation

Before presenting the final procedure adopted to determine atmospheric attenuation from the data collected, a justification for using secant of zenith angle instead of air mass in the data reduction is presented. When using ALGOL programming in the Burroughs 220, the secant φ for various values of φ is accomplished very rapidly and accurately by using an established series approximation program. This is a "standard" program under this system, and thus requires no additional effort to the basic data reduction related to this investigation. The other possible

choices were either to solve the geometrical equation for air mass as a function of zenith angle or to store the table of such calculations which are presented in Handbuch Der Astrophysik (37). Both of these approaches would require more computer time and effort and would result in less than 3 percent change for the zenith angles encountered. Below are a few values for comparison:

Zenith angle (φ)	Secant φ	Air Mass
30	1.155	1.154
45	1.414	1.413
60	2.000	1.995
75	3.864	3.816
80	5.759	5.600

Having determined that the signals from the sky are essentially the same for all filters and that the secant of the zenith angle is essentially the same as air mass, the total atmospheric attenuation per air mass can be determined from the signal levels recorded for the sun as a function of secant zenith angle. The procedure for this evaluation is as follows:

1. Estimate two exponential curves, each passing through the data points from two adjacent filters.

2. At some value of sec φ, calculate the logarithm of the difference between the curves.

3. Move to a larger value of sec φ and again calculate the logarithm of the difference between the curves.

4. Compute the attenuation per air mass from the equation

$$\Gamma = -10 \frac{\log [V_{sun_1} - V_{sun_2}]_{A_1} - \log [V_{sun_1} - V_{sun_2}]_{A_2}}{A_1 - A_2} \text{ in db/air mass,}$$

where

V_{sun_1} = voltage from sun for Filter No. 1,

V_{sun_2} = voltage from sun for Filter No. 2,

A_1 = value of sec φ at position one, and

A_2 = value of sec φ at position two.

5. Repeat steps 2, 3, and 4 at different values of sec φ to establish the relative slopes of the two estimated curves to give a nonincreasing value of Γ as A is increased.

This is the first estimate of 1) the attenuation per air mass and of 2) the exponential curves which fit the data points. Now from a table of logarithm of differences as a function of air mass for a given attenuation value, construct a new set of exponential curves which have a better fit to the data points. Repeat this estimating process by choosing new values of attenuation per air mass and/or by assuming new values of voltage differences until the best set of curves is obtained for all the data points related to the two filters.

Having established these two curves, then the voltage curve for the next adjacent filter must be estimated in the same manner by assuming values of voltage difference and attenuation per air mass relative to one of the established curves and continuing in the same manner until the third exponential curve is obtained which is a good fit to the data points for the third filter. Repeating this process for the data points of the fourth and fifth filters yields the exponential curves for these

data. Since this procedure makes the third, fourth, and fifth curves depend upon the first two curves, it is necessary to reestimate the curves for the first two filters until the data points for all five filters are simultaneously the best fit for the appropriate exponential curves and calculated attenuation per air mass.

For example, this requires for the afternoon of 24 March 1963 that the attenuation in the region from 40 to 49 gc/s be 1.0 db/air mass; from 49 to 59 gc/s be 1.8 db/air mass; from 59 to 69 gc/s be 2.0 db/air mass; and from 69 to 74 gc/s be 0.8 db/air mass. Although a 1 db variation could exist in values which would estimate the attenuation in the frequency band between any two adjacent filters, when data for all five filters are satisfied simultaneously there is little room for adjusting the curves for any two filters. It is estimated that the value of atmospheric attenuation, in decibels per air mass, has an error of less than 1/4 db by this requirement of simultaneously fitting five curves.

Curves fitted to the data of the afternoon of 24 March 1963 are shown in Figure 19.

Water Vapor Content

Radiosonde measurements made by the U. S. Weather Bureau provide the only daily source of information about the lower atmosphere from which the water vapor content can be determined. A radiosonde system consists of a ground station recording system, and an electronic transmitter which is lifted by a helium filled balloon. The transmitting equipment contains an aneroid capsule for measuring pressure, a chemically treated element for measuring humidity, and a temperature sensitive resistance

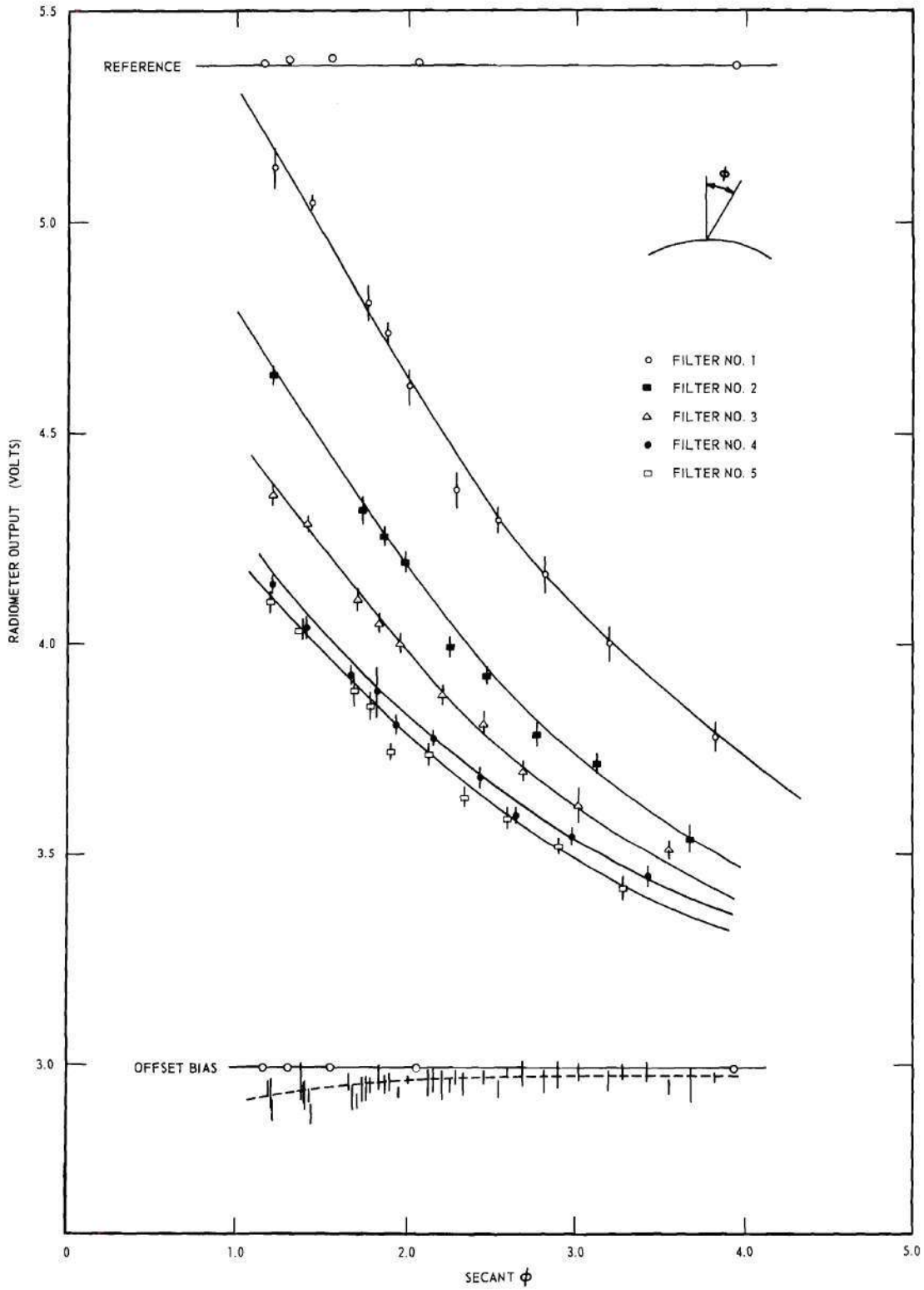

Figure 19. Atmospheric Attenuation from Data for March 24, 1963.

element. Electronics equipment in the airborne system are used to detect variations in these meteorologically sensitive elements and to transmit a signal to the ground station which gives the temperature, pressure, and relative humidity as the balloon ascends. The closest radiosonde stations to the Atlanta area are at Montgomery, Alabama, and Athens, Georgia; no such measurements are made in the Atlanta Area because of the extremely heavy aircraft traffic. Each station makes two observations daily, one beginning at 0000 hours and one beginning at 1200 hours Greenwich Standard Time. Radiosonde data for the two stations were obtained from the National Weather Records Center in Asheville, North Carolina, for each day corresponding to recordings made with the radiometer.

From the geographical locations of Montgomery, Athens, and Atlanta, it is reasonable to assume that when the two reporting stations observe the same water vapor content in the atmosphere then the atmosphere is homogeneous between the two stations, and thus the Atlanta area should have about this same amount of water vapor.

The water vapor density in the atmosphere was calculated for each altitude where radiosonde data were available, using the following equation which was developed by Goff and Gratch (38),

$$Q = (2.1668)\,\frac{W}{T}\,10\,\exp\left\{-7.9028\,\left(\frac{373.2}{T} - 1.0\right) + 5.02808\,\log\left(\frac{373.2}{T}\right) - 1.3816 \times 10^{-7}\left[10\,\exp 11.344\left(1.0 - \frac{T}{373.2}\right) - 1.0\right] + 8.1328 \times 10^{-3}\cdot \left[10\,\exp\left(-3.49149\right)\left(\frac{373.2}{T} - 1.0\right)\right] - 1.0 + \log 1013.246\right\} \text{ in } gm/m^3 ,$$

where

Q = water vapor density,

T = observed temperature in °K, and

W = observed relative humidity in percent.

A graph of the results of these computations gives a profile of the moisture content in the atmosphere from ground level to approximately 9600 meters above the recording station. In order to obtain a common denominator, for comparing daily conditions, the total water vapor in grams per square centimeter was computed from each profile record to obtain the integrated water vapor which existed in a column one square centimeter in cross section from ground level to 9600 meters. The water vapor values are discussed in the next chapter.

Values of temperature, pressure, relative humidity, and water vapor density as a function of altitude for 24 March 1963 are present in Figure 20. Examples of the water vapor density profile with altitude existing when measurements were made with the radiometer in 1963 are shown in Figure 21. Also, the total moisture content in a column 1 centimeter square for each calculated profile is given. For reference purposes, the water vapor density profile and the total moisture content were computed for the Standard International Atmosphere as used by Hogg (14); the ARDC Model Atmosphere as used by Schmelzer (7), and the "medium" atmosphere used by Theissing and Caplan (8).

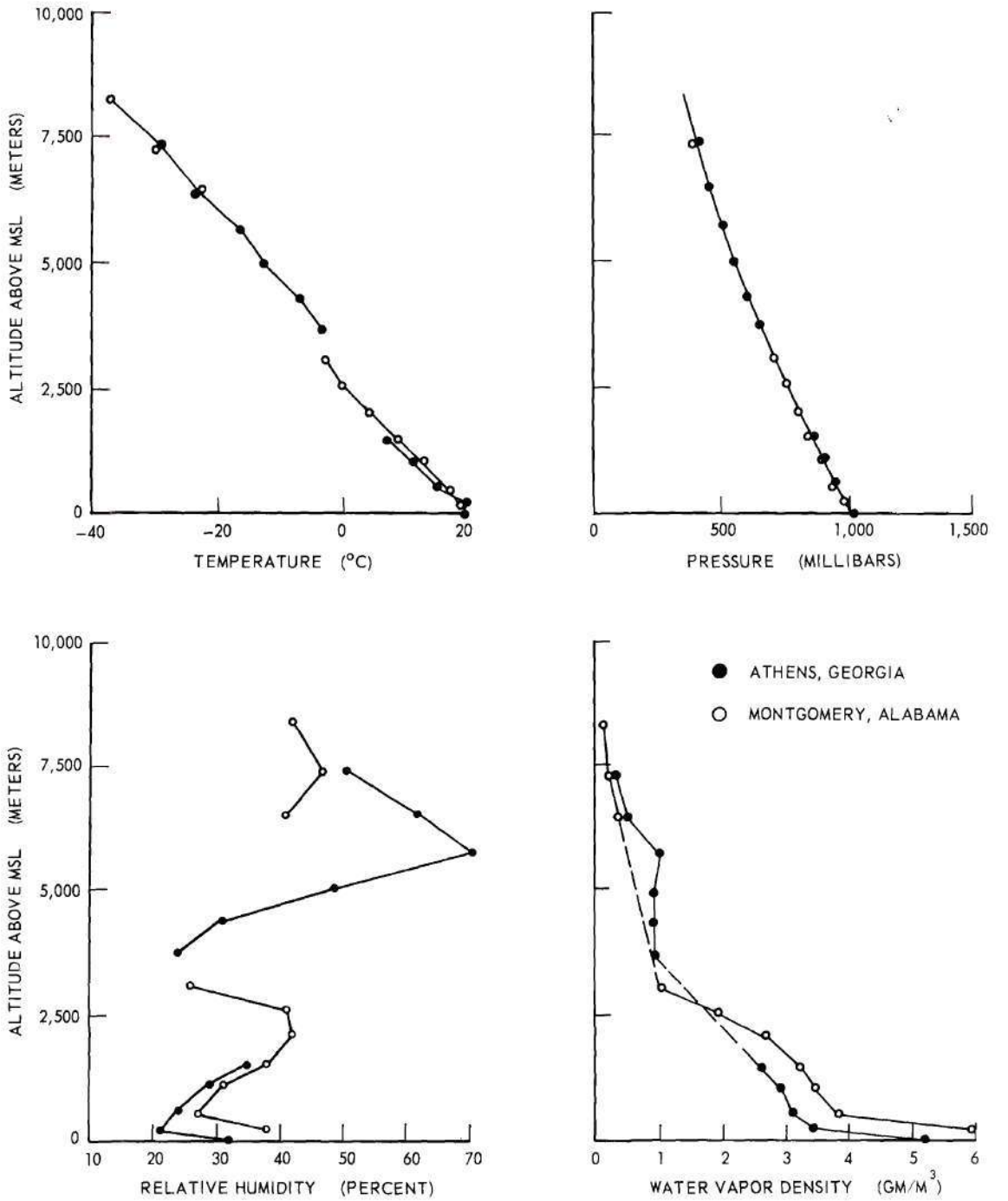

Figure 20. Meteorological Conditions for Afternoon of March 24, 1963.

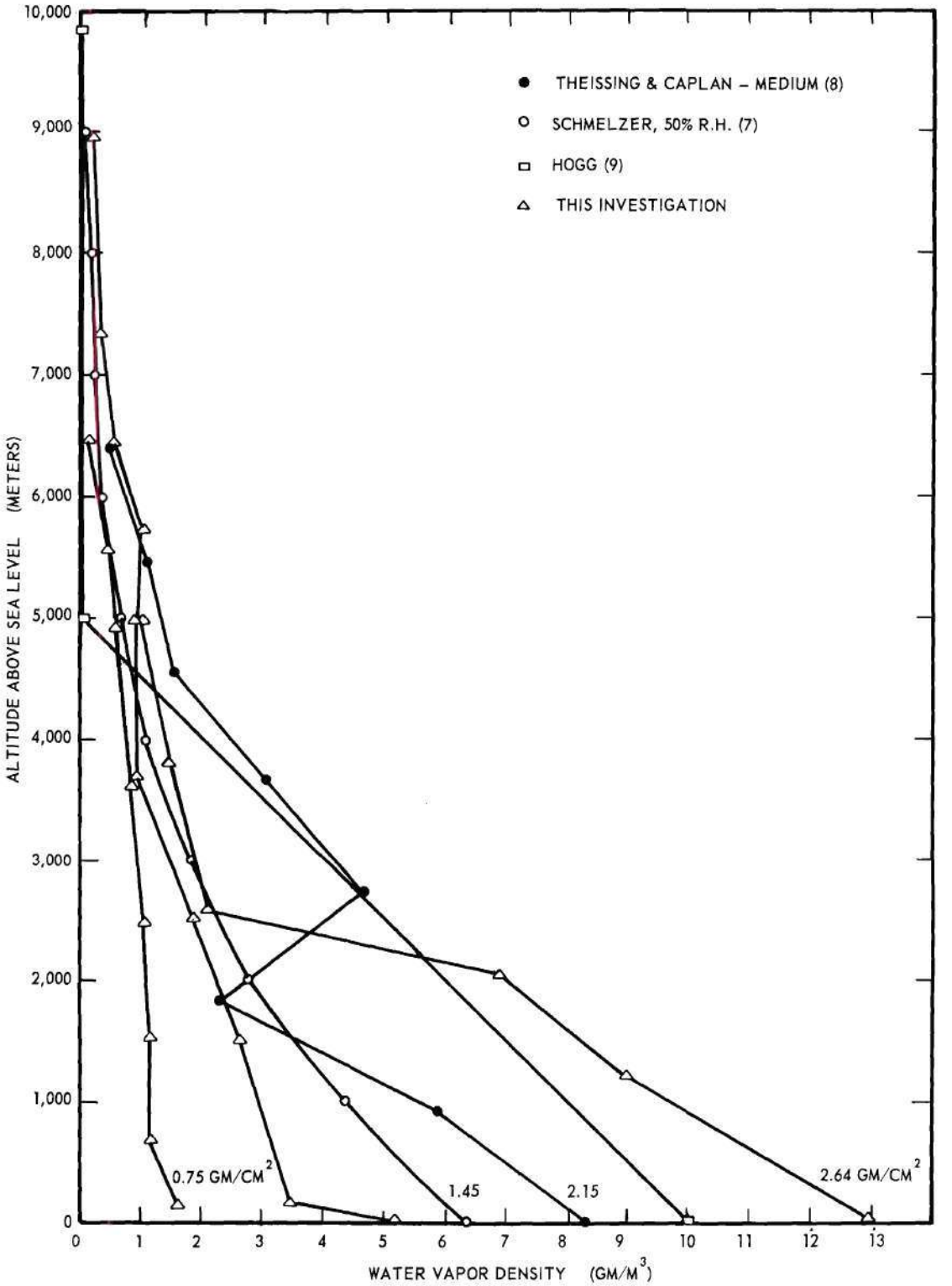

Figure 21. Sample Water Vapor Density Profiles.

CHAPTER VI

DISCUSSION OF EXPERIMENTAL DATA

The waveguide filters used in the direct-detection radiometer have characteristic cut-off frequencies which are sufficiently separated that the atmospheric attenuation is not constant over the frequency band between two filters. Methods are presented in the following paragraph for determining the effective center frequency of each frequency band which was investigated. Having established such effective frequencies, comparisons of the data collected during this investigation with previous investigations are made at discrete frequencies in the electromagnetic spectrum from 40 to 140 gc/s.

Calculation of Frequency Bands

As discussed in Chapter IV, the average attenuation per air mass (See Table 2) was calculated by the author for each frequency band delimited by two waveguide filters. These calculations convert an attenuation function which is continuous with frequency to a discontinuous function which takes on the computed average value for each frequency band. For any frequency band, the effective center frequency of the band is defined as that frequency at which the attenuation value of the continuous function is equal to the calculated average value of attenuation. The average attenuation is of course a result of atmospheric attenuation and both of the filter attenuation functions. The effective center frequency has been determined for each band by comparing the calculated

attenuation values in Table 2 of Chapter IV with the values presented in Figure 5 of Chapter II for both the Schmelzer and Theissing and Caplan (Medium Humidity) predicted attenuation curves. The results of the process are shown in Table 3. Except for the band between Filters No. 3 and 4, the effective center frequencies are within the band defined by the 10-db cut-off frequencies for the waveguide filters. For air masses of 2.0 or greater, the average atmospheric attenuation predicted by Theissing and Caplan in the frequency band of 59.7 to 69.4 gc/s exceeds that of either Filter No. 3 or Filter No. 4. The result is that the effective center frequency which has been calculated using these two filters is outside the frequency band defined by the cut-off frequencies of the waveguide filters.* Since the effective center frequencies determined from the two predicted attenuation functions are between the cut-off frequencies for the filters, except as noted above, a compromise frequency was chosen

---

*The cut-off frequency (59.7 gc/s) of Filter No. 3 is in the center of the wide oxygen absorption band near 60 gc/s; the predicted (see Figure 5) atmospheric attenuation is in excess of 100 db/air mass in the frequency band between 58 and 62 gc/s. Thus essentially no energy passes through the atmosphere at these frequencies and therefore, the cut-off frequency of the system employing Filter No. 3 is for practical purposes defined by the atmosphere and not the filter. Using the predictions of Theissing and Caplan in the region near the cut-off frequency (69.4 gc/s) of Filter No. 4, the values of atmospheric attenuation are very large and are comparable to the attenuation of Filter No. 4. This results in the effective center frequency being higher than the defined 10-db cut-off frequency of Filter No. 4. In the case of Schmelzer's predictions, the values of atmospheric attenuation are lower than those for waveguide Filter No. 4; therefore the upper cut-off frequency is controlled more by Filter No. 4 than by the atmosphere. This causes the resulting effective center frequency to be at a lower frequency than 69.4 gc/s.

Table 3. Effective Center Frequency for Each Frequency Band

Frequency Band (gc/s)	Filter Nos.	Schmelzer		Theissing and Caplan		Frequency Used (gc/s)
		Average Attenuation (db/air mass)	Effective Frequency (gc/s)	Average Attenuation (db/air mass)	Effective Frequency (gc/s)	
40.1-49.6	1-2	0.605	46	0.862	46	46
49.6-59.7	2-3	2.649	51	2.618	51	51
59.7-69.4	3-4	2.911	69	3.212	73.2	69*
59.7-74.6	3-5	2.071	71.6	3.173	73.3	72
69.4-74.6	4-5	1.822	72.3	3.158	73.5	73
72.7-92.4	6-7	1.268	77	1.368	82.8	80
92.4-107.7	7-8	2.474	99.6	1.212	101.8	101
92.4-121.5	7-9	2.869	104.4	1.400	103.4	104
107.7-121.5	8-9	4.276	113.5	2.803	108.5	110
121.5-138.3	9-10	6.236	127.5	1.223	130	130

*See footnote on preceding page.

which is between the two calculated values. These compromise values are listed in Table 3, column "Frequency Used," and they are used throughout the remainder of this chapter. In determining these center frequencies, the atmospheric attenuations calculated between 2 and 2.5 air masses were used from Table 2. This was done because the data collected during this investigation were primarily obtained between 1.5 and 3.5 air masses.

Effect of Uncondensed Water Vapor on Atmospheric Attenuation

The effect of uncondensed water vapor on atmospheric attenuation in the frequency region from 40 to 140 gc/s was determined from the data collected during this investigation. The water vapor content in the atmosphere was calculated from radiosonde observations made at Athens, Georgia, and Montgomery, Alabama. From the calculated profiles of water vapor density at these two observing stations, it was observed that the lower atmosphere (below 9.6 km) was nearly homogeneous between the two stations and the moisture content in the Atlanta area was taken as the average between these calculated values.

Values of atmospheric attenuation per air mass were determined, by the technique discussed in Chapter V, from radiometer observations of the sun. The values obtained are presented in Table 4 as a function of frequency and water vapor content. The date of each set of observations is listed only for historical reference.

For each frequency listed (i.e. each column of data), standard statistical tests, such as discussed by Hoel (39), were performed to establish the relation between atmospheric attenuation and water vapor

content. The linear correlation coefficient was computed for each center frequency to determine if a straight line could be used to estimate the data; and the "Student t" distribution was used to establish the hypothesis that the calculated correlation coefficient did not occur simply by chance. These statistical tests have shown that a straight line is a valid approximation to the data points at each center frequency except 69 and 72 gc/s.

Straight line estimates to the data points for the other eight center frequencies were then calculated. The process of linear regression, as explained by Hoel (39), was used to obtain a straight line relation between atmospheric attenuation per air mass, Γ, and water vapor content, ρ, and is given by

$$\Gamma = m\rho + c \tag{6.1}$$

or

$$\Gamma = m(\rho - \bar{\rho}) + \bar{\Gamma}$$

where $\bar{\rho}$ and $\bar{\Gamma}$ are the average values respectively of water vapor and attenuation, and m is the slope for N data points and is given by

$$m = \frac{\sum^{N} \rho\Gamma - N\,\bar{\rho}\,\bar{\Gamma}}{\sum^{N} \rho^2 - N\,\bar{\rho}^2}$$

The value of the slope, m, calculated for each center frequency

Table 4. Atmospheric Attenuation from Sun-Sky Radiometer Measurements

Frequency (gc/s) Filter Nos.		46 1 - 2	51 2 - 3	69 3 - 4	72 3 - 5	73 4 - 5	80 6 - 7	101 7 - 8	104 7 - 9	110 8 - 9	130 9-10
Date	Water Vapor gm/cm^2	Attenuation (db/air mass)									
1-16-63	0.65	0.24	1.62	1.50	1.10	0.5	0.8	0.8	.7	2.25	0.8
1-25-63	0.72	0.6	1.75	1.75	1.25	0.6					
1-28-63 AM	0.75						0.76	1.0	1.5	2.24	1.0
1-28-63 PM	0.75						0.8	1.0	1.5	2.24	1.0
1-2-63	0.79						0.8	0.8	1.7	2.25	0.8
12-31-62	0.81	0.80	1.75	1.75	1.50	0.7					
1-22-63 AM	0.85	1.00	1.75	1.75	1.50	0.8	1.0	1.0	1.55	2.24	0.76
1-22-63 PM	0.85	0.60	1.75	1.75	1.50	0.6	1.0	1.0	1.6	2.25	0.8
2-4-63	0.87	0.24	1.5	1.4	1.25	0.76					
12-14-62	0.88	0.8	1.75	2.0	1.65	0.8					
10-27-61	0.88						1.0		1.5		1.0
1-1-63	0.91	0.8	1.8	1.4	1.20	0.48					
3-22-63	0.94	1.0	2.0	1.5	1.5	0.6					
3-23-63	0.98	0.8	1.75	1.5	1.5	0.6	0.76	0.8	1.7	2.25	1.0
10-26-61	0.99	0.76	1.8		1.4		1.0		1.4		1.0
2-8-63	1.10	0.8	2.0	2.0	1.6	1.0					
3-24-63	1.12	1.0	1.8	2.0	1.65	0.8	1.0	1.0	1.75	2.25	1.25
1-4-63 AM	1.14	0.4	2.0	2.0	1.85	1.0					
1-4-63 PM	1.14	0.76	1.4	1.4	1.12	0.76					
1-3-63	1.15	1.0	2.24	1.4	1.23	0.8	0.8	0.8	1.5	2.25	0.8
5-2-63	1.18	0.76	2.24	1.5	1.25	0.8	0.76	0.76	1.4	2.24	1.0
1-9-63	1.24	0.8	1.4	2.0	1.7	0.8					
11-21-61	1.26	0.76	2.24		1.5						
11-24-61	1.28	0.48	1.75		1.4		0.76		1.4		0.76
5-1-63	1.29	1.0	1.75	2.25	1.7	0.8	1.0	1.0	1.5	2.24	1.0

(Continued)

Table 4. (Continued)

Frequency (gc/s) Filter Nos.		46 1 - 2	51 2 - 3	69 3 - 4	72 3 - 5	73 4 - 5	80 6 - 7	101 7 - 8	104 7 - 9	110 8 - 9	130 9-10
Date	Water Vapor gm/cm^2	Attenuation (db/air mass)									
4-13-63	1.30	0.8	1.4	1.75	1.5	0.8	1.0	1.0	1.5	2.25	1.0
3-27-63 AM	1.48						1.25	1.4	1.8	2.25	1.25
3-27-63 PM	1.48						1.25	1.0	1.7	2.25	1.0
4-8-63	1.57	1.0	2.24	2.0	1.7	0.8					
5-3-63	1.72						1.4	1.4	1.6	2.24	1.25
11-10-61	1.72	1.0	2.24		1.4		1.25		1.50		1.25
11-17-61	1.80	1.15	2.24		1.6						
5-4-63	1.95						1.0	1.4	1.9	2.24	1.0
10-10-61	2.03	1.0	2.24		1.5						
10-9-61	2.20						1.25		1.5		1.25
4-2-63 AM	2.25						1.4		2.25		1.75
4-2-63 PM	2.25						1.0	1.0	1.4	2.25	1.25
10-19-61	2.25	0.76	2.0		1.5						
5-5-63	2.27						1.25	1.25	1.70	2.24	1.5
5-7-63	2.43						1.5	1.75	2.1	2.25	1.5
4-10-63 AM	2.53						1.75	1.75	2.5	2.25	1.75
4-10-63 PM	2.58						1.5	1.4	1.75	2.24	2.25
4-3-63	2.64						1.75	1.75	2.3	2.25	1.25
4-4-63	2.64						1.0	1.5	1.8	2.0	1.5
11-2-61	3.08	0.8	2.0		1.5						
9-27-61	3.09	1.0	2.24		1.5						
9-25-61 AM	3.12	1.0	2.24		1.8						
9-25-61 PM	3.50	1.76	2.24		1.5						
9-23-61	3.70	0.8	2.0		1.5						
9-22-61	3.72	1.0	2.24		1.5						
9-4-61	4.38	1.0	2.25		1.5						

is shown in Figure 22 and is drawn as a horizontal bar extending across the frequency band defined by the filter numbers listed in Table 4. In addition to the values of atmospheric attenuation per gram per square centimeter obtained from this investigation, the values reported by Straiton et al. (11) at the University of Texas are included in Figure 22. The large value of water vapor influence reported by Straiton at 114 gc/s was not obtained by this investigation. But these data reported here do not rebut the findings at the University of Texas; as it will be noted in the next section, the measurements made with Filters Nos. 8 and 9 resulted in large values of attenuation for the frequency range from 108 to 121 gc/s.

Since the linear correlation coefficient and "Student t" tests do not suggest a relation of attenuation to water vapor in the frequency regions delimited by Filters No. 3 and 4 and No. 3 and 5, estimates of linear relations have been made for these regions. The slope of the estimated line is shown by the dashed lines in Figure 22.

The data presented in Table 4 are also presented in graphical form in Figures 23 through 32 for each frequency band considered. Solutions to Equation (6.1), $\Gamma = m\rho + c$, are also shown in each figure by a solid line when the statistical tests indicate a linear regression is applicable. For Figures 25 and 26, the slope of the regression lines were estimated from Figure 22 and straight line estimates are drawn in dashed lines. In each of these figures, two dashed lines have been drawn to include 90 percent of the data points and thus set upper and lower limits for vatiations caused by daily fluctuations. No estimate was made in the frequency band around 110 gc/s because of the constant value of attenuation

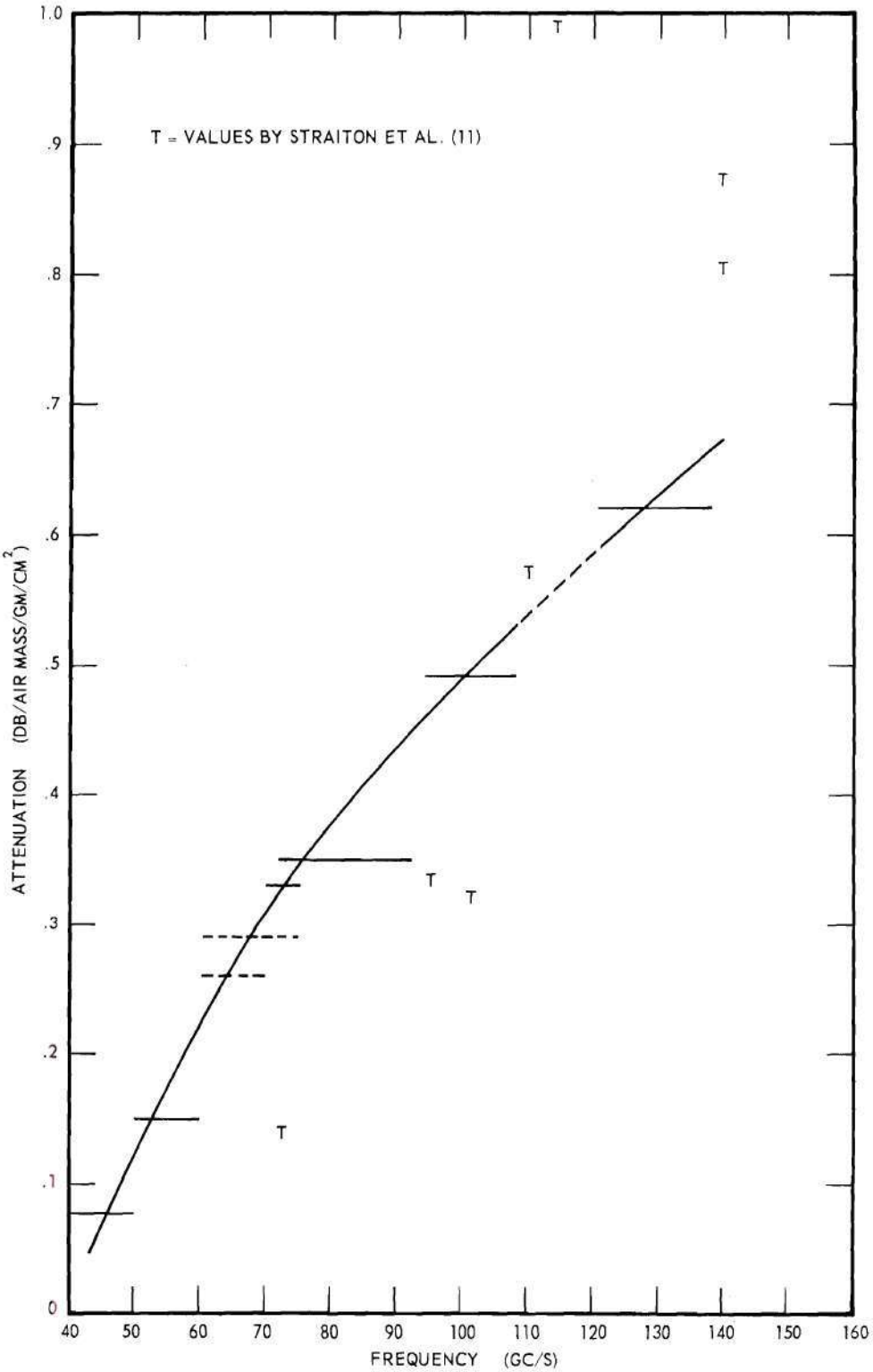

Figure 22. Measured Water Vapor Influence on Atmospheric Attenuation.

obtained over a wide range of water vapor content, which is inconsistent with the data obtained for other regions between 40 and 140 gc/s. This inconsistency is caused by high absorption over the frequency band and the effects of separate gases are not resolvable by the wide band system employed in this investigation. It does not appear likely that the single oxygen line at 120 gc/s could cause sufficient absorption over the band from 107 to 121 gc/s to limit the effective frequency region to a much more narrow band and thus result in the constant attenuation observed. It does lend support perhaps to the proposal by the Texas group that large attenuation values are a result of water vapor, either from additional water vapor resonant lines or strong water vapor-oxygen interaction in the frequency region between 110 and 118 gc/s.

Effect of Oxygen on Atmospheric Attenuation

Since statistical tests have shown straight line estimates are applicable to the data obtained in most frequency bands, and since linear regression has been used to obtain the straight lines, extrapolation of each straight line to larger and smaller values of water vapor content is appropriate. The intersection of the vertical axis (zero water vapor) and the regression line is thus the amount of the total atmospheric attenuation caused by all other gases in the atmosphere. The value of this intersection is the constant, c, in the regression line Equation (6.1). Since it has been predicted that all other gases which have resonant absorption lines in this frequency region cause negligible attenuation compared to oxygen and water vapor, it was assumed that the atmospheric attenuation due to oxygen is estimated by the value of the constant in the equation of the regression line.

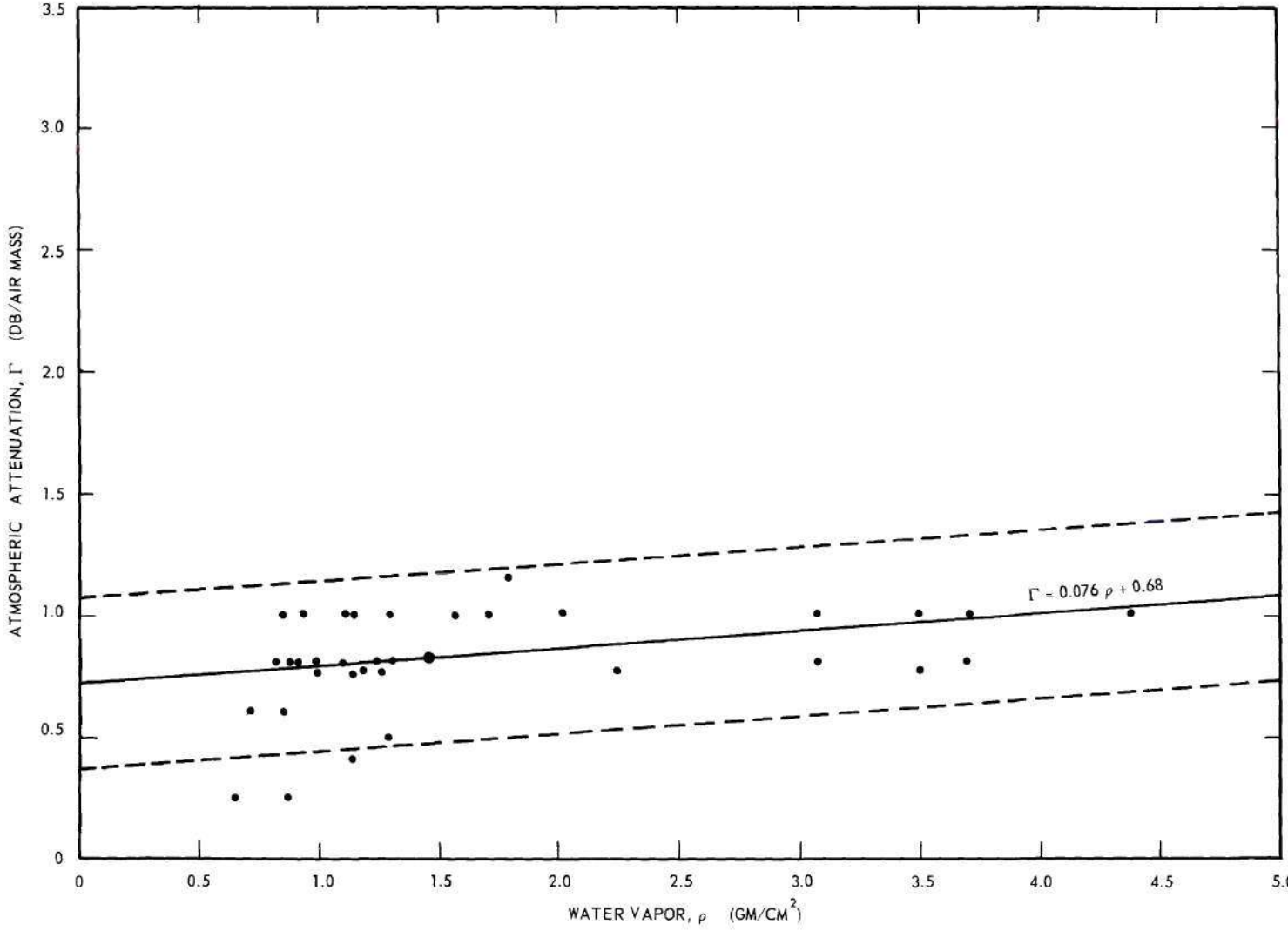

Figure 23. Measured Atmospheric Attenuation in 40 to 49 gc/s Band.

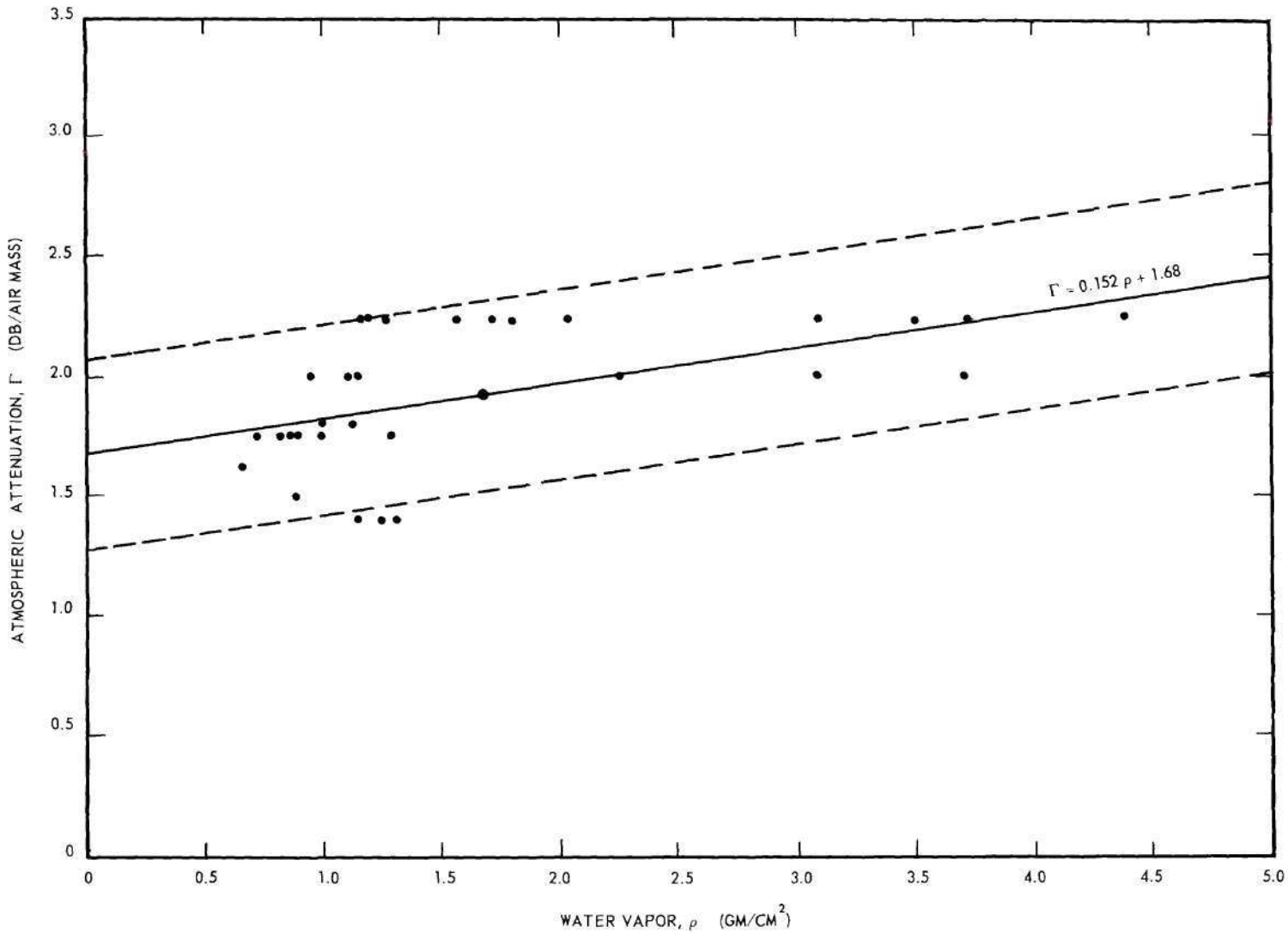

Figure 24. Measured Atmospheric Attenuation in 49 to 59 gc/s Band.

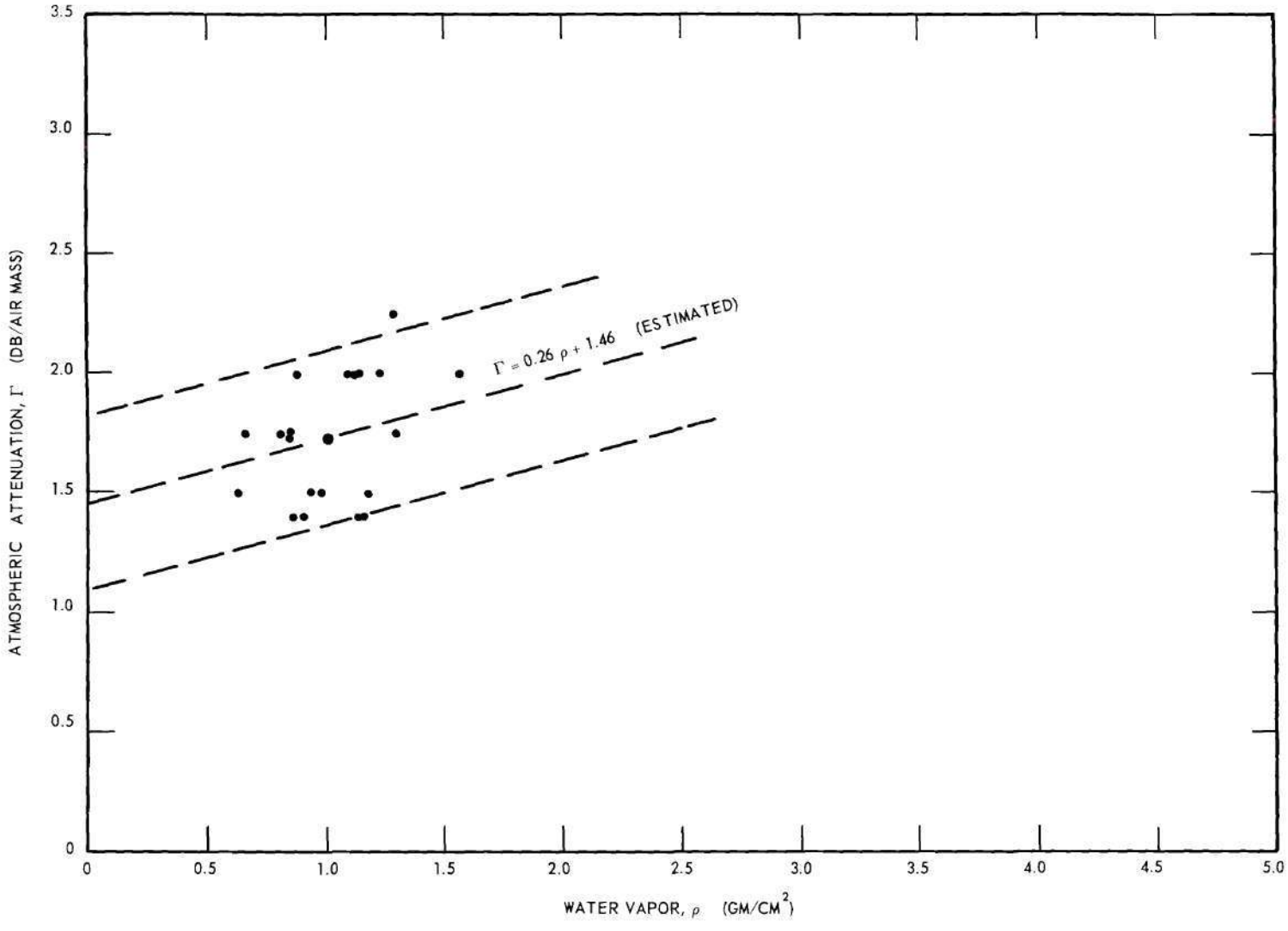

Figure 25. Measured Atmospheric Attenuation in 59 to 69 gc/s Band.

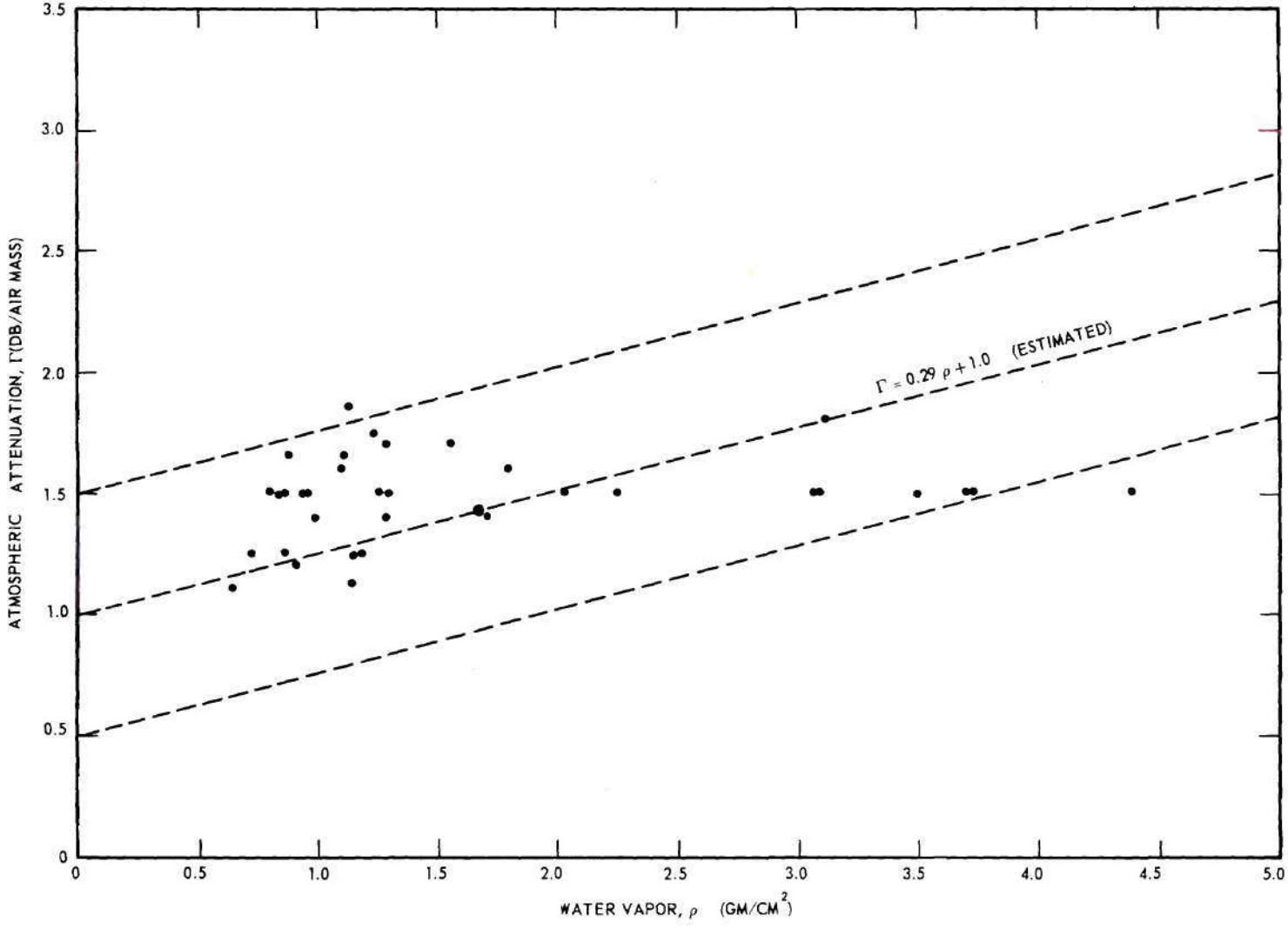

Figure 26. Measured Atmospheric Attenuation in 59 to 74 gc/s Band.

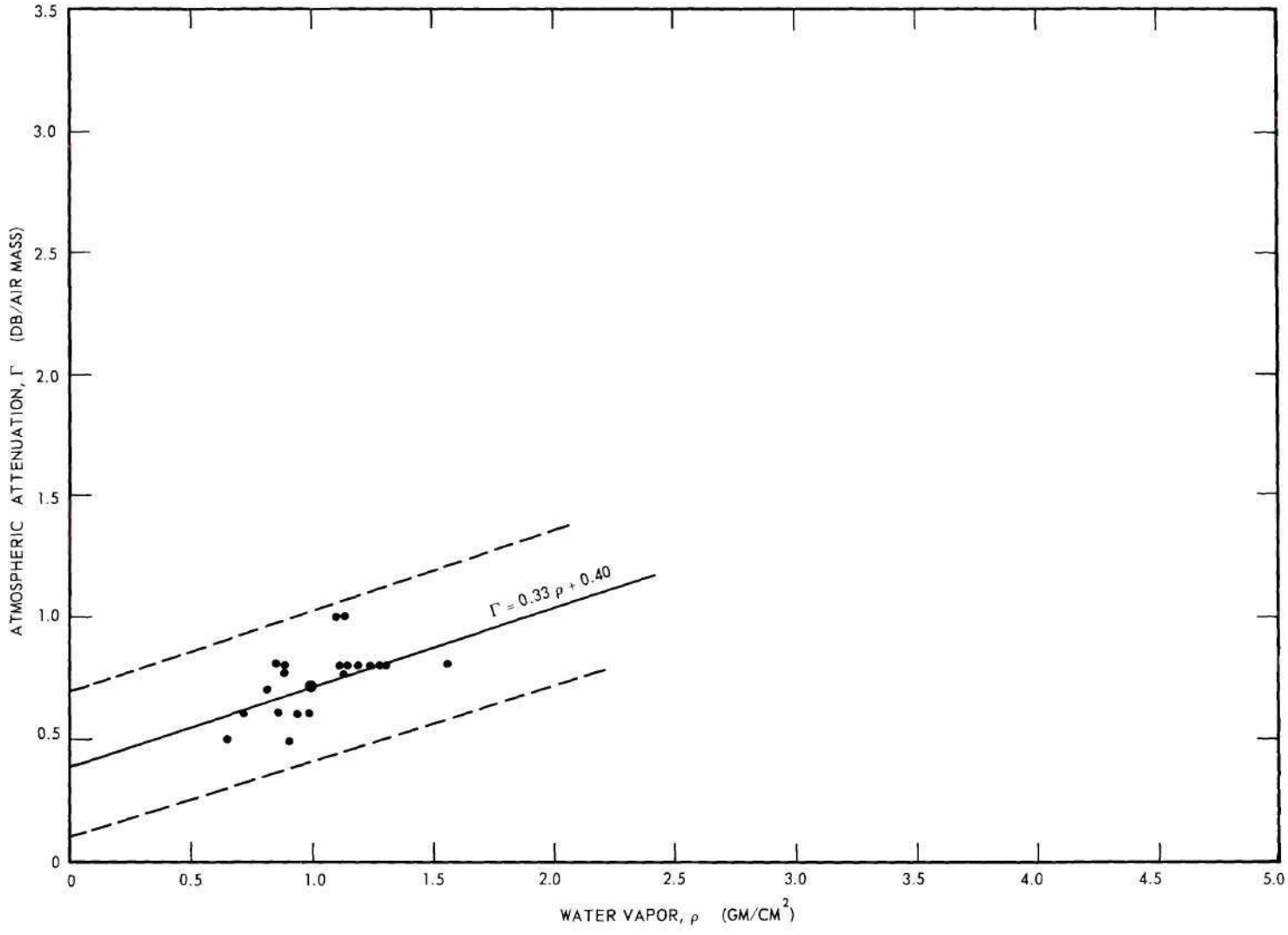

Figure 27. Measured Atmospheric Attenuation in 69 to 74 gc/s Band.

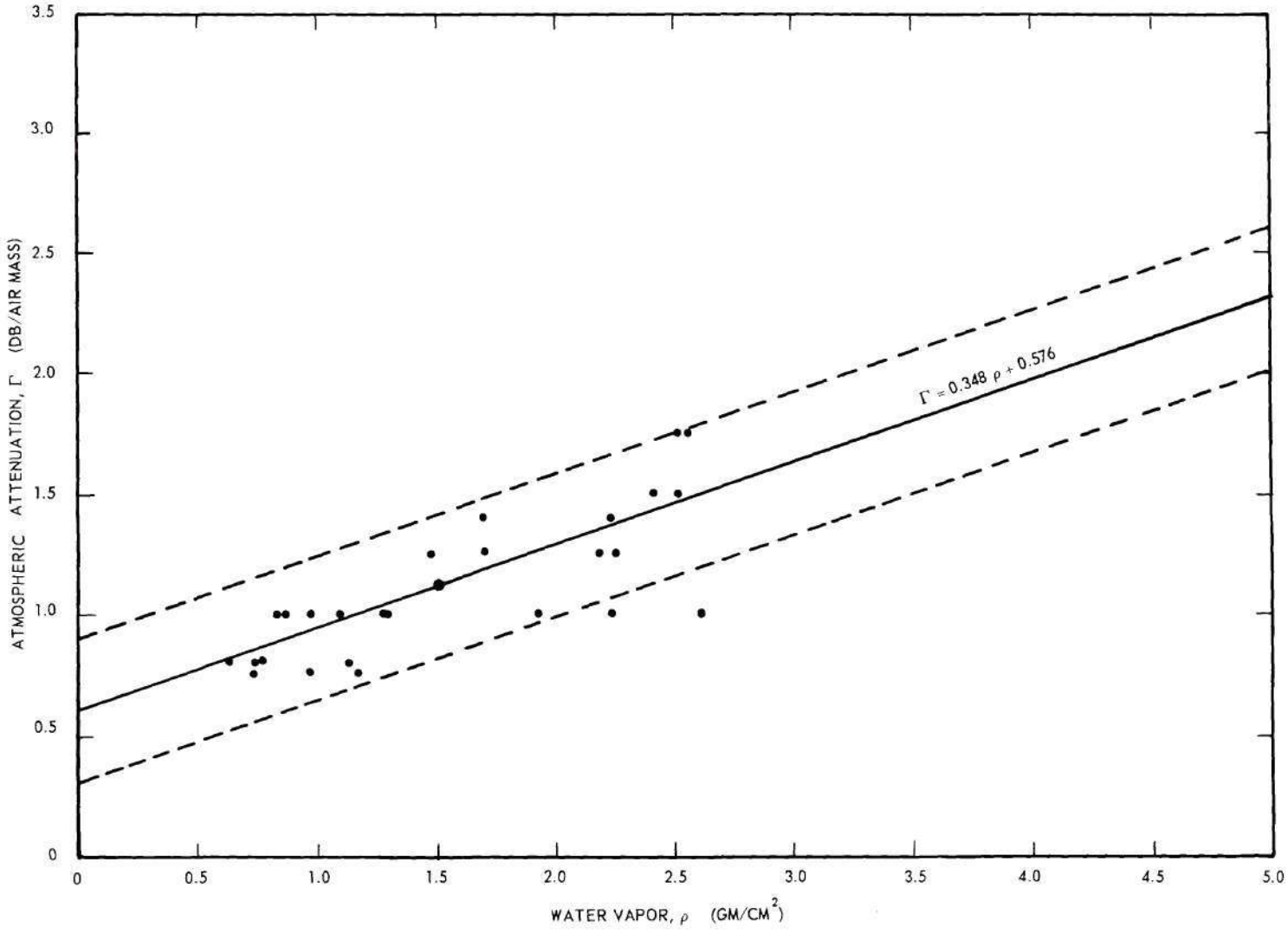

Figure 28. Measured Atmospheric Attenuation in 72 to 92 gc/s Band.

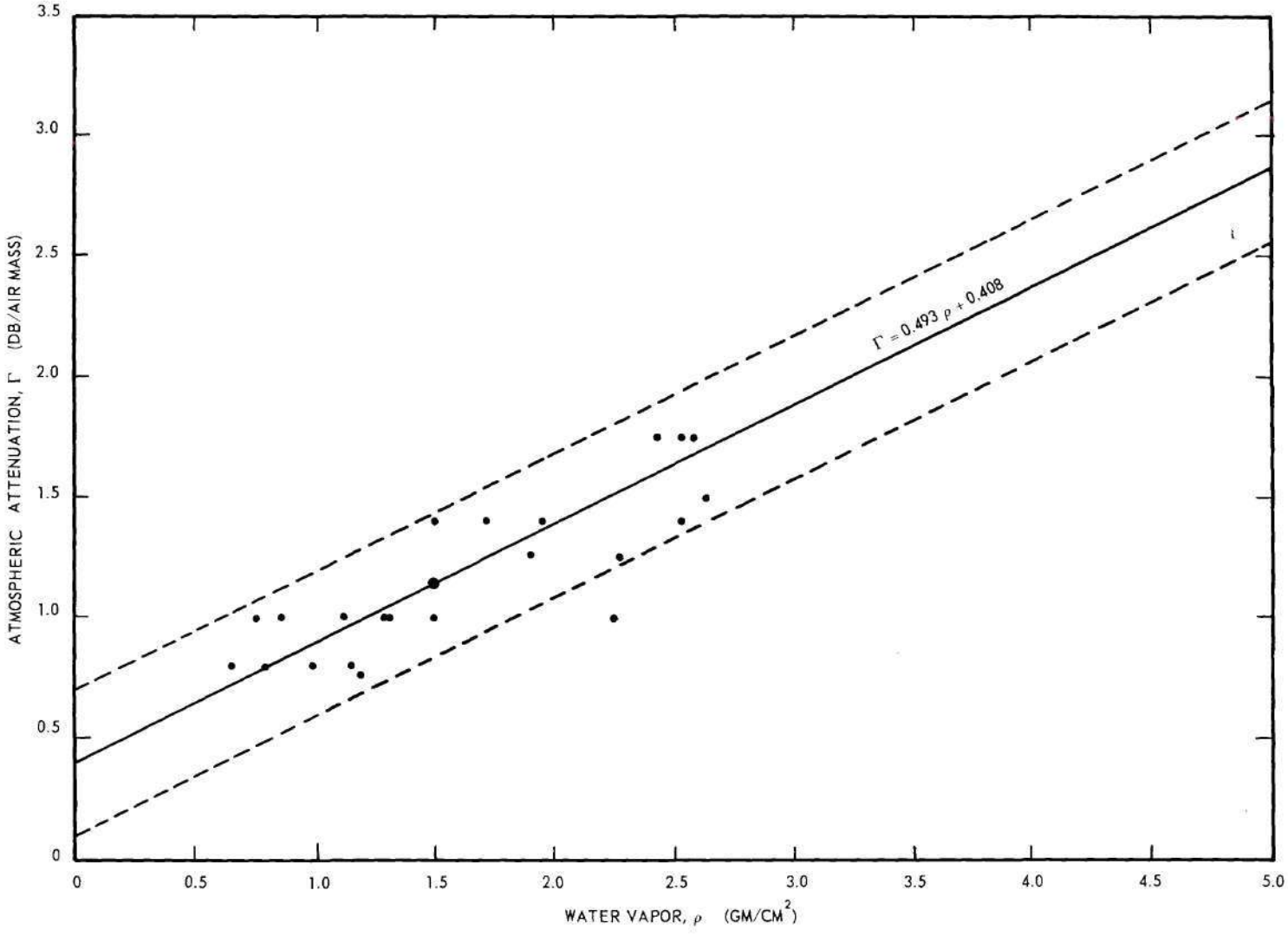

Figure 29. Measured Atmospheric Attenuation in 92 to 107 gc/s Band.

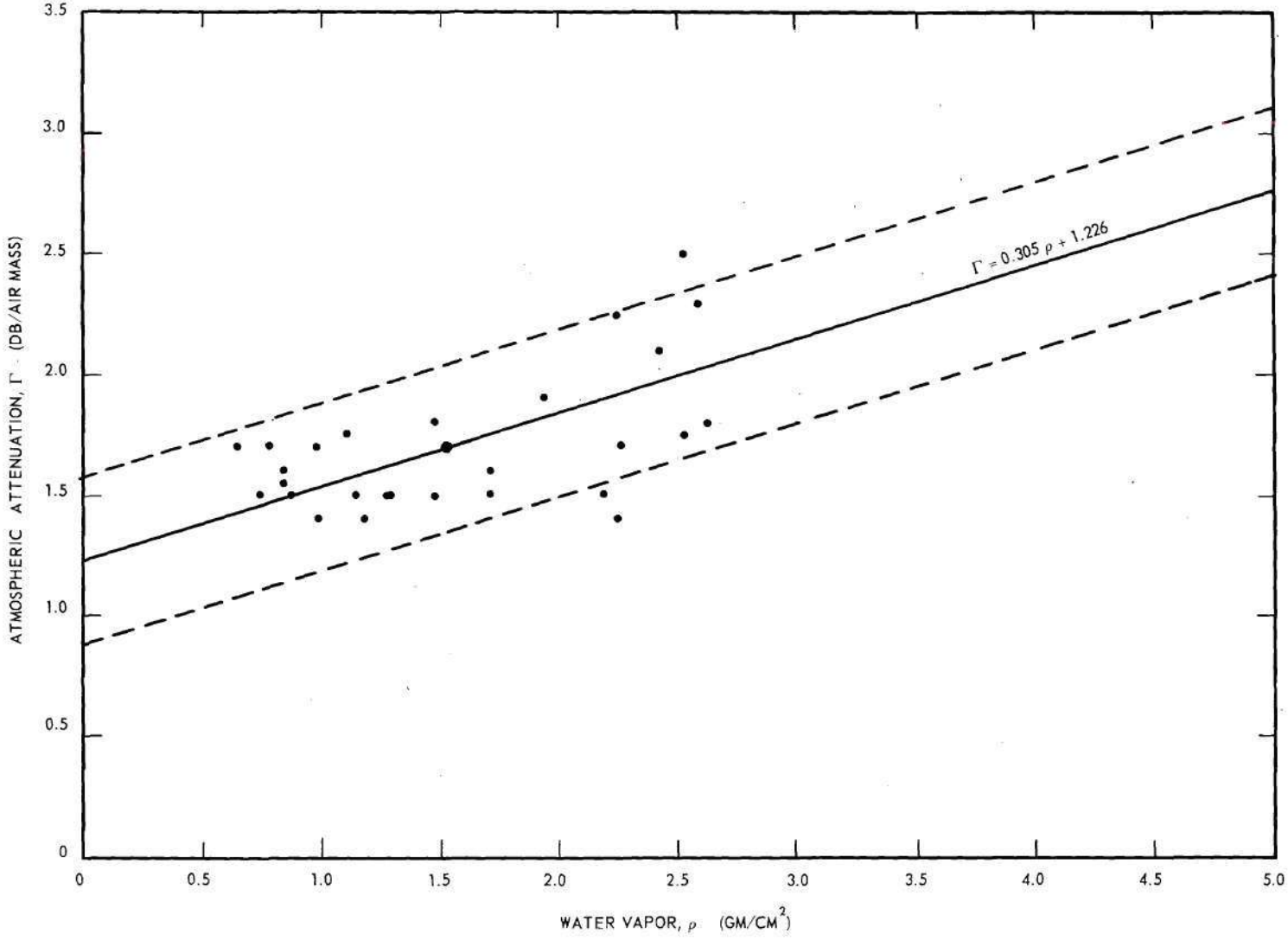

Figure 30. Measured Atmospheric Attenuation in 92 to 121 gc/s Band.

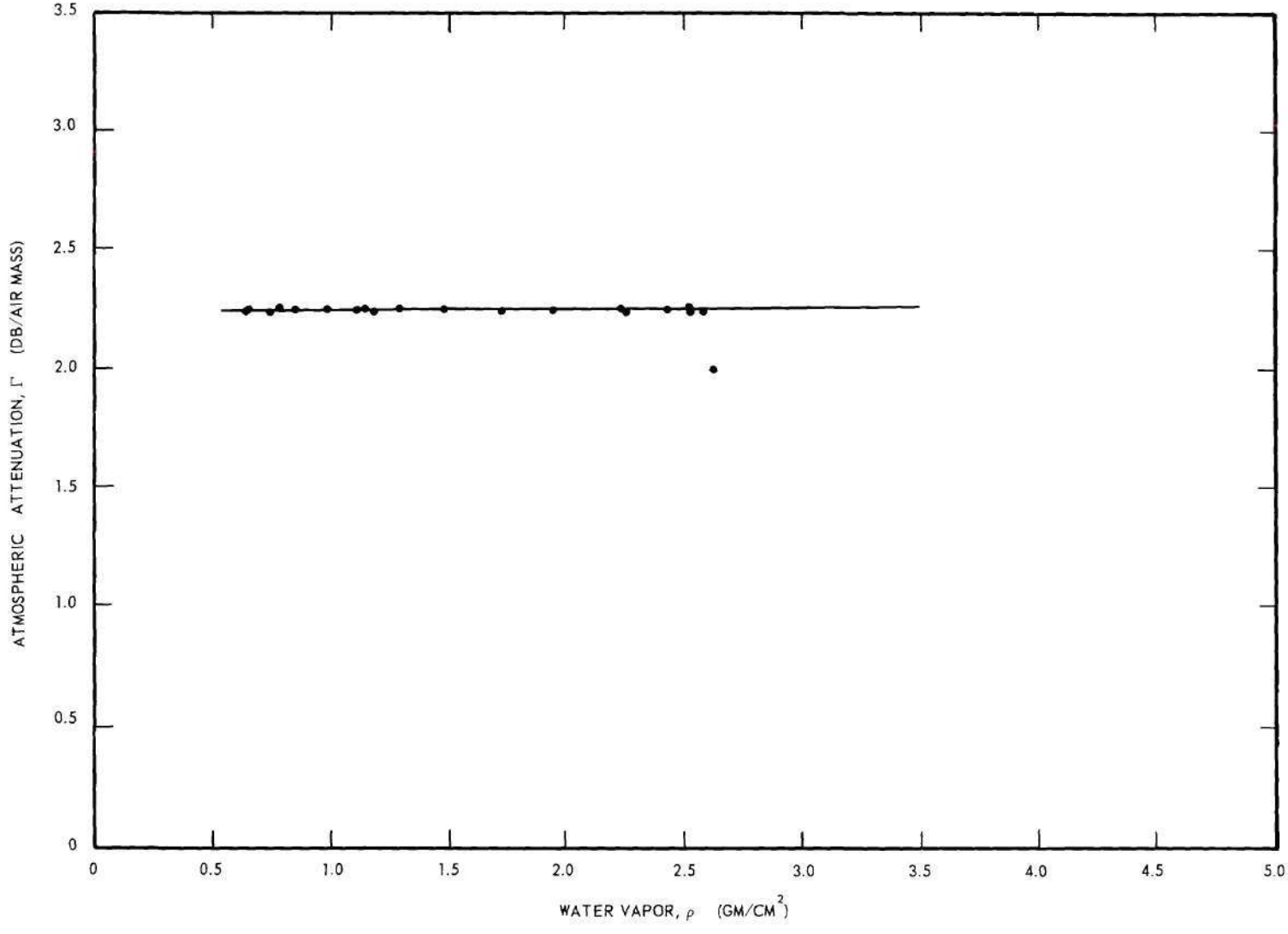

Figure 31. Measured Atmospheric Attenuation in 107 to 121 gc/s Band.

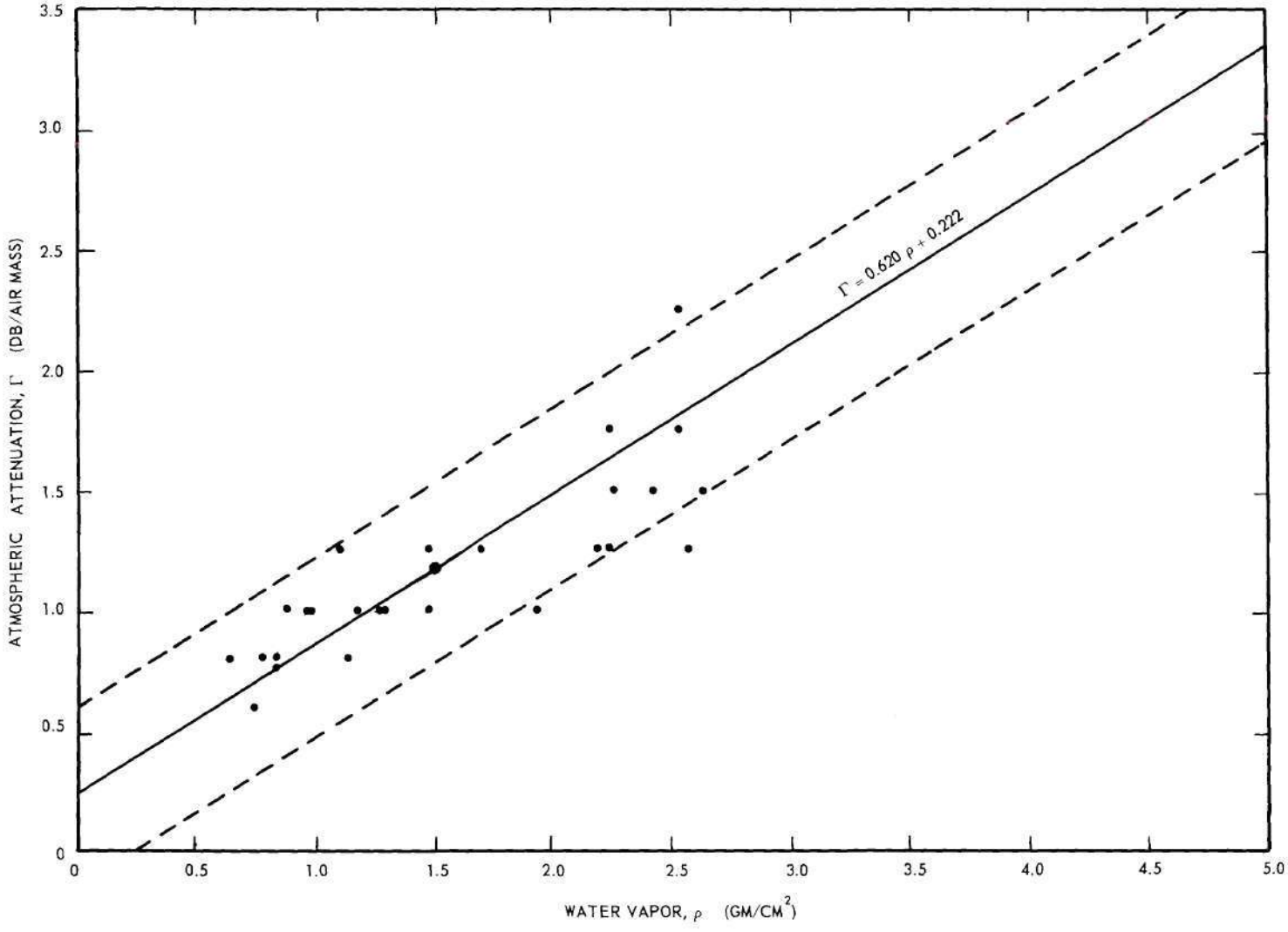

Figure 32. Measured Atmospheric Attenuation in 121 to 138 gc/s Band.

There are two frequency bands, 59 to 69 gc/s and 108 to 121 gc/s, where the straight lines were estimated for the data and true regression lines were not calculated. Although the values presented in Figure 25 and 31 are valid measurements of total atmospheric attenuation, these data do not reveal the separate influence of attenuation due to oxygen and to water vapor. This results in more uncertainty in values of attenuation due to oxygen in these frequency bands.

Summary

Table 5 is a summary presentation of the total atmospheric attenuation in the frequency regions from 40 to 140 gc/s determined during this investigation. The attenuation has been listed by water vapor content so that comparisons can be made with the predicted attenuations presented by Meeks (6), Schmelzer (7), and Theissing and Caplan (8).

Errors related to the atmospheric attenuation are from two primary sources. First, there was a 1/4 db estimated error when drawing the curves of sun signal as a function of air mass and from which the values of attenuation per air mass were obtained. This has been discussed in Chapter V. Secondly, variations in daily values of attenuation as shown in Figures 23 through 32 of this chapter were estimated by the upper and lower limits of the regression lines. Since these two sources of errors are independent, the total error was obtained by calculating the square root of the sum of the individual errors squared. These resultant "over all" errors are presented in Table 5 for each frequency band investigated.

Table 5. Calculated Atmospheric Attenuation For Water Vapor Content

Frequency Center (gc/s)	Frequency Range (gc/s)	Atmospheric Attenuation, Γ (db/air mass) ρ = zero gm/cm²	0.53 gm/cm²	1.45 gm/cm²	2.15 gm/cm²	3.2 gm/cm²	Equation Relation Γ = mρ + c	Error
46	40.1-49.6	0.68	0.72	0.79	0.86	0.93	0.077ρ+0.68	±0.43
51	49.6-59.7	1.68	1.76	1.90	2.01	2.17	0.15ρ+1.68	±0.47
69	59.7-69.4	1.46	1.60	1.84	2.02	2.29	0.26ρ+1.46*	±0.43
72	59.7-74.6	1.0	1.15	1.42	1.62	1.93	0.29ρ+1.0*	±0.56
73	69.4-74.6	0.4	0.57	0.88	1.11	1.46	0.33ρ+0.4	±0.39
80	71.7-92.4	0.58	0.76	1.08	1.32	1.69	0.348ρ+0.576	±0.39
101	92.4-108.0	0.41	0.67	1.12	1.47	1.99	0.493ρ+0.408	±0.39
104	92.4-121.5	1.23	1.39	1.67	1.88	2.20	0.305ρ+1.226	±0.43
110	108.0-121.5	2.25	2.25	2.25	2.25	2.25	0.0ρ+2.25	±0.50
130	121.5-138.3	0.22	0.55	1.12	1.55	2.20	0.620ρ+0.222	±0.47

*Estimates

Figure 33 presents the predicted and measured values of total atmosphere attenuation in the frequency region from 40 to 140 gc/s which are known to the author. The predicted values of attenuation presented by Meeks (6), Schmelzer (7), and Theissing and Caplan (8) are shown as continuous functions with frequency. The measured data reported by Nicoll (34) and Coates (20) for clear days, and by Whitehurst et al. (19) for both clear days and days with thin clouds are shown with bars to indicate the variation in attenuation values obtained at the specific frequencies. Measured values reported by Straiton et al. (11) have appeared in both summary form without the variations noted and in detailed form with variations noted. Their data are presented in Figure 33 with a bar to show the variation if known. All the Texas data are listed for a water vapor content of 3.2 gm/sq cm. (The same value as Theissing and Caplan's "humid" condition.)

In addition to these previously reported values of atmospheric attenuation, the values determined during this investigation are shown at the effective center frequencies for each frequency band studied. To aid the reader in making comparisons between the values determined during this study and those predicted by other investigators, the same values of water vapor are used, namely, zero, 0.53, 1.45, 2.15, and 3.2 gm/sq cm. In addition, the estimated errors of the author's data are shown by a bar centered about the attenuation values for 1.45 gm/sq cm of water vapor.

The radiometer used for collecting the basic data from which these measurements were made was located at an elevation of 300 meters above sea level. Since the Van Vleck-Weisskopf attenuation function is proportional to the number of absorbing molecules and since there is less

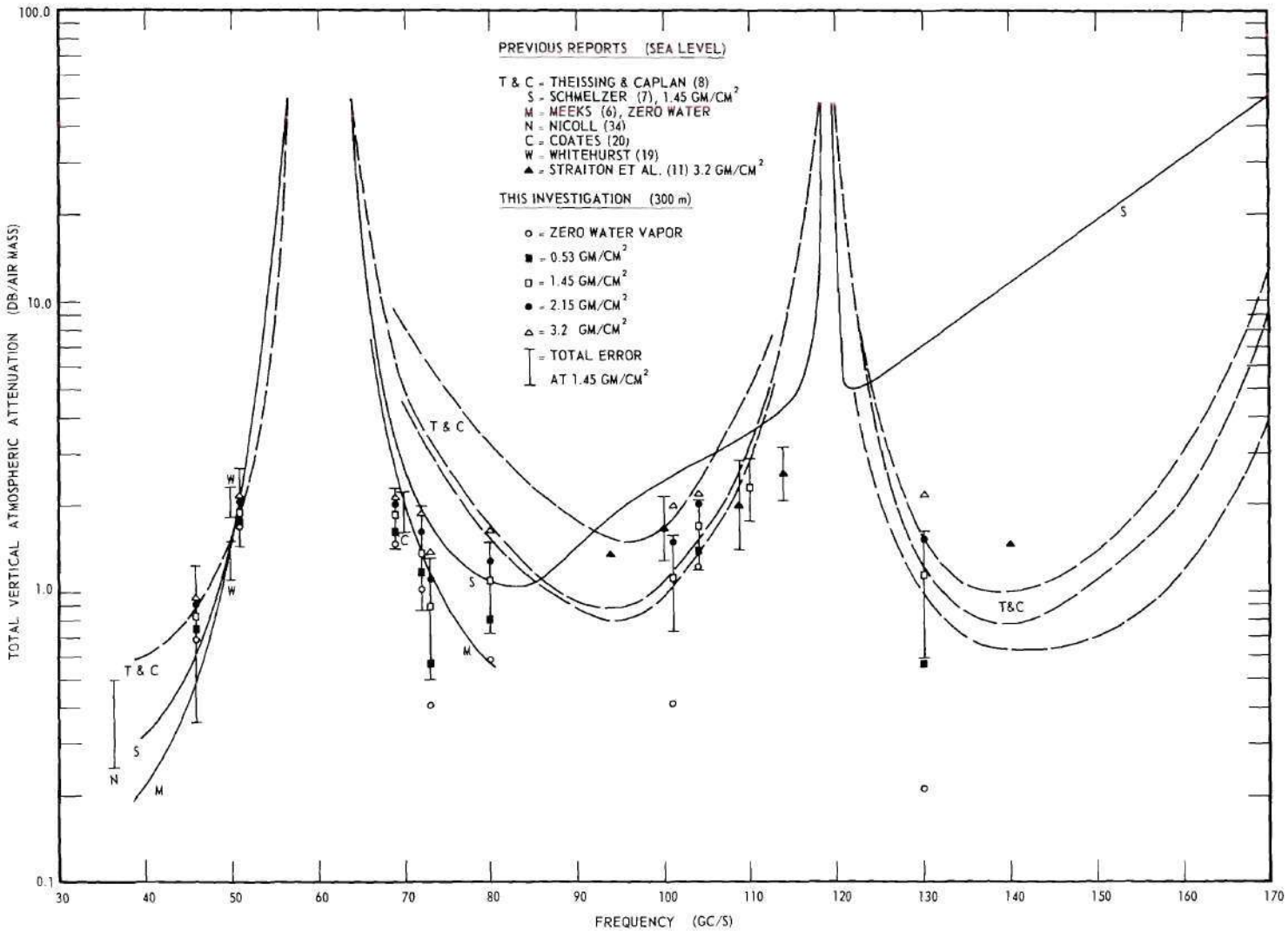

Figure 33. Measured and Predicted Atmospheric Attenuation from 40 to 140 gc/s.

than a 5 percent decrease in molecular density when changing from sea level to 300 meters, this elevation difference should not cause appreciable error in measured attenuation. Certainly this error is small compared to the daily fluctuations in temperature and pressure, which have a stronger influence on the Van Vleck-Weisskopf attenuation function.

Conclusions can be drawn from the data presented in Figure 33. Atmospheric attenuations measured by previous investigators using narrow band superheterodyne systems (11, 20, 34) are confirmed by the measurements made with this wideband direct-detection radiometer.

Total atmospheric attenuation values predicted by Schmelzer (7) appear to be reasonable in the frequency region from 40 to 70 gc/s where the major source of attenuation is a result of oxygen absorption. However in the frequency region from 70 to 140 gc/s, the values of attenuation measured during this investigation are appreciably less than those predicted by Schmelzer. This conflict is a result of predicted water vapor absorption and probably caused by the large "off resonant" linewidth parameter used by Schmelzer.

The atmospheric attenuation calculated by Theissing and Caplan (8), and also presented by Rosenblum (13), as a result of oxygen absorption are too large in the frequency region from 50 to 120 gc/s. This is a result of the simplified oxygen linewidth parameter used by Theissing and Caplan, which as they mentioned is adequate for the region of their measurements near 300 gc/s, but as shown by this investigation are inadequate at frequencies below 140 gc/s. If their predicted values of attenuation were corrected for oxygen, then the attenuation due to water vapor absorption would be slightly less than the values measured during this investigation.

This agrees in general with their conclusions that the Van Vleck-Weisskopf equation gives a reasonable prediction of the atmospheric attenuation in the region near absorption lines but predicts low absolute values of attenuation between resonant lines due to water vapor.

Therefore, it appears that the effect of water vapor, in a frequency region removed from a resonant absorption line, is less than that calculated by Schmelzer, but greater than that calculated by Theissing and Caplan. In his original discussion, Van Vleck (4) made note of the fact that the linewidth parameter he suggested may not be accurate in the region away from a resonant line. The data obtained during this investigation confirms that the linewidth parameter is different for regions on a line and the regions away from a line.

The degree of influence of water vapor on total atmospheric attenuation in the frequency region from 70 to 140 gc/s reported by Straiton et al. (11) at the University of Texas, agrees reasonably well with the data reported here. Although they have reported very strong water vapor influence at 114 gc/s, this investigation neither confirmed nor disproved this degree of influence. This investigation does show a discontinuity in the attenuation function in the frequency region from 108 to 121 gc/s, and it is suspected that it could be caused by water vapor-oxygen interaction.

Finally, it is of importance to note that atmospheric attenuation resulting from oxygen absorption in dry air as calculated by Meeks (6), is within the experimental error of the data determined from this investigation. The data presented in Table 5 and Figure 33 therefore represent the most complete and up-to-date information on the atmospheric attenuation in the frequency region from 40 to 140 gc/s.

CHAPTER VII

CONCLUSIONS AND RECOMMENDATIONS

The Van Vleck-Weisskopf theory of gaseous absorption due to molecular resonances has been accepted by most investigators studying the earth's atmosphere. Using this theory, with laboratory measured molecular parameters and estimated dependences of absorption linewidth on temperature and pressure, Schmelzer (7) and Theissing and Caplan (8) predicted the total vertical atmospheric attenuation resulting from oxygen and from uncondensed water vapor at frequencies above 40 gc/s. The author used these predicted atmospheric attenuations for oxygen and water vapor to calculate the expected total vertical attenuation which should be obtained from measurements using a wide band detecting system.

A wide band, low noise direct-detection radiometer was constructed and used successfully to measure the signal strength of the sun as a function of the zenith angle. From the measured data, the total vertical atmospheric attenuation was obtained for the frequency region from 40 to 140 gc/s in eight adjacent frequency bands. To the author's knowledge, this is the first reporting of the use of a wide band radiometer with replaceable high-pass waveguide filters which has been used to obtain such data. The values of attenuation obtained during this investigation are in conflict with the predicted values mentioned above. It is therefore concluded that the values of certain parameters used by these previous investigators are in error, when applied to the conditions of the atmosphere.

These measurements show that the values calculated by Schmelzer are reasonable in the frequency region from 40 to 80 gc/s, but are too high in the region from 80 to 140 gc/s. This appears to be caused by an incorrectly large attenuation attributed to water vapor at frequencies removed from the resonant water lines. It appears to be appropriate for the calculations to be made again, using a smaller linewidth parameter for water vapor in the far wing regions removed from the water lines.

Theissing and Caplan used a simple approximation of the attenuation function for oxygen, which was valid for their analysis in the frequency region near 300 gc/s, but produces excessively large attenuation near the oxygen resonant lines. With a revised oxygen linewidth, their excellent work should be appropriate for frequencies down to 40 gc/s. In the frequency region between 125 and 138 gc/s, their calculated values of total atmospheric attenuation are smaller than the values obtained by this investigation. They reached two conclusions which agree with the data of this investigation except near 110 gc/s; that is, 1) the Van Vleck-Weisskopf equation properly describes the general shape of the relation of atmospheric attenuation as a function of frequency, but 2) fails to give the proper absolute magnitude of attenuation in frequency regions between resonant absorption lines.

In the frequency region from 107 to 121 gc/s, no measurable dependence of atmospheric attenuation on water vapor was obtained for water vapor content from 0.65 to 2.65 gm/sq cm. This is indicative of a broad resonant absorption line causing a large value of attenuation throughout the bandpass region and preventing an analysis of the separate influence from oxygen and water vapor. The oxygen line at 120 gc/s has a strong

influence in this frequency band, but with a predicted linewidth of 600 mc/s, it should not be so large as to predominate and completely mask the influence of water vapor. Measurements at the University of Texas (11, 19) also indicate anomalies in the absorption of electromagnetic energy at these frequencies. If true, as postulated by Straiton (11), that either additional water vapor lines or strong water vapor-oxygen interaction exists in this region, then the total attenuation would be large and a wide band system would not reveal separate influences by the two gases.

The calculations made by Meeks (6) result in values of attenuation for dry air which are only slightly larger than the values obtained from data measured during this investigation in the frequency regions from 40 to 50 and from 70 to 80 gc/s. The slight difference appears to be caused by the value of oxygen linewidth parameter which he calculated based on atmospheric measurements in air containing water vapor although he considered the air to be dry.

The atmospheric attenuation measurements made by Nicoll (34), Coates (20), Whitehurst *et al.* (19), and Straiton *et al.* (11), were obtained with superheterodyne systems (5 to 10 mc/s bandwidth) operated at various different frequencies in the 40 to 140 gc/s region. The values they reported are consistent with the values obtained during this investigation, in which a wide band direct-detection radiometer was used.

The technique reported here appears to be reliable. Measurements should be extended to higher frequencies. The limitations of the technique will occur in obtaining waveguide filters, parabolic reflectors,

and bolometer detectors. Yet all of these items can be produced to operate as high as 300 gc/s. Using steel mandrels, it should be possible to construct waveguide filters for 300 gc/s operation; a smaller antenna will offer adequate resolution and thus optical grinding or liquid-spun epoxy-cast techniques can be used to construct accurate parabolas; and Mullard photodetectors (40) have been reported to operate satisfactorily at frequencies even above 300 gc/s.

It is also recommended that a system with greater frequency resolution than presently employed be used to investigate the frequency region between 107 and 121 gc/s to resolve the conflict of water vapor and oxygen interaction which appears to exist at these frequencies. If a highly sensitive bolometer element, such as has been developed by Texas Instruments, Incorporated (41) could be mounted in a waveguide holder and operated efficiently in this frequency region, then a series of waveguide filters designed with closely spaced cut-off frequencies would produce a radiometer with sufficient frequency resolution. When selecting the pair of filters to define the frequency band to be investigated, the cut-off frequency of one filter should be sufficiently separated from the absorption line that the frequency band is delimited by the filters and not the absorption line. When the location or shape of the line is unknown, then judicious selection of the cut-off frequency for each high pass waveguide filter will be obtained only be repeated selection of the cut-off frequency and making attenuation measurements. A tunable filter such as reported by Long and Butterworth (27) has possible application and should be investigated for use in the frequency region from 100 to

140 gc/s. The same technique employed during this investigation could be used to advantage and would result in obtaining valuable information in this anomalous region.

A P P E N D I C E S

APPENDIX A

DESCRIPTION OF MODEL ATMOSPHERES

I. The International Standard Atmosphere is defined as follows:

1. The air is dry, and its chemical composition is the same at all altitudes.

2. The temperature and pressure at MSL (mean sea level) are 15° C and 1013.2 millibars.

3. At any altitude h (meters) measured above MSL and between 0 and 11,000 meters the temperature of the air is equal to $t = 15 - 0.0065\,h$ °C.

4. For altitudes above 11,000 meters, the temperature of the air is constant and equal to -56.5° C.

5. The pressure at any altitude h is given by

$$P = 1{,}013.2\left(1 - \frac{0.0065h}{288}\right)^{5.2568} \text{ millibars.}$$

II. Theissing and Caplan Atmospheres

H	Dry			Medium			Humid		
	P	T	ρ	P	T	ρ	P	T	ρ
0	770	278	2.81	761	289	8.28	758	295	12.65
3	683	269	1.68	683	285	5.83	783	290	11.28
6	609	270	0.55	609	282	2.26	609	285	7.56
9	544	266	0.46	544	277	4.43	544	281	3.22
12	482	264	0.55	482	270	2.86	482	275	2.81
15	428	258	0.27	428	264	1.40	428	270	1.89
18	378	252	0.16	378	259	0.98	378	264	0.64
21	333	245	0.08	333	252	0.34	333	257	0.35

H = height in 1000 feet
P = pressure in mm Hg
T = temperature in °K
ρ = partial pressure of water vapor in mm Hg

III. ARDC Model Atmospheres (42)

	1957 (for Schmelzer)		1960 (for Meeks)	
Height km	Temperature °K	Pressure mm Hg	Temperature °K	Pressure mm Hg
0	288	760	288	760
1	282	674	282	674
2	275	596	275	596
3	269	525	269	526
4	262	562	262	462
5	256	405	256	405
6	249	354	249	354
7	243	308	243	308
8	236	267	236	267
9	230	230	230	231
10	223	198	223	199
11	217	170	217	170
12	217	145	217	146
15	217	90.3	217	90.8
20	217	41.1	217	41.5
25	217	18.7	217	19.0
30	232	8.71	231	8.89
40	262	2.18	261	2.25
50	283	0.629	283	0.659
60	258	0.181	254	0.193
70	223	0.0435	210	0.0452
80	199	0.00835	166	0.00756
90	218	0.00158	166	0.00102
100	245	0.000359	199	0.000160

APPENDIX B

WAVEGUIDE FILTERS

The attenuation characteristics of rectangular waveguides have been developed for the dominant TE_{10} mode of propagation and are well defined functions of the physical dimensions (23, 24, 43). In general, power capacity is determined by the height of the waveguide, cut-off frequency is determined by the width of the waveguide, and impedance is determined by the ratio of height to width. In the frequency range of interest, any standard waveguide has more than adequate power handling capacity (watts) compared to power received (picowatts) from the sun. This simplifies the waveguide design by using constant heights to mate with standard commercial units and adjusting the width for the desired attenuation and impedance as a function of frequency. Five filters were designed and constructed to mate with standard RG-98 waveguide, two double linear transitions were constructed in addition to the filters for impedance matching the RG-98 waveguide with the RG-138 waveguide with dimensional design following that suggested by Johnson (43).

The first (lowest cut-off frequency) filter in each waveguide set has the standard dimensions of the appropriate waveguide. The remaining four filters each have a narrow center section which is connected to the standard waveguide by a linear H-plane taper on each end. Width of the narrow section was chosen for the desired cut-off frequency of each filter and a mandrel was machined from a plexiglas blank for each unit.

Figure 34 presents sketches of mandrels used for the ten filters and the two double linear taper transitions.

Each mandrel was splattered with gold by placing the mandrel in a belljar and evaporating a gold filament at the flash temperature of gold. Copper was deposited to a thickness of approximately 0.15 inch on this thin layer of gold by standard electroforming techniques. The units were removed from the electroforming bath and machined on each end to produce flat rectangular surfaces for later installation of standard UG-385 flanges. After machining, methylene chloride, which dissolves plexiglas but does not attack copper, was used to remove the mandrels. Then the flanges were installed and each unit checked dimensionally with a 150 power Tool-makers microscope. Johansson blocks were used to calibrate the microscope and accuracy of the final measurements is estimated to be better than ±0.0002 inch. Results of the measurements of the inside dimensions are listed in Table 6, where the alphabetical quantities are shown in Figure 34 for the mandrels.

Attenuation values over the frequency region of 40 to 200 gc/s were calculated for each unit from the dimensions presented in Table 6. In the frequency region above cut-off, $f > \frac{c}{2A}$, the following equation derived by Kuhn (23) was used to calculate the waveguide attenuation

$$\alpha = 0.0009225A^{-3/2}\left[\frac{c}{2Af}\left(1-\frac{c^2}{4A^2f^2}\right)\right]^{-1/2}\left[\frac{c^2}{4A^2f^2}+\frac{A}{2B}\right] L \text{ in db.}$$

In the frequency region below cut-off, $f < \frac{c}{2A}$, the following equation given by Ragan (24) was used to calculate the waveguide attenuation

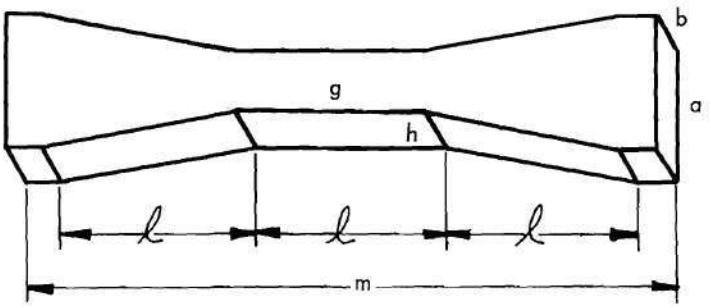

WAVEGUIDE FILTER

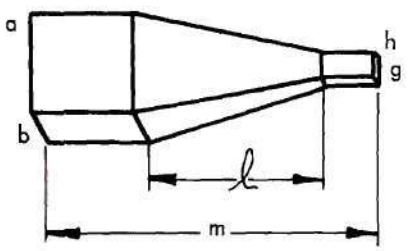

DOUBLE LINEAR TAPER WAVEGUIDE TRANSITION

Figure 34. Sketches of Mandrels for Waveguide Units.

Table 6. Inside Dimensions of Waveguide Filters and Transitions.

Filter No.	a	b	g	h	ℓ	m
1	0.1473	0.0747	0.1473	0.0747	1.00	2.30
2	0.1475	0.0752	0.1191	0.0742	1.00	2.30
3	0.1513	0.0736	0.0989	0.0733	1.00	2.30
4	0.1475	0.0740	0.0851	0.0742	1.00	2.30
5	0.1486	0.0750	0.0791	0.0744	1.00	2.30
6	0.0823	0.0424	0.0823	0.0424	0.54	1.96
7	0.0816	0.0419	0.0639	0.0398	0.54	1.96
8	0.0808	0.0401	0.0547	0.0404	0.54	1.78
9	0.0814	0.0406	0.0486	0.0397	0.54	1.96
10	0.0809	0.0408	0.0427	0.0399	0.54	1.96
Transitions						
1	0.1501	0.0735	0.0811	0.0382	1.00	1.33
2	0.1484	0.0735	0.0806	0.0399	1.00	1.33

All units in Inches. Accuracy ±0.0002 inch.

$$\alpha = 27.3 \frac{L}{A} \left[1 - \left(\frac{2Af}{c}\right)^2\right]^{\frac{1}{2}} \text{ in db ,}$$

where

A = a or g = wide dimensions of waveguide in inches,

B = b or h = narrow dimension of waveguide in inches,

L = ℓ or m = length of waveguide in inches,

c = velocity of light in inches per sec, and

f = frequency in cycles per sec.

The H-plane taper sections in each filter were approximated by sections of straight waveguide having a width of $(g + a)/2$ and a length of $(m-\ell)$. The attenuation values obtained using this simple approximation for Filter No. 5 were found to differ by less than 3 percent from the attenuation values obtained by the more standard five step approximations suggested by Johnson (43).

A graphical investigation of attenuation per unit length was made in the region of frequency cut-off, $f_c = c/2A$, for waveguides to determine the magnitude of the discontinuity resulting from using Kuhn's equation for $f > f_c$ and Ragan's equation for $f < f_c$. The actual dimensions of Filters No. 1 and 5 (RG-98 waveguide) and Filters No. 6 and 10 (RG-138 waveguide) were used in these calculations. From Figures 35 and 36, it can be seen that discontinuities in values of attenuation are not serious even for changes in the A dimension by a factor of two.

A more critical examination was made concerning Filters No. 1 and 5 by expanding the data presented in Figure 35. This is shown in Figure 37, where the attenuation per unit length is presented for a 0.3 percent change in frequency near the cut-off region. For a given filter (using

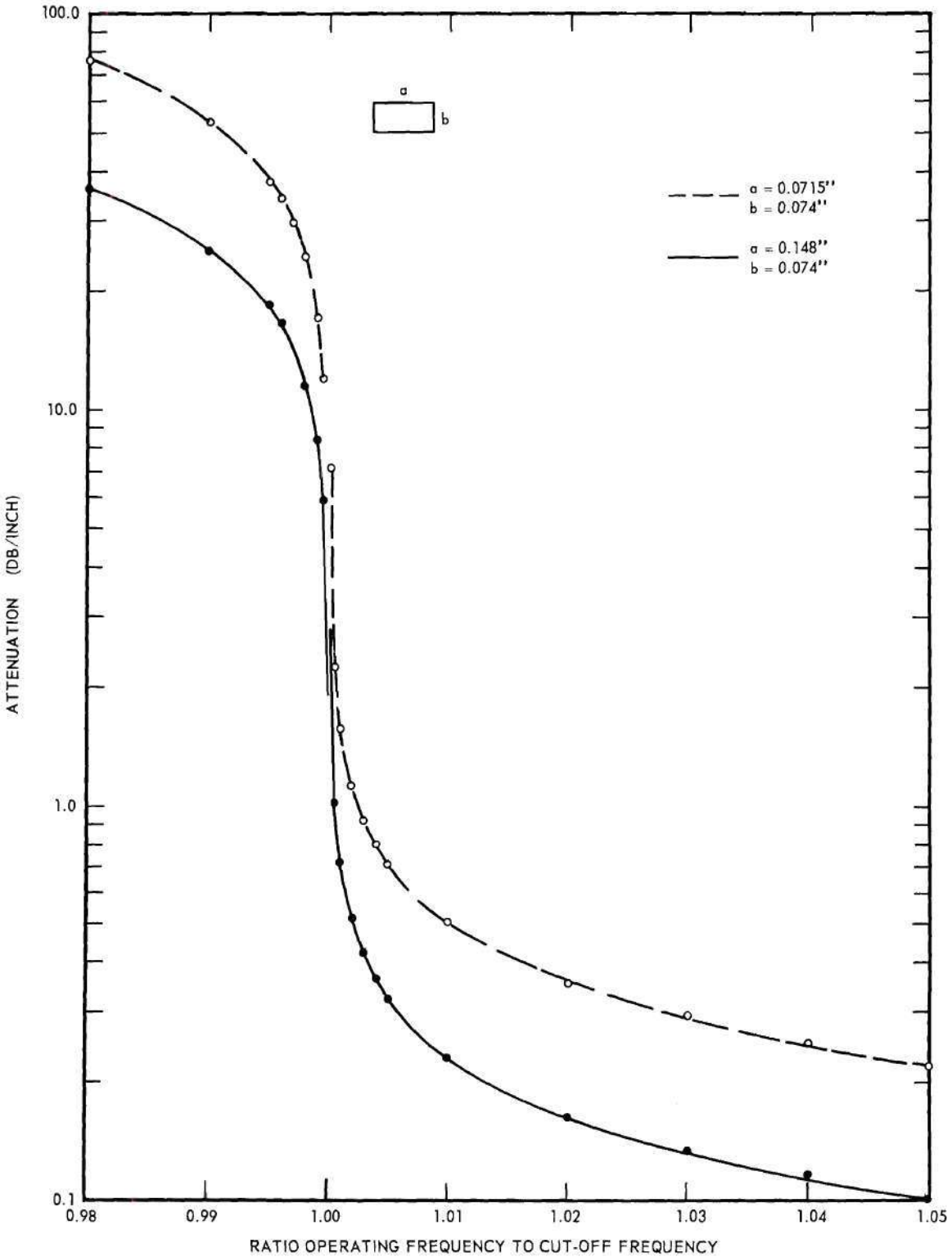

Figure 35. Calculated Attenuation of RG-98 Waveguide.

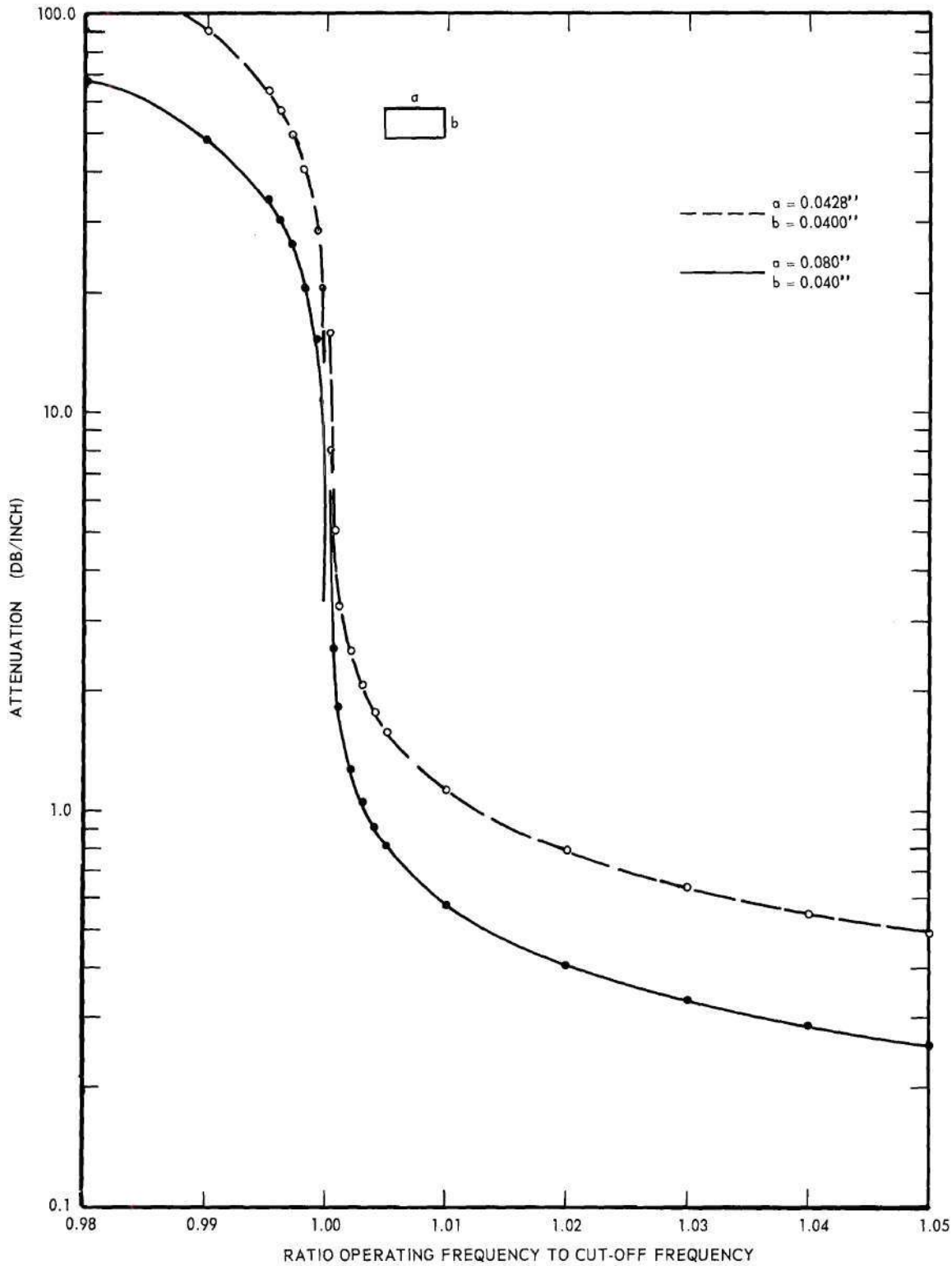

Figure 36. Calculated Attenuation of RG-138 Waveguide.

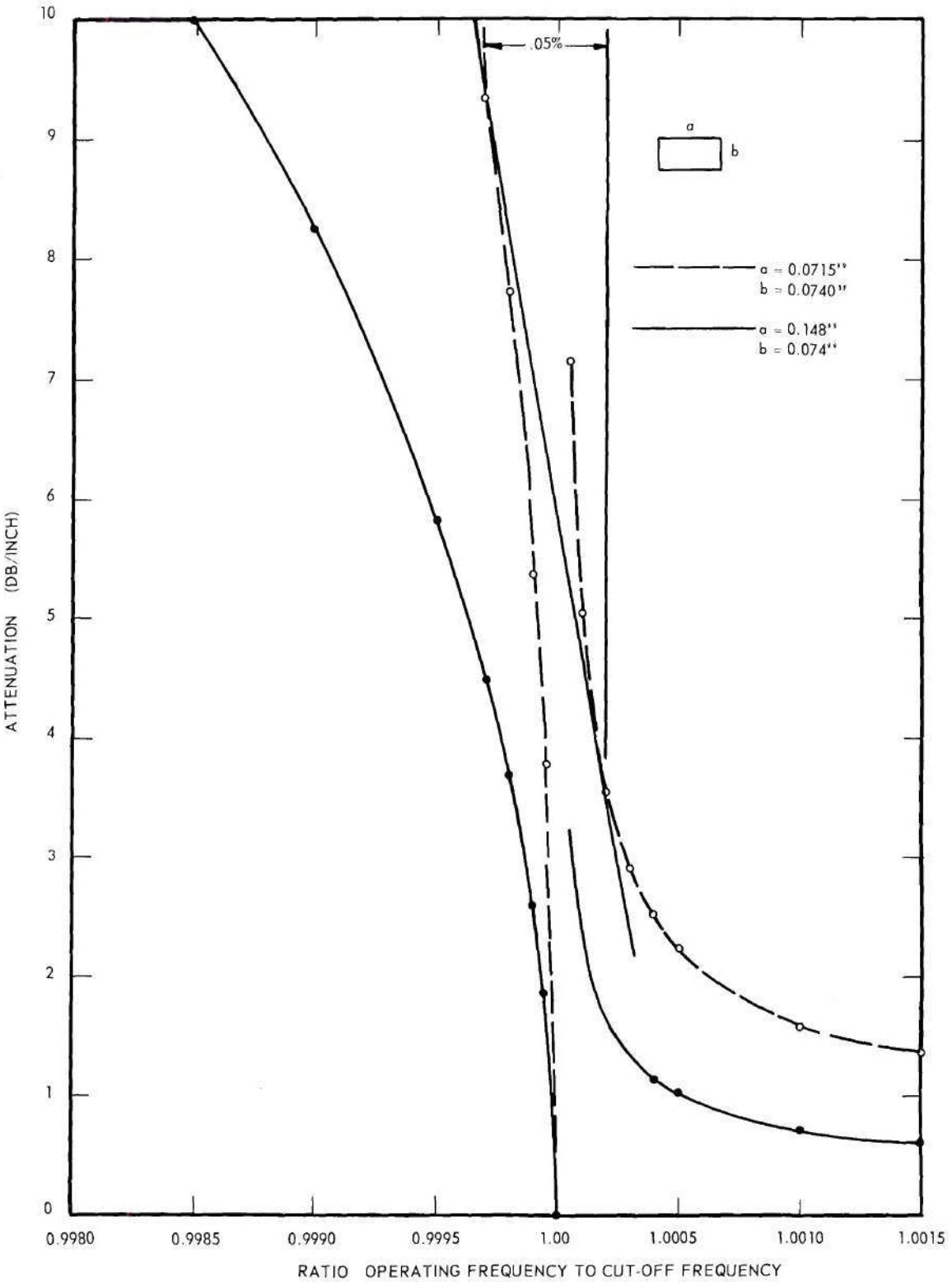

Figure 37. Calculated Attenuation of RG-98 Waveguide at Cut-off.

Filter No. 5 as an example), a straight line is constructed which is tangent to both calculated curves. These two tangency points are separated by less than 0.06 percent of the value of the cut-off frequency, f_c. Thus if the attenuation function with regard to frequency is correctly defined by Kuhn's equation for $f > 1.0003\ f_c$, Ragan's equation for $f < 0.9997\ f_c$, and a linear equation for $0.9997\ f_c \leq f \leq 1.0003\ f_c$, a good first order approximation is obtained. In a wide band system, such as the one used in this investigation, where the values of f_c for two adjacent filters are separated by 10 percent, then a 0.06 percent frequency region of uncertainty in filter attenuation is certainly a small fraction of the total bandwidth. Thus no effect should be noticed by assuming a straight line connection between Kuhn's and Ragan's equations. The curves presented in Figure 10 of Chapter III were obtained using this approximation.

APPENDIX C

THE VAN VLECK-WEISSKOPF ABSORPTION COEFFICIENT

For completeness of this investigation, the following summary is presented from the original article by Van Vleck and Weisskopf (2).

The resonant absorption theory by Lorentz and the nonresonant absorption theory by Debye have been revised and unified. We assume the condition of thermal equilibrium between molecules undergoing hard collisions and the surrounding electromagnetic field. Then, the phases of the molecular motion are not randomly distributed as assumed by Lorentz, but instead follow the Boltzmann distribution. However, under these conditions, the case of resonant absorption for a harmonic oscillator can be treated in a manner similar to that used by Lorentz. These assumptions will also permit the absorption coefficient to reduce to the Debye case for negligible rotational energy of the molecule.

Let ω be the angular frequency of the incident wave, and ω_o be that of the oscillator, whose charge and mass are denoted by e and m, respectively. Then the equation of motion for the molecule is

$$m(\ddot{x} + \omega_o^2 x) = e E \cos \omega t \qquad \text{(C-1)}$$

when the applied electric field intensity is of the form $E \cos \omega t$. The general solution of Equation (C-1) is

$$x = \mathrm{Re}\left[\frac{eEe^{i\omega t}}{m(\omega_o^2 - \omega^2)} + C_1 e^{i\omega_o t} + C_2 e^{-i\omega_o t} \right]$$

where the symbol Re denotes the real part of the quantity following the symbol.

Suppose now that at a time $t - \theta$, the oscillator has last experienced a collision. The constants C_1 and C_2 are then obtained from the boundary conditions on x and $\dot{x}$ under the assumption that the distribution after collision follows the Boltzmann distribution law. If the collisions occur at random, with a mean frequency $f = \frac{1}{\tau}$, then the distribution of collisions in time is $(1/\tau)e^{-\theta/\tau}\, d\theta$. When we average the expression for x over the various times of last collisions, the result is

$$x = \mathrm{Re}\left[\frac{eEe^{i\omega t}}{m(\omega_o^2-\omega^2)}\left\{1 - \frac{(\omega+\omega_o)\,\omega/\omega_o^2\tau}{2[(1/\tau) - i(\omega_o-\omega)]} + \frac{(\omega_o-\omega)\,\omega/\omega_o^2\tau}{2[(1/\tau) + i(\omega_o+\omega)]}\right\}\right] \qquad \text{(C-3)}$$

We may write (C-3) in the form

$$x = \mathrm{Re}\left[Ee^{i\omega t}\,(x' - ix'')\right] \qquad \text{(C-4)}$$

where x' and x'' are real quantities given by

$$x' = \frac{e}{m(\omega_o^2-\omega^2)}\left\{1 - \frac{(\omega_o^2-\omega^2)(\omega/\omega_o^2\tau)}{2[(1/\tau)^2 + (\omega_o-\omega)^2]} + \frac{(\omega_o^2-\omega)(\omega/\omega_o^2\tau)}{2[(1/\tau)^2 + (\omega_o+\omega)^2]}\right\}$$

and

$$x'' = \frac{e}{2m}\,\frac{\omega}{\omega_o^2}\left\{\frac{(1/\tau)}{(1/\tau)^2 + (\omega_o-\omega)^2} + \frac{(1/\tau)}{(1/\tau)^2 + (\omega_o+\omega)^2}\right\}$$

The polarization, $\mathcal{P}$, or dipole moment per unit volume, resulting from the charge e having a displacement x in an electric field is given by

$$\mathcal{P} = ex \tag{C-5}$$

By substituting Equation (C-4) for x, we obtain

$$\mathcal{P} = e \cdot \mathrm{Re}\left[Ee^{i\omega t}(x' - ix'')\right]$$

In an absorbing medium containing N molecules per cm^3, the the absorption coefficient, γ, is related to the polarization by

$$\gamma = \frac{4\pi\omega Ne}{c} x''$$

in as much as this is the same as the mean work $\langle Ed\mathcal{P}/dt\rangle_{av}$ done on the molecule divided by the energy flow $cE^2/8\pi$ in the incident radiation. Thus

$$\gamma = \frac{4\pi\omega Ne}{c} \frac{e}{2m} \frac{\omega}{\omega_o^2} \left\{ \frac{(1/\tau)}{(1/\tau)^2 + (\omega_o - \omega)^2} + \frac{(1/\tau)}{(1/\tau)^2 + (\omega_o + \omega)^2} \right\} \tag{C-6}$$

Equation (C-6) has been derived from the classical point of view and therefore must be generalized to the quantum mechanical system. The quantity e^2/m in this classical expression corresponds to $(8\pi^2/3h)|\mu_{ij}|^2 f_{ij}$ and the term ω_o to $2\pi f_{ij}$ in the quantum-mechanical expression. Here μ_{ij} is the matrix element of the dipole moment connecting two stationary states i, j of energy W_i, W_j respectively. The matrix element may be either electric or magnetic. In addition, the total number of molecules, N, in the volume must be summed over the various states according with the Boltzmann law. Thus Equation (C-6) becomes

$$\gamma = \left(\frac{8\pi^3 fN}{3hc}\right) \frac{\sum_j \sum_i |\mu_{ij}|^2 F(f_{ij},f)\, e^{-W_j/kT}}{\sum_j e^{-W_j/kT}} \qquad \text{(C-7)}$$

where

$$F(f_{ij},f) = -F(f_{ji},f) = \frac{1}{\pi}\frac{f}{f_{ij}}\left[\frac{\Delta f}{(f_{ij}-f)^2 + (\Delta f)^2} + \frac{\Delta f}{(f_{ij}+f)^2 + (\Delta f)^2}\right]$$

and

$$\Delta f = \frac{1}{2\pi\tau}$$

In the case of oxygen and water vapor, $|f_{ij}| \ll kT/h$ at microwave frequencies and normal atmospheric temperatures. Thus the positive and negative terms from $hf_{ij} = W_i - W_j = -hf_{ji}$ nearly cancel, permitting simplification of Equation (C-7) to

$$\gamma = \frac{8\pi^2 f^2 N}{6ckT} \frac{\sum_j \sum_i |\mu_{ij}|^2 e^{-W_j/kT}}{\sum_j e^{-W_j/kT}} \left[\frac{\Delta f}{(f_{ij}-f)^2 + (\Delta f)^2} + \frac{\Delta f}{(f_{ij}+f)^2 + (\Delta f)^2}\right] \qquad \text{(C-8)}$$

In the presentation of the equation for atmospheric absorption in Chapter II, additional simplifications were made. The total number of molecules in the atmosphere is $N = 9.66 \times 10^{18}\ (P/T)$, where P is the total pressure in millimeters of mercury; also γ is proportional to the partial pressure p/P. To convert Equation (C-8) to decibels per km,

it is necessary to multiply by the factor $10^6 \log e$. The constant K also includes the ratio of the square of the moment matrix element, μ_{ij}, and the partition function in the denominator, thus

$$K = \frac{4\pi^2 \, (9.66) \, 10^{24} \, \log e \sum_j \sum_i |\mu_{ij}|^2}{3 \, ck \sum_j e^{-W_j/kT}} \qquad \text{(C-9)}$$

Equation (C-8) reduces to that presented in Chapter II, namely

$$\gamma = \frac{pKf^2}{T^2} \; e^{-W/kT} \left[\frac{\Delta f}{(f_{ij}-f)^2 + (\Delta f)^2} + \frac{\Delta f}{(f_{ij}+f)^2 + (\Delta f)^2} \right]$$

LITERATURE CITED

(1) T. F. Rogers, "Factors Affecting the Width and Shape of Atmospheric Microwave Absorption Lines," ARDC No. E5078, ATI 121123.

(2) J. H. Van Vleck and V. F. Weisskopf, "On the Shape of Collision-Broadened Lines," Reviews of Modern Physics, vol. 17, p. 227; April-July, 1945.

(3) J. H. Van Vleck, "The Absorption of Microwaves by Oxygen," The Physical Review, vol. 71, p. 413; April, 1947.

(4) J. H. Van Vleck, "The Absorption of Microwaves by Uncondensed Water Vapor," Phys. Rev., vol. 71, p. 425; April, 1947.

(5) S. N. Ghosh and H. D. Edwards, Geographical Research Directorate, AFCRC Report No. 82; 1956.

(6) M. L. Meeks, "Atmospheric Emission and Opacity of Millimeter Wavelengths Due to Oxygen," Journal of Geophysical Research, vol. 66, p. 3749; November, 1961.

(7) R. J. Schmelzer, "Total Molecular Absorption in the Atmosphere from Frequencies below 380 kmc," LMSD Report No. 895084; March, 1961. AD 256896.

(8) H. H. Theissing and P. J. Caplan, "Atmospheric Attenuation of Solar Millimeter Wave Radiation," Journal of Applied Physics, vol. 27, p. 538; May, 1956.

(9) D. C. Hogg and A. B. Crawford, "Measurement of Atmospheric Attenuation at Millimeter Wavelength," Bell System Technical Journal, vol. 35, p. 907; July, 1956.

(10) D. E. Kerr, "Propagation of Short Radio Waves," Vol. 13, Ch. 8, M.I.T. Radiation Laboratory Series, McGraw-Hill Book Company, Inc., New York, N. Y., 1948.

(11) A. W. Straiton, C. W. Tolbert, et al., "Anomalies in the Absorption of Radio Waves by Atmospheric Gases," Proceedings of the Institute of Radio Engineers, vol. 48, p. 898, May, 1960. Also Technical Laboratory Reports 5-43, 5-45, 6-39, 6-42, 93, 107, 109, 117, and 125; and "Atmospheric Transmission Characteristics of Millimeter Radio Waves," paper presented at Johns Hopkins University, published February 1964 in A Symposium on Electromagnetic Waves. Technical Report AF-106.

(12) W. M. Sinton, Atmospheric Transmission Between 300 and 2,000 Microns, Progress Report on Contract N-onr 248(01), November 15, 1952.

(13) E. S. Rosenblum, "Atmospheric Absorption of 10-4000 kmcps Radiation. Summary and Bibliography of 1960," Lincoln Laboratory Report No. 82G-0021, August 1960. Also -- "Summary and Bibliography to 1961," The Microwave Journal, vol. 4, p. 91; March 1961. See also J. Lurye, Survey of the Literature on Millimeter and Submillimeter Waves, TRG, Inc., June, 1960. AD-243 242.

(14) D. G. Hogg, "Effective Antenna Temperatures Due to Oxygen and Water Vapor in the Atmosphere," J. Appl. Phys., vol. 30, p. 1417; September, 1959.

(15) D. C. Hogg and W. W. Mamford, "The Effective Noise Temperature of the Sky," Microwave J., vol. 3, p. 80; March, 1960.

(16) D. C. Hogg and R. A. Semplak, "The Effect of Rain and Water Vapor on Sky Noise at Centimeter Wavelength," Bell System Tech. J., vol. XL, p. 1331; September 1961.

(17) H. H. Theissing and P. J. Caplan, "Measurements of the Solar Millimeter Spectrum," Journal of the Optical Society of America, vol. 46, p. 971; November, 1956.

(18) J. O. Artman and J. P. Gordon, "Absorption of Microwaves by Oxygen in the Millimeter Wavelength Region," Phys. Rev., vol. 96, p. 1237; December, 1954.

(19) R. N. Whitehurst, J. Copeland and F. H. Mitchell, "Solar Radiation and Atmospheric Attenuation at 6-mm Wavelength," J. Appl. Phys., vol. 28, p. 295; March, 1957.

(20) R. J. Coates, "Measurements of Solar Radiation and Atmospheric Attenuation at 4.3-Millimeters Wavelength," Proc. IRE, vol. 46, p. 122; January, 1958.

(21) A. E. Schulze and C. W. Tolbert, "Shape, Intensity and Pressure Broadening of the 2.53-Millimeter Wave-Length Oxygen Absorption Line," Nature, vol. 200, p. 747; November 23, 1963.

(22) S. Silver, Microwave Antenna Theory and Design, MIT Rad. Lab. Ser. vol. 12, Chapter 10, McGraw-Hill, 1949.

(23) S. Kuhn, "Calculations of Attenuation in Wave Guides," The Journal of the Institute of Electrical Engineers, vol. 93, Part III, p. 633; May, 1946.

(24) G. L. Ragan, Microwave Transmission Circuits, MIT Rad. Lab. Ser., vol. 9, chapter 10, McGraw-Hill; 1948.

(25) W. M. Sinton, "Observations of Solar and Lunar Radiation at 1.5 Millimeters," J. Opt. Soc. Am., vol. 45, p. 975; November, 1955.

(26) W. M. Sinton, "Observation of a Lunar Eclipse at 1.5 MM," The Astrophysical Journal, vol. 123, p. 325; March, 1956.

(27) M. W. Long and J. C. Butterworth, "New Technique for Microwave Radiometry," IEEE Trans. Microwave Theory and Tech., vol MTT-11, p. 389, Sept. 1963.

(28) R. H. Dicke, "The Measurement of Thermal Radiation at Microwave Frequencies," Review of Scientific Instruments, vol. 17, p. 268; July, 1946.

(29) R. P. Sallen and E. L. Key, "A Practical Method of Designing RC Active Filters," IRE Transactions on Circuit Theory, vol. CT-2, p. 74; March, 1955.

(30) N. T. Larsen, "Low-Level Low-Frequency Detection System," Rev. Sci. Instr., vol. 33, p. 1200; November, 1962.

(31) D. B. Harris, "Microwave Radiometry," Part I, The Microwave J., p. 41; April, 1960; Part II, Microwave J., vol. 3, p. 47; May, 1960.

(32) E. W. Richter, "Millimeter Radiometers," Microwave J., vol. 3, p. 63; October, 1960.

(33) F. D. Drake and H. I. Ewen, "A Broad-Band Microwave Source Comparison Radiometer for Advanced Research in Radio Astronomy," Proc. IRE, vol. 46, p. 53; January, 1958.

(34) G. R. Nicoll, "The Measurement of Thermal and Similar Radiations at Millimeter Wavelengths," Proc. IEE, No. 104-B, p. 519; 1957.

(35) J. L. Pawsey and R. H. Brasewell, Radio Astronomy, Oxford; 1955.

(36) J. D. Kraus, "Solar System Radio Radiation," The Ohio State University Research Foundation Scientific Report No. 1-A, R.F. Project 673; December, 1958.

(37). K. F. Bottlinger, and E. Schoenberg, Handbuch Der Astrophysik, vol. 2, Part I; 1929, pp. 268-272.

(38) J. A. Goff and S. Gratch, "Low-Pressure Properties of Water from -160 to 212° F," Transactions of American Society of Heat and Ventilating Engineers, vol. 52, p. 95; 1946.

(39) P. G. Hoel, Introduction to Mathematical Statistics, Chapter V, John Wiley and Sons; 1947.

(40) E. H. Putley, "The Detection of Sub-Millimeter Radiation," Proc. IEEE, vol. 51, p. 1412; November 1963.

(41) F. J. Low, "Low Temperature Germanium Bolometer," J. Opt. Soc. Am. vol. 51, p. 1300; November, 1961.

(42) United States Air Force, Handbook of Geophysics, Revised Edition, Macmillan Company; 1960.

(43) R. C. Johnson, "Design of Linear Double Tapers in Rectangular Waveguides," IRE-Trans. on Microwave Theory and Tech., vol. MTT-7, No. 3, p. 374; July, 1959. Corrections vol. MTT-8, p. 458, July, 1960.

VITA

Robert Deming Hayes was born on March 11, 1925, in Lexington, Kentucky, the son of Roy B. and Esther B. Hayes. He was married in 1947 to Miss Nancy Ellen Taylor, and they have four children.

He attended public schools in Lexington, Kentucky, and graduated from Henry Clay High School in February 1943. He entered Kenyon College in February 1943 and was assigned by the U. S. Army Air Corps to the Pre-Meterology Program at Kenyon College in April 1943. He completed the Pre-Meterology program in February 1944 and was assigned to duty in the U. S. Army Air Corps as a weather observer. During his military service, he completed the Radio and Electronics School at Harvard University, the Radiosonde Maintenance School at Fort Monmouth, N. J., and the Radiosonde-Rawin Observers School at Chanute Field, Ill. He was discharged in the spring of 1946 and entered the University of Kentucky.

He received the BSEE degree from the University of Kentucky in 1948 and the MS (Physics) degree in 1950. While at Kentucky, he was an undergraduate assistant in 1947 and a graduate assistant from 1948 to 1950, teaching courses in Electrical Engineering.

He was employed as a Field Engineer with the Western Electric Company from 1950 to 1954 providing technical assistance to the U. S. Air Force on airborne radar navigational and bombing systems.

Mr. Hayes started his employment at the Georgia Institute of Technology in 1954 as an Assistant Research Engineer. Since 1955, he has been a Research Engineer and Director of several radar projects relating

to the national defense efforts. He has also taught part time in the School of Electrical Engineering since 1958.